Machine learning-based investigation of disease progression of structural changes in the brain in people with epilepsy and its association with treatment response of anti-epileptic medications

Seymour Mark Lopez

A dissertation submitted in partial fulfilment

Of the requirements for the degree of

Master of Philosophy

Of Biomedical engineering and medical physics.

University College London.

Department of Medical Physics and Biomedical Engineering

I, Seymour Mark Lopez, confirm that the work presented in this thesis is my own. Where information has been derived from other sources, I confirm that this has been indicated in the thesis.

Abstract

Epilepsy is a neurological disease associated with structural and functional changes in the brain, genetic mutations, as well as factors mediated through brain injury. While extensive research has documented structural changes in the brains of people with epilepsy, it remains unclear whether these changes follow a distinct pattern of progression from one brain region to another. Furthermore, existing antiepileptic drugs often show limited effectiveness in treating epilepsy, posing challenges in clinical management. Therefore, I investigate if there are image-derived subtypes of epilepsy based on the unique progression of structural changes in the brain and if staging these patients helps identify the response to antiepileptic drugs. This will help identify patients that require personalised or alternate treatments during the early diagnostic stages of epilepsy. Furthermore, it is unclear if there is a link between structural changes in the brain and the subtle facial asymmetry seen across a subset of people with epilepsy. Therefore, I aim to investigate this association, which will improve our understanding of the underlying mechanisms that cause facial asymmetry in people with epilepsy.

This report is structured in 7 chapters, where: Chapter 1 which serves as the introduction, I outline the main motivations and objectives of the research conducted here; Chapter 2 explains the causes, diagnosis, treatments in epilepsy and subsequently outlines the motivations for my research, Chapter 3 gives an overview of machine learning techniques used across the research presented here; Chapter 4 investigates the association of structural changes in the brain with the asymmetry of facial features; In Chapter 5, using one of the world's largest epilepsy cohorts, from the ENIGMA-Epilepsy working group, I estimate the progressive sequence of structural changes in the brain; Chapter 6 extends the work of Chapter 5 by investigating imaging-derived subtypes of epilepsy based on the unique progressive changes in the brain. Lastly, Chapter 7 outlines the conclusions and future work of the research reported here.

Impact statement

Our collaborators, Dr. Simona Balestrini and colleagues, showed that people with lateralised focal epilepsies carrying structural variants in the genome exhibit a subtle yet quantitative increase facial asymmetry, compared to people with idiopathic generalized epilepsy or controls without epilepsy. However, the pathological mechanisms that cause facial asymmetry has not been explored. Here, I help demonstrate that the facial asymmetry observed in these patients is independent to the structural changes in the brain. This affirms that the pathological mechanisms that cause structural changes in the brain are independent to that of facial asymmetry. Future research can focus on investigating the link between facial asymmetry and other clinical variables such as seizure semiology, comorbidities, genetic mutations or other phenotypic traits.

Utilizing the largest cohort of T1W and DTI MRI data in epilepsy research, we introduce a novel imaging-derived subtype and disease stage assignment based on the unique sequence in which structural changes progress in the brain. This sequence was estimated using cross-sectional data and validated using the duration of illness. Here, we established four imaging-derived subtypes which had majority of people with focal epilepsies grouped in the two limbic-led subtypes and two white matter-led subtypes that contained both people with focal and generalized epilepsies. This reaffirms the common disease pathology between the epilepsy syndromes.

We also show here that early disease stages can represent changes in grey matter regions as well as changes in white matter tracts. The estimated disease stages were not very useful in predicting the treatment responses in patients. However, by incorporating the use of additional clinical features we may help improve its application in clinical management strategies such as treatment responses and surgical planning. Finally, in future, investigating the associations between disease stages and genetic variation or changes in gene expression we can help provide novel drug targets that prevents progressive structural changes in the brain or epileptogenesis.

UCL Research Paper Declaration Form

referencing the doctoral candidate's own published work(s)

a) What is the title of the manuscript?
Increased facial asymmetry in focal epilepsies associated with unilateral lesions

b) Please include a link to or doi for the work
https://doi.org/10.1093/braincomms/fcab068

c) Where was the work published?
Brain Communications

d) Who published the work? (e.g. OUP)
Dr. Simona Balestrini, Oxford Academic is Oxford University Press's (OUP) academic research platform

e) When was the work published?
April 2021

f) List the manuscript's authors in the order they appear on the publication
Simona Balestrini, Seymour M. Lopez, Krishna Chinthapalli, Narek Sargsyan, Rita Demurtas, Sjoerd Vos, Andre Altmann, Michael Suttie, Peter Hammond and Sanjay M. Sisodiya.

g) Was the work peer reviewed?
Yes

h) Have you retained the copyright?
Yes

i) Was an earlier form of the manuscript uploaded to a preprint server? (e.g. medRxiv). If 'Yes', please give a link or doi)
No

If 'No', please seek permission from the relevant publisher and check the box next to the below statement:
☒
I acknowledge permission of the publisher named under 1d to include in this thesis portions of the publication named as included in 1c.

UCL Research Paper Declaration Form

referencing the doctoral candidate's own published work(s)

a) What is the title of the manuscript?
Event-based modeling in temporal lobe epilepsy demonstrates progressive atrophy from cross-sectional data

b) Please include a link to or doi for the work
https://doi.org/10.1111/epi.17316

c) Where was the work published?
Epilepsia

d) Who published the work? (e.g. OUP)
Seymour Lopez, Wiley, Online Library.

e) When was the work published?
June 2022

f) List the manuscript's authors in the order they appear on the publication
Seymour M. Lopez, Leon M. Aksman, Neil P. Oxtoby, Sjoerd B. Vos, Carrie R. McDonald, Daniel C. Alexander, Sanjay M. Sisodiya, Andre Altmann, the ENIGMA-Epilepsy Working Group

g) Was the work peer reviewed?
Yes

h) Have you retained the copyright?
Open access article

i) Was an earlier form of the manuscript uploaded to a preprint server? (e.g. medRxiv). If 'Yes', please give a link or doi)
No

If 'No', please seek permission from the relevant publisher and check the box next to the below statement:

☒

I acknowledge permission of the publisher named under 1d to include in this thesis portions of the publication named as included in 1c.

Acknowledgments

I am deeply grateful to Dr Andre Altmann (Centre for Medical Image Computing (CMIC)) for his guidance, advise and tutoring throughout these past years, in the field of machine learning. I would also like to thank Dr Sanjay Sisodiya for his insights on the clinical relevance and applications of my findings. I would also like to thank Dr Simona Balestrini for including me in her research project. Moreover, I have gained an immense knowledge of; processing and evaluating MRI scans through Dr Sjoerd Vos; EBM application with help from Dr Leon Aksman, Neil Oxtoby, as well as other members of the POND UCL group.

Table of Contents

Chapter 1 Introduction

1.1 Overview of epilepsy

Epilepsy is a group of neurological diseases mainly characterised by reoccurring seizures, and affects about 0.6-1.5% of the worldwide population (Sander, 2014; Beghi *et al.*, 2019). This equates to around 7 million people in total. A seizure is a sudden temporary firing of electrochemical signals from neurons that disrupts the normal function of the brain (Scharfman, 2007). Broadly speaking, epilepsy is a diverse disease exhibiting various clinical syndromes. These epilepsy syndromes are classified based on the brain regions where the seizure originates, seizure symptoms and etiology of the disease (Engel, 2001; Berg and Scheffer, 2011; Fisher *et al.*, 2017). The brain regions where seizures originate are referred to as the epileptogenic focus or seizure onset. There are two broad categories based on the seizure onset: focal epilepsies where seizures originate in either one of the two brain hemispheres, and generalized epilepsies where the seizure onset involves both hemispheres (Fisher *et al.*, 2017). The seizure onset is therefore considered to be lateralized in a single brain hemisphere in focal epilepsy. Furthermore, research has demonstrated that pathological mechanisms in focal and generalized epilepsy affect the network of neurons across the brain and not necessarily localised to a single brain region (Bernhardt *et al.*, 2011; Blumenfeld, 2014; Fisher *et al.*, 2017).

Epilepsy is diagnosed by a specialist from the semiology of seizures and other supplementary information including a patient' medical history, example reports of previous seizures if available (Engel, 2001; Harris and Angus-Leppan, 2020; Riney *et al.*, 2021). In cases that require additional information to classify the seizure, a clinician may use videos brought in by family, or EEG recordings depending on their availability (Fisher *et al.*, 2017; Riney *et al.*, 2021). Epilepsy can be ruled out if any of the imitators of epileptic seizures are detected such as: syncope caused by reduced global cerebral perfusion; psychogenic non-epileptic seizures (PNES) caused due to behavioural phenomena that inhibits self-control

or seizures caused from withdrawal of alcohol and recreational drugs (Engel, 2001; Brodtkorb, 2013).

People with epilepsy (PWE) are usually prescribed a single or a combination of anti-seizure medications (ASMs). However, it is important to note that ASMs are not effective in approximately one third of PWE and are categorised as having resistance to ASMs (Kwan et al., 2010). Due to this, patients are advised to take precautions and avoid engaging in activities that could potentially jeopardize their safety or that of others until their treatment becomes effective. These precautions are particularly crucial in case a seizure occurs during activities such as driving, swimming, or participating in physically demanding tasks, as they could result in a loss of control and potential harm or even fatality. Consequently, PWE can face social and or economic repercussions depending on the disease severity, as determined by factors such as seizure frequency and symptoms during the seizure. Hence, an effective treatment plan is required to enhance the well-being and overall quality of life for people living with epilepsy.

PWE that are resistant to ASMs may be considered for surgery, where the brain region considered as the epileptogenic focus is resected (Casazza *et al.*, 1997; Jayakar *et al.*, 2016). Electrophysiological methods sometimes used to aid in the diagnostic process include the electroencephalogram (EEG) or intracranial-EEG, whereas neuroimaging methods such as magnetic resonance imaging (MRI) are predominantly used to plan surgery (Jayakar *et al.*, 2016; Vogt *et al.*, 2017; Bernasconi *et al.*, 2019). These techniques are detailed in Section 2.5. Current research efforts involve the analysis of brain imaging data from PWE to investigate structural alterations in the brain and their associations with clinical variables or phenotypic traits. This can help understand the underlying mechanisms of epilepsy which is crucial for enhancing the management and treatment outcomes.

A study by Chinthapalli *et al.*, (2012) demonstrated that PWE with structural variations in the genome exhibit subtle atypical facial features. Furthermore, they showed that patients with abnormality in their MRI scans had a greater degree of facial asymmetry. However, the underlying relationship between facial

asymmetry in PWE and brain pathology remains largely unknown. Previous research has indicated that individuals with focal epilepsy often exhibit a higher degree of brain asymmetry compared to those with generalised epilepsy, due to lateralized structural changes (Bernasconi *et al.*, 2004; Thom *et al.*, 2012; Bernhardt, Bonilha and Gross, 2015; Vaughan *et al.*, 2017; Whelan *et al.*, 2018). Therefore, in Chapter 4, we explore whether facial asymmetry quantified in PWE is associated with structural changes in the brains of individuals with lateralized focal epilepsy.

Recent research using data derived from neuroimaging have shown PWE have widespread thinning of the cortical and subcortical regions. (Alhusaini *et al.*, 2012; Whelan *et al.*, 2018). Furthermore, it is established that the progression of cortical thinning or structural changes in the brain is associated with the duration of illness (Bernasconi, Natsume and Bernasconi, 2005; Bonilha *et al.*, 2006; Bernhardt *et al.*, 2009; Coan *et al.*, 2009; Whelan *et al.*, 2018; Galovic *et al.*, 2020). However, the disease progression of these structural changes from one brain region to another is not well understood. Uncovering this pattern can help us better understand if there are imaging-derived subtypes of epilepsy based on a specific trend in the progression of structural changes and how they relate to epilepsy syndromes and treatment response. We start by investigating the progression of structural changes of the brain in patients with left and right mesial temporal lobe epilepsy with hippocampal sclerosis (MTLE-HS) in Chapter 5 and subsequently investigate imaging-derived subtypes of epilepsy based on their unique disease progression patterns from a cohort of patients with common epilepsies in Chapter 6. Lastly, Chapter 7 outlines the conclusions and future work.

Chapter 2 Background

2.1 Underlying biology of neurons and epilepsy

The brain is composed of approximately 86 billion neurons or nerve cells, with diameters ranging from 4 to 100 micrometers. These neurons form an intricate communication network, exchanging neurotransmitters or biomolecules, that creates an action potential (electric discharge) as shown in Figure 2.1 (Yamazaki, Igarashi and Yamaura, 2021). Imbalances of neurotransmitters such as γ-aminobutyric acid (GABA), glutamate, dopamine, noradrenaline, serotonin, acetylcholine in PWE can lead to seizures (Covenas, 2015). Seizures can also be caused by synchronous or redirected ions flowing through the network, that arise from damage in the brain due to injury, brain hypoxia, or infections, as well as malformations of cortical development (MCD) (Sisodiya, 2004; Hossain, 2005; Jiruska *et al.*, 2013; Löscher *et al.*, 2020). During a seizure, people often undergo temporary and involuntary alterations in muscle activity, which can manifest as convulsions, spasms, or jerking movements (Fisher *et al.*, 2005; Riney *et al.*, 2021). About one third of the PWE also suffer from anxiety and depression (Kwon and Park, 2014).

In 2014, the International League Against Epilepsy (ILAE) defined epilepsy as a group of diseases which are characterised by at least two unprovoked seizures occurring >24 hour apart or a high risk of seizure reoccurrence after a first unproved or reflex seizure (Fisher *et al.*, 2014). In this context, "unprovoked" indicates the absence of a temporary or reversible factor causing a seizure. The latter risk of seizure reoccurrence is evaluated based on diagnosis of a specific epilepsy syndrome, presence of structural lesions, central nervous system (CNS) infection, or traumatic brain injury among others. Seizures usually last for 3-5 minutes (mins), after which the individual gradually recovers to a normal state. However, it is vital to get medical help if seizures continue for more than 5 mins, a condition referred to as status epilepticus which can cause significant damage in the brain (Lowenstein and Alldredge, 1998; Bengzon *et al.*, 2002; Trinka *et al.*, 2015).

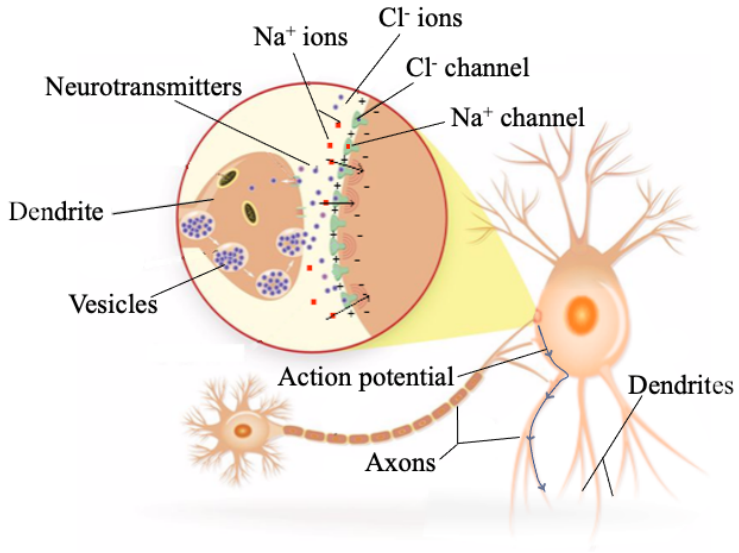

Figure 2.1 Generation of action potential in a neuron: Figure shows the transition of sodium (Na^+) and chloride (Cl^-) ions entering and leaving the neuron through their channels located on the membrane. This creates an action potential (electric discharge) along the axon which releases biomolecules or neurotransmitters stored in dendrite vesicles. The released biomolecules activate neighbouring neurons or cells that regulate organ functions. Adapted from (Asadi et al., 2019).

2.2 Anatomy of affected brain regions in epilepsy

Functional and structural changes in both grey matter (cortical and subcortical) regions and white matter tracts have been found to play a crucial role in the development and manifestation of various neurological disorders. A basic anatomy of these brain regions is shown in Figure 2.2. Here, grey matter regions interact with one another and various brain regions through complex connections of white matter tracts.

Previous studies have identified definitive thinning of sub-structures within grey matter regions, such as the superior frontal and superior temporal gyri, hippocampus and thalamus among others, in PWE compared to healthy individuals (Hardiman *et al.*, 1988; Lee *et al.*, 1995; Woermann *et al.*, 2000; Scanlon *et al.*, 2013; Whelan *et al.*, 2018; Galovic *et al.*, 2019). In addition,

changes in microstructural properties of white matter tracts, in particular tracts of the frontal, parietal, limbic system thalamo-cortical regions, corpus callosum which connects the two (left and right) hemispheres have also been identified in PWE (Focke *et al.*, 2008; Lee *et al.*, 2014; Szaflarski *et al.*, 2016; Hatton *et al.*, 2020). Studies have also suggested that structural changes in the cerebellum is associated with the occurrence of seizures (Marcián *et al.*, 2016). Depending on the brain regions affected, symptoms and etiology of the disease, epilepsy is classified into syndromes to manage and monitor treatments.

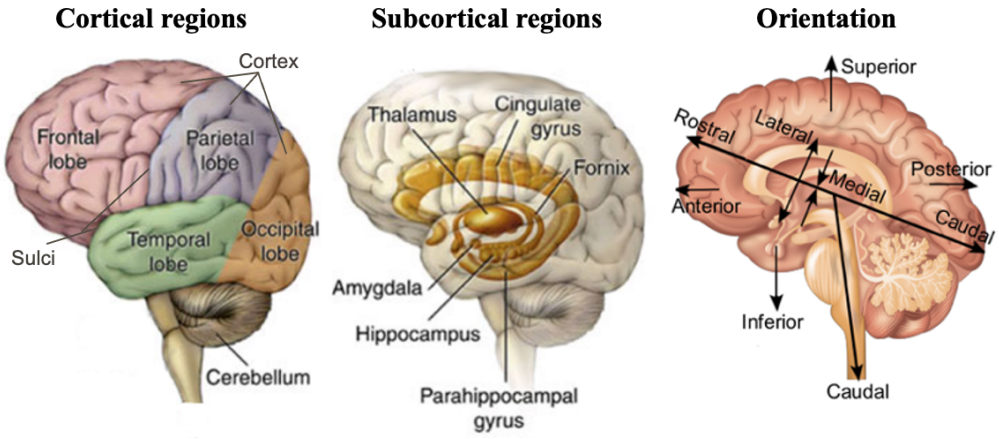

Figure 2.2 Anatomy of cortical and subcortical regions: In each hemisphere, three main sulci or tissue depressions distinguish the cortical structure into the four lobes as shown. These brain regions individually govern memory, behaviour, personality, speech, sense of touch, and interpret vision, among other functions. The orientation labels are affixed to sub-structures of the cortex for clear and concise identification. Reproduced from [1,2].

[1] https://sharpbrains.com/blog/2020/04/09/the-frontal-lobes-the-little-brain-down-under-and-stayin-alive-3-3/
[2]https://en.wikiversity.org/wiki/WikiJournal_of_Medicine/Medical_gallery_of_Blausen_Medical_2014

2.3 Classification and causes of epilepsy

2.3.1 Classification of epilepsy

Epilepsy is broadly classified based on the origin and type of seizures. In March 2017 the ILAE published the revised classification protocol for PWE that defined three diagnostic levels including 1) seizure type, 2) epilepsy type, and 3) epilepsy syndrome (Fisher *et al.*, 2017). Figure 2.3 illustrates examples of seizure types under which a patient may be classified. Here, the classification lays out two main types of epilepsy we briefly mentioned earlier: focal and generalized onset, where the seizure originates within brain networks of one and both hemispheres respectively (Fisher *et al.*, 2017). If the seizure onset cannot be identified from the information available at the time of diagnosis, the seizure can be classified as unknown onset. Seizures can be sub-classified as motor onset or nonmotor onset based on seizure characteristics. Here, motor activity encompasses various forms of muscular engagement and can manifest either as an increase or decrease in muscle contractions, resulting in distinct movements that are indicative of a seizure. (Fisher *et al.*, 2017). Focal seizures can optionally be further characterized based on the presence or absence of retained awareness.

Specific semiologies in focal epilepsies provide an insight into the localization of the seizure onset zone, which is particularly useful for diagnosis. For example the amygdala which is part of the mesial temporal lobe, is involved in emotion processing and autonomic regulation, including control of heart rate and breathing. When focal seizures originate or propagate to the amygdala, it may present with experiential aura (fear, déjà vu or jamais vu) or tachycardia (Bancaud *et al.*, 1994; Illman *et al.*, 2012; Du *et al.*, 2015; Chowdhury *et al.*, 2021). In addition to localisation, some symptoms of a focal seizure may also be lateralized in the left or right side of the body. For example, unilateral tonic or unilateral clonic movements which indicate onset in the contralateral hemisphere (McGonigal and Chauvel, 2004; Stoyke, Bilgin and Noachtar, 2011; Tufenkjian and Lüders, 2012).

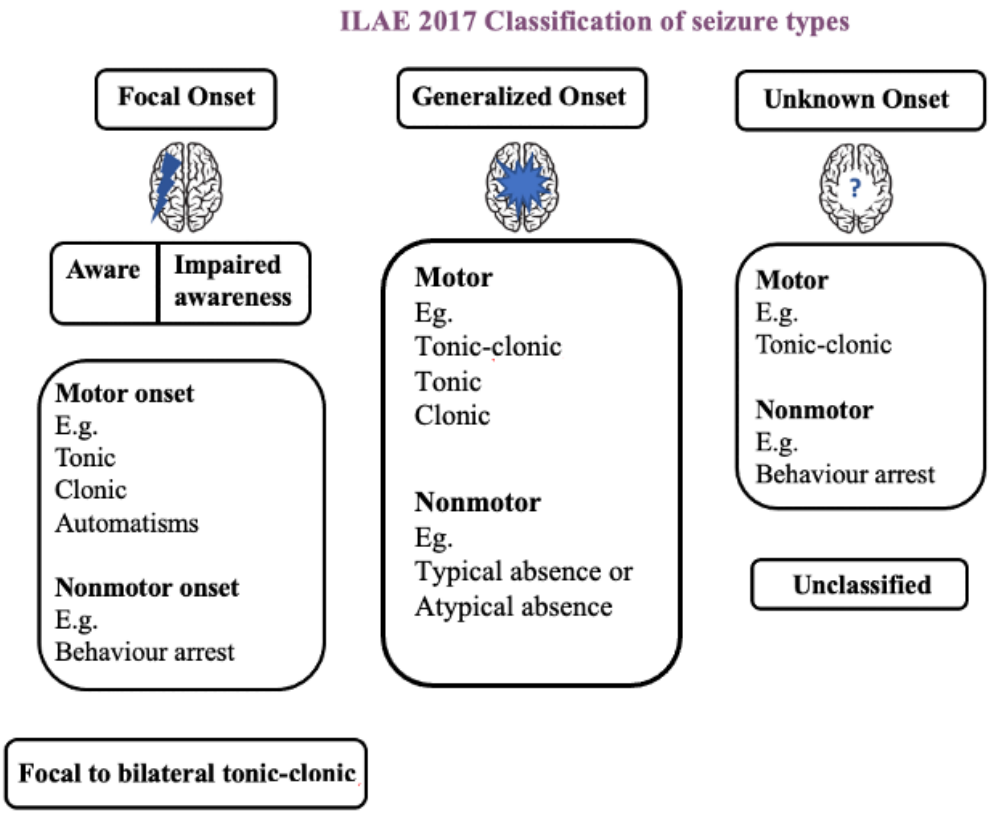

Figure 2.3 Epilepsy classification: As per the ILAE 2017 classification, the seizure type can be a focal seizure or a generalized seizure. These can be further sub-classified as motor or nonmotor based on the seizure symptoms. Cases where the origin of onset is not clear, or those with inadequate clinical data are categorised as unknown onset or unclassified respectively. Adapted from (Fisher et al., 2017).

The 'focal to bilateral tonic-clonic' classification reflects the propagation pattern of seizures to bilateral networks and serve to distinguish from generalized seizures (Jobst *et al.*, 2001; Hemery, Ryvlin and Rheims, 2014; Yoo *et al.*, 2014; Sinha *et al.*, 2021). For example, a patient may have an initial sense of fear and lip smacking, which progresses to a bilateral tonic-clonic seizure. The symptoms of the tonic-clonic seizure are illustrated in Figure 2.4.

Typical absence seizures are characterised by a sudden onset, interruption of ongoing activities, a blank stare or unresponsiveness, and may involve a brief upward deviation of the eyes (Roger *et al.*, 1989; Fisher *et al.*, 2017). Absence seizures are considered atypical when changes in muscle tone are more

pronounced than in typical absence seizures. Atypical absence seizures are also be characterised by their slow onset or termination of the seizure.

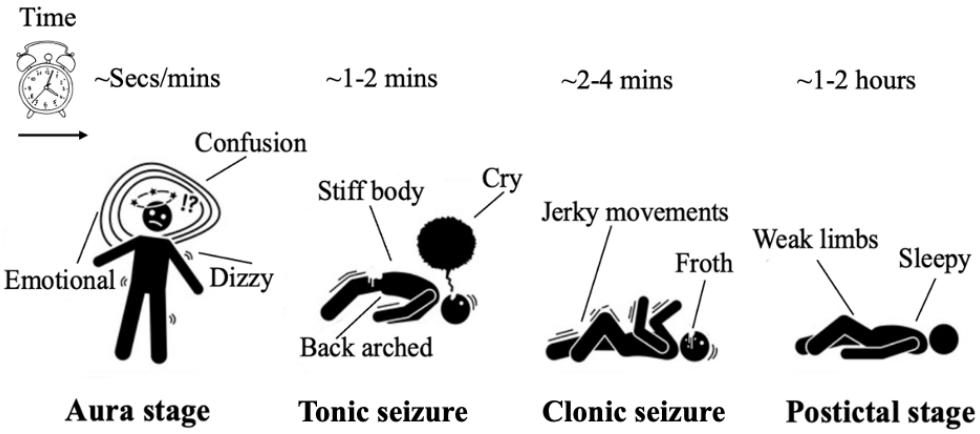

Figure 2.4 Tonic-clonic seizures stages: Patients may experience the aura stage before tonic-clonic seizures, followed by the postictal stage. Symptoms experienced during these stages are shown with their duration. Adapted from [3].

The second level of classification is the epilepsy type and assumes that the patient has a diagnosis of epilepsy based on the definition of epilepsy discussed earlier. Depending on the seizure type, a patient may be diagnosed into one of the four categories 1) focal epilepsy, 2) generalized epilepsy, 3) combined generalized and focal epilepsy, or 4) an unknown epilepsy group (Scheffer *et al.*, 2017). The new group of combined generalized and focal epilepsies exists as there are patients who have both generalized and focal seizures. Patients may be categorised as having an unknown epilepsy if the clinician is not able to distinguish the epilepsy type as focal or generalized due to insufficient information available to infer the seizure type.

Lastly, the third level of classification is an epilepsy syndrome diagnosis (Scheffer *et al.*, 2017). An epilepsy syndrome refers to a group of features incorporating seizure types, symptoms, EEG and neuroimaging features that usually occur together. It often has age-dependent features such as age of onset,

[3] https://www.vectorstock.com/royalty-free-vector/stages-and-phases-a-seizure-depicts-phases-vector-26129105

severity, remission, seizure triggers, diurnal variation, co-morbidities, and sometimes prognosis. An epilepsy syndrome may not have a direct association with an etiological diagnosis and serves a different purpose such as guiding management of the disease. The idiopathic generalized epilepsies (IGE)s are a sub-group within the generalized epilepsies that encompasses four well-established epilepsy syndromes: childhood absence epilepsy, juvenile absence epilepsy, juvenile myoclonic epilepsy and generalized tonic-clonic seizures alone. Here, the term "idiopathic" is derived from the Greek word "idios" that refers to self, own or personal, and is thus meant to reflect the genetic etiology without explicitly stating so. However, in order to accommodate the fact that IGEs can have some genetic cause that are not necessarily inherited, the ILAE task force recommended to refer to this group of syndromes as genetic generalized epilepsies (GGEs) (Scheffer *et al.*, 2017).

2.3.2 Causes of epilepsy

From the onset of the patient' first epileptic seizure, clinicians should aim to identify the underlying cause of the epilepsy. This is essential because knowledge of the etiology may hold potential therapeutic implications. As per the recommendations made by the ILAE in 2017, a clinician may state the etiology as one of the following: structural, genetic, infectious, immune, metabolic or unknown factors and are listed in Figure 2.5 (Scheffer *et al.*, 2017). Structural etiologies may be genetic such as MCD or acquired as a result of a stroke, injury or infection (Annegers and Rocca, 1996; Guerrini, Sicca and Parmeggiani, 2003; Sisodiya, 2004; Myint, Staufenberg and Sabanathan, 2006; Guerrini, Dobyns and Barkovich, 2008). Previous studies have reported that MCD arises from macroscopic alterations of brain structure like double cortex, absent or small gyri caused due to genetic mutations or environmental factors (Pilz *et al.*, 1998; Parrini *et al.*, 2016; Guarnieri *et al.*, 2018).

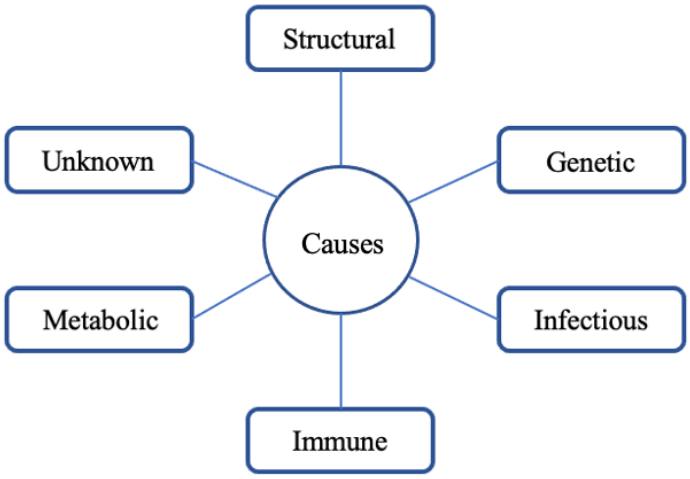

Figure 2.5 Causes of epilepsy: The different causes of epilepsy are shown above. Mechanisms from one or more of the above causes may lead to epilepsy.

Epilepsy can also be caused by changes in a persons' genome that alter the function of proteins or ion channels located on neurons. The malfunction of these proteins that regulates the activation of neurotransmitters and ions leads to the abnormal firing of neurons. Some of these ion channels affected in epilepsy are the voltage-gated sodium channels, voltage-gated potassium channel, voltage-gated calcium channel, voltage-gated chloride channel and gamma-aminobutyric acid (GABA) receptors (Petroff *et al.*, 1996; Singh *et al.*, 1998; Claes *et al.*, 2001; Lossin *et al.*, 2003).

A typical example of a genetic cause is that in Dravet syndrome, where more than 80% of patients have a pathogenic variant of *SCN1A* gene (Depienne *et al.*, 2009; Marini *et al.*, 2009; Bender *et al.*, 2012). Infectious etiologies of epilepsy may arise from conditions like neurocysticercosis, tuberculosis, human immunodeficiency virus (HIV), or cerebral malaria (Pal, Carpio and Sander, 2000; Singhi, 2011; Moyano *et al.*, 2014; Vezzani *et al.*, 2016). Metabolic causes involve epilepsy linked to metabolic disorders such as porphyria or uremia. An immune etiology is considered when there is evidence of autoimmune-mediated central nervous system inflammation. If the cause cannot be determined at the time of diagnosis, the etiology may be classified as unknown until new information becomes available.

In Chapter 4, some of the legacy terms are in line with the ILAE report published in 1989. According to this report, epilepsy with an acquired or genetic cause, associated with gross neuroanatomic or neuropathologic abnormalities, and/or clinical features such as brain injury, developmental abnormalities, or infections, was categorized as symptomatic epilepsy (Roger *et al.*, 1989; Shorvon, 2011; Shorvon, Guerrini and Andermann, 2011). Cases where the cause cannot be identified due to unknown mechanisms were classified as cryptogenic epilepsy.

2.4 Epidemiology

Epilepsy stands as a prominent global health challenge, contributing to diminished work productivity, increased mortality rates, societal stigma, and heightened strain on healthcare systems (Fiest *et al.*, 2014; Thurman *et al.*, 2017). In 2016, the global prevalence of active epilepsy reached 45.9 million people, with 24.0 million specifically diagnosed with active IGE (Beghi *et al.*, 2019). Notably, between 1990 and 2016, the prevalence of IGE remained relatively stable, yet mortality rates exhibited a significant 24.5% decrease, coupled with a 19.4% decline in disability-adjusted life years (DALYs) (Beghi *et al.*, 2019). These positive trends can be linked to advancements in perinatal care, improved control of infectious diseases, and enhanced access to treatments, resulting in a reduced risk of death and milder disease severity. The global epidemiology chart for IGE, depicted in Figure 2.6 and sourced from Beghi *et al.*, (2019), provides a comprehensive overview.

Furthermore, Beghi (2020) reported the prevalence and incidence of epilepsy tends to be slightly lower in women compared to men, and that focal seizures were more commonly observed than with generalized seizures. The meta-analysis by Vaughan et al. (2019) estimated that from a population of 51.7 million people currently diagnosed with epilepsy, that 10.1 million patients were potential candidates for surgical treatment, with an annual projection of 1.4 million new cases. According to the world health organisation (WHO), the estimated annual incidence of new cases is 49 per 100,000 people in high-

income countries and 139 per 100,000 in low- and middle-income countries [4]. However, this report does not account for the underreporting of cases in low-income regions, where cultural beliefs and stigma may lead to many incidents going unreported. Overall, the epidemiological insight highlights the global effect of epilepsy, inspiring our pursuit of improving tools to predict treatment outcomes and a comprehensive exploration of disease progression.

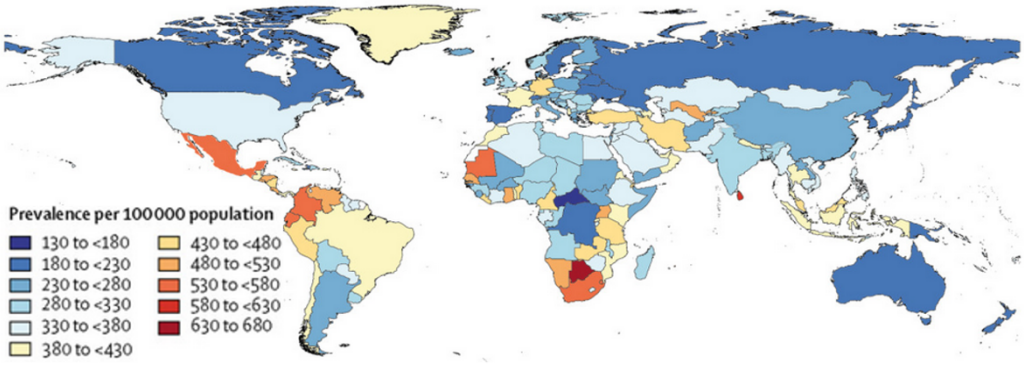

Figure 2.6 Global epidemiology chart for IGE: Global distribution of annual prevalence of IGE, prevalence per 100,000 people both sexes, 2016. Prevalence is higher in low-income countries, particularly sub-Saharan Africa, which can be linked to inadequate treatment facilities in these countries. Reproduced from (Beghi, 2020).

2.5 Epilepsy diagnosis and tools to aid in treatments

PWE manifest a variety of symptoms depending on the seizure type. Epilepsy is primarily diagnosed from the seizure semiology reported by the patient or care giver (Fisher *et al.*, 2017; Riney *et al.*, 2021). For example, a report of brief seizures with stiffening of the right arm and leg, during which responsiveness and awareness is retained would be classified as focal aware tonic seizure. If a patient experiences the "hair on my arms standing on edge", a feeling of being flushed and retained awareness, the seizure would be classified as focal aware autonomic seizure. Generalized clonic seizures begin, progress, and end with sustained rhythmic jerking of limbs on both sides of the body and often head,

[4] https://www.who.int/news-room/fact-sheets/detail/epilepsy

neck, face, and trunk. In addition, the patients' medical history can provide information about past seizures, which the clinician can use to make an informed decision on the diagnosis. (Angus-Leppan, 2008; Nass *et al.*, 2017; Nobili *et al.*, 2020; Riney *et al.*, 2021). In certain cases where the epilepsy syndrome is unclear, the clinician may utilize EEG to aid in the diagnostic process. For patients requiring surgery, magnetic resonance imaging (MRI) scans are conducted to localize the epileptogenic areas in the brain.

2.5.1 EEG

The EEG records electrochemical activity in the brain using electrodes placed on the patient' scalp. The EEG recordings obtained during ictal and interictal states in PWE are distinctive compared to healthy people. (Jung and Berger, 1979; Tatum *et al.*, 2018). Interictal spikes are characterized by a high amplitude, short duration waveforms with morphological characteristics of a spike lasting 20-70 millisecond (ms) or a sharp wave with a duration of 70-200 ms. In, addition, the generalized spike-and-wave (GSW) patterns on EEG are noted as a hallmark of GGEs, with discharges bursts of about 3 Hz (Tatum *et al.*, 2018). EEG may also be used in combination with a video recording to diagnose epilepsy syndromes (Mishra, Gautier and Glasscock, 2018). However, EEG may not be able to detect epileptogenic activity arising from deep sources such as orbitofrontal cortex. In such cases, electrochemical changes may not be detectable at the scalp, or if present, they may be widely distributed. Though sometimes this can be addressed by intracranial EEG, the procedure may not be suitable for all patients.

2.5.2 MRI

MRI emerges as the primary neuroimaging method employed to pinpoint epileptogenic regions or lesions in the brains of PWE. This diagnostic approach is not only instrumental in surgical planning but is also extensively employed for research purposes to provide insights on structural changes in the brain (Salmenpera and Duncan, 2005; Zhao *et al.*, 2017; Bernasconi *et al.*, 2019). The

analytical framework presented in this research relied on data extracted from MRI scans.

2.5.1.1 Tissue composition-based contrast

MRI uses strong magnetic fields and a radio frequency (RF) pulse to produce detailed images of the anatomy inside the body (Damadian, 1971; Koutcher, Goldsmith and Damadian, 1978). In an MRI scan, a magnetic field B_0 is present which aligns hydrogen nuclei (protons) present in water in the body. This is followed by the application of the RF pulse that causes the protons to absorb energy and flip the protons' direction out of alignment with respect to the B_0 field. The moment spins are out of alignment with B_0, they start to precess (rotate) around B_0. This precession can be measured by a receive coil as it acts as a moving magnetisation which induces a current in a coil. Over time, the protons realign with B_0 (relaxation).

Different tissues have different molecular compositions which result in different relaxation rates. This provides a contrast between tissue types which is translated into an image by a computer. There are two main magnetic relaxation properties with respect to B_0 field, T1 (relaxation along B_0) and T2 (relaxation in the plane transverse to B_0). Depending on the sequence timings, images can be created of varying contrast, from strongly T2-weighted (T2W) to strongly T1-weighted (T1W), or anything in between. The T1W and T2W scans illustrated in Figure 2.7.

The location of the individual hydrogen nuclei is identified by spatial encoding, which is achieved with the help of gradient coils. First a slice is selected from one of the three dimensions by a RF pulse with bandwidth in the megahertz (MHz) range. Following this, the signal along one axis of the anatomy is located by frequency encoding gradients, where current is passed through a coil that produces a sloped magnetic field strength that is superimposed on B_0. This alters the precession frequency of the hydrogen nuclei along the long axis. Similarly, the signal along the other axis is located by phase encoding gradients, by applying a sloped magnetic field that alters the phase of the precession hydrogen

nuclei. The composite signal containing spatial encoding information is recorded as a k-space matrix. In k-space, we essentially record the frequencies of signal intensities across space. To reconstruct the image from k-space, we use the inverse fast fourier transform algorithm which converts the frequency-domain information in k-space back into spatial signal intensities. Once the spatial domain data is obtained, greyscale values are assigned to the image pixels depending on the amplitudes of the sampled composite signal. This process results in the creation of a grayscale image.

MRI is a non-invasive neuroimaging technique unless a contrast agent needs to be administered. Furthermore, in an MRI scan, patients are exposed to RF radiation which is not harmful, in contrast to other methods, eg. ionising radiation from computed tomography (CT) scans (Kuzniecky, 2005; Martin and Semelka, 2006). In clinical practice, MRI scans are also used to identify lesions in the brain as shown in Figure 2.7, which play a crucial role in monitoring treatment outcomes. Previous studies have used measures derived from T1W MRI scans to identify cortical thinning and volume loss, across cortical and subcortical structures in PWE (McDonald *et al.*, 2008; Bernhardt *et al.*, 2010; Kemmotsu *et al.*, 2011; Labate *et al.*, 2011; Whelan *et al.*, 2018).

Based on T1W and T2W MRI scans from PWE, lesions often show as abnormal masses with varying degrees of contrast compared to healthy tissue or blurring on the scan, along with changes in the grey and white matter signal intensity (Bernasconi *et al.*, 2011). The use of T2-fluid-attenuated inversion-recovery (T2-FLAIR) enhances the visibility of lesions by suppressing cerebrospinal fluid (CSF) signals, leading to improved contrast between grey matter structures and reduced partial volume artifacts. This technique has proven effective in detecting lesions that might be overlooked in conventional T1W and T2W scans.

A study conducted by Focke *et al.*, (2009), demonstrated the capability of T2-FLAIR to identify abnormal signal clusters in cortical regions corresponding to seizure onset that were not visible on T1W scans. However, limitations exist, as T2-FLAIR may be less sensitive to detecting hippocampal sclerosis due to inherent hyperintensity in limbic structures (Adler *et al.*, 2018). Consequently,

the selection of the most appropriate MRI technique depends on the specific characteristics of the pathology under investigation and the desired diagnostic or research requirements. The research presented here primarily utilized data derived from T1W MRI given its widespread adoption across epilepsy treatment centers.

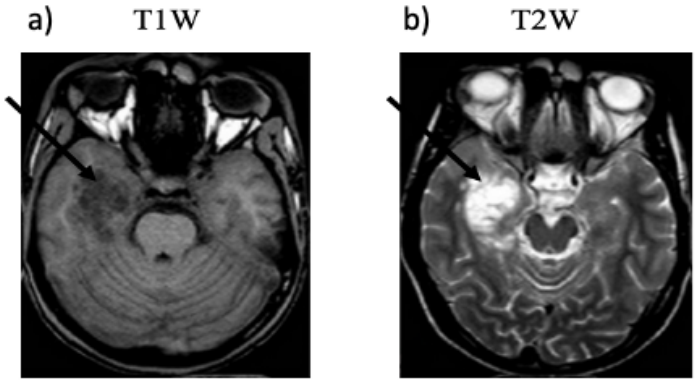

Figure 2.7 Identifying lesions in the brain from MRI scans: Figures show an axial slice selected from the MRI scan, of a plane through the brain that can help visualise the lesion in the temporal lobe area, taken from a patient with dysembryoplastic neuroepithelial tumour (DNET) which causes epilepsy. In a T1W scan white matter of the brain which contains myelin (a fatty substance) appears bright, whereas cerebrospinal fluid (CSF) is dark and vice versa for the T2W scan. Air appears dark in both T1W and T2W MRI scans. Depending on the disease pathology investigated, T1W, T2W or alternative MRI techniques are used to highlight specific modalities. Figure a) shows the lesion in black which represents loss of internal structure of the tissue whereas b) shows lesion as hypersensitivity which can be due to a variety of factors including ischemia, breaches of CSF or deformed myelin sheath. Reproduced from (Bano et al., 2011).

2.5.1.2 Molecular diffusion-based contrast

Fibre tracts that form the white matter in the brain are tightly packed together which makes it difficult to evaluate microstructural changes on T1W and T2W scans. However, by tracking the net diffusion of water molecules across these tracts we can infer their structural integrity. White matter tracts exhibit

anisotropic diffusion of water molecules in axons, differing along various directions, primarily because of faster diffusion along the long axis compared to the perpendicular direction (Bihan and Breton, 1985; Kang *et al.*, 2005). In contrast, grey matter neurons, being more spherical in shape, demonstrate more isotropic diffusion, characterized by equal diffusion rates in all directions.

Diffusion tensor imaging (DTI) is an MRI technique that capitalizes on these variations in diffusion properties to estimate the diffusion of water molecules within white matter tracts. (Bihan and Breton, 1985). In DTI, scans obtained at different orientations of diffusion-weighting are fitted to the diffusion tensor model, where diffusion within each voxel can be visualized as vectors in three dimensions called eigenvectors and magnitude as eigenvalues. The 3D representation of these eigenvectors and eigenvalues forms an ellipsoid as shown in Figure 2.8.

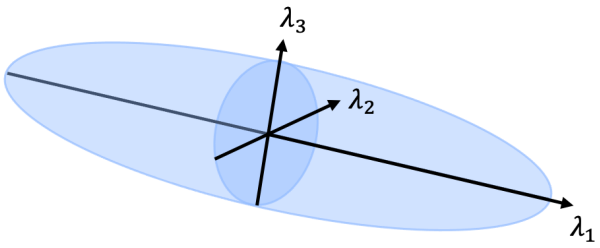

Figure 2.8 Diffusion tensor model: Three eigenvectors and the corresponding eigenvalues (λ_1, λ_2, λ_3) quantify the water diffusion in three orthogonal axes of the diffusion ellipsoid in each voxel. The principal eigenvalue λ_1, measures the diffusion along the tract, whereas the eigenvalues λ_2 and λ_3 describes how uniform the radial diffusion is. Adapted from (Alexander *et al.*, 2007).

The eigenvalues from the tensor are used to calculate the fractional anisotropy (FA), which quantifies the dominance of the principal eigenvalue along the axons' main axis. FA values range from 0 to 1, where 0 represents isotropic diffusion, or lack of anisotropic displacement, and 1 represents a high degree of anisotropic diffusion. Thus, lower FA values are typically assumed to reflect decreased white matter integrity, which is usually due to an underlying disease. On the other hand, mean diffusivity (MD) is the average of the three diffusion

tensor eigenvalues, quantifying the average rate of diffusion within each voxel. A higher MD generally indicates loss or expansion of white matter tracts. Therefore, the utilization of measures derived from DTI scans in Chapter 6 enables a comprehensive exploration of microstructural changes within white matter tracts, offering valuable insights into underlying brain alterations.

2.6 Treatments in epilepsy

As discussed earlier, ASMs are the primary line of treatment for PWE. Typically, the prescription of ASMs is determined by factors such as the characteristics of the seizures, their frequency, and a careful assessment of the potential benefits in improving the patient' condition weighed against any known side effects. ASMs work towards preventing seizures in individuals with epilepsy by reducing neuronal excitation. The current class of ASMs operates by modulating voltage-gated ion channels, neurotransmitter levels (e.g., GABA), and synaptic activation. For individuals who do not respond favourably to ASMs, alternative treatments may be considered, with the choice tailored to each case. These alternatives include dietary therapies, resective surgery and neurostimulation. Several dietary approaches, altering the body's energy source, show efficacy in epilepsy treatment. Of these therapies, the ketogenic diet which is based on a high-fat, low-carbohydrate, and adequate protein intake is most popular. While the ketogenic diet shows promise as a therapy for epilepsy, its effectiveness may vary, suggesting it may not be universally effective for everyone.

Resection surgery entails the removal of brain tissue suspected to be the source of seizures. For instance, in cases of mesial temporal lobe epilepsy (MTLE) resistant to ASMs, resection procedures such as selective temporal, amygdalo-hippocampectomy, lesionectomy or corticectomy are considered. (Wieser, 1988; Clusmann *et al.*, 2002; Jobst and Cascino, 2015). While these procedures are successful for most cases, it is essential that these patients undergo regular medical check-ups to monitor pathological progression.

For those patients ineligible for surgery, neurostimulation techniques like vagus nerve stimulation present a viable option, where an electronic device with electrodes are implanted to stimulate the vagus nerve (Handforth *et al.*, 1998). This stimulation aims to modulate norepinephrine levels or trigger the release of anticonvulsant neurochemicals in potential epileptogenic regions. In summary, these diverse treatment modalities offer hope and improved quality of life for PWE, emphasizing the importance of personalized care and identifying candidates for the alternate treatments during diagnosis.

2.7 Mechanisms and features of ASM resistance

As the occurrence of seizures is an intermittent phenomenon, the period of being classified as seizure-free needs to be defined clearly in order to aid clinicians and researchers in accurately categorizing patients. We therefore first define ASM resistance in epilepsy as per the ILAE.

2.7.1 Defining ASM resistance in epilepsy

Resistance to ASMs is defined by the ILAE as the failure to achieve 'substantial' (discussed below) seizure freedom from adequate trials of two tolerated, appropriately chosen and clinically used drug schedules (Kwan, Arzimanoglou, *et al.*, 2010). The criteria that was set out is summarised in Table 2.1, follows a hierarchical order where: Level 1 defines a standard measure of characterising a patient as seizure-free following therapeutic intervention, along with the minimum information required of the intervention; Level 2 provides the definition for treatment failure, and is based on the response from Level 1; Level 3 are for those patients who's ASM response is unknown (Kwan, Arzimanoglou, *et al.*, 2010). Each of the three levels are further sub-classified based on the occurrence of adverse effects.

Level 1 defines substantial seizure-free period as the period that is at least three times the longest inter-seizure interval experienced by the patient prior to starting the treatment (Kwan, Arzimanoglou, *et al.*, 2010). In consensus the

seizure-free period is considered to be at least 12 months after commencing treatments. Treatment failure is defined based on recurrent seizure(s) after the intervention has been adequately (strength of dose and intervention duration) applied.

Table 2.1 Categorisation criteria for drug resistance: Level 1 evaluates the presence of seizures after administering ASMs, and Level 2 defines treatment failure. Each level is sub-classified into A, B and C based on occurrence of adverse effects. Reproduced from (Kwan, Arzimanoglou, et al., 2010).

Outcome dimension[a]		
Seizure control	Occurrence of adverse effects	Outcome category
1. Seizure-free	A. No	1A
	B. Yes	1B
	C. Undetermined	1C
2. Treatment failure	A. No	2A
	B. Yes	2B
	C. Undetermined	2C
3. Undetermined	A. No	3A
	B. Yes	3B
	C. Undetermined	3C

[a]See text for definitions of "seizure-free," "treatment failure," and "undetermined." The numeric and alphabetic nomenclature of categories does not imply gradation or hierarchy.

Furthermore, the intervention must also be applied appropriately (sufficient dosage) to be considered for categorisation in Level 1 or Level 2. If the previous two conditions are not met, then the outcome is categorised as undetermined in Level 3. Similarly, if the patient drops out before the seizure-free assessment period is complete, or an incorrect dose of an ASM known to be effective was administered, then the patient being evaluated is classified as undetermined (Level 3) for that ASM. Understanding the factors contributing to resistance to ASMs is crucial for tailoring effective therapeutic strategies.

2.7.2 Patterns and mechanisms of resistance to ASMs

Resistance to ASMs can arise at multiple stages of treatments and may follow one of these patterns: 1) de novo (or ab initio) ASM resistance, which is when

the patient never achieves seizure freedom upon commencing treatments; 2) delayed resistance, where the ASMs are initially effective but after some time period (several years) seizures recur and become uncontrolled; 3) a fluctuating pattern of being effective for set time periods (>2 years) and incurring seizures in-between; or 4) the ASMs are not effective initially but are able to control the seizures after some time period (Schmidt and Löscher, 2005). Of these, the de novo pattern is most common among patients and indicates that the condition is present even before the first ASM is administered (Camfield *et al.*, 1997; Kwan and Brodie, 2001; Berg, 2004).

Resistance to ASMs can stem from various factors, including damage to the neural network, which hampers ASM accessibility to their targets, as well as alterations in neurotransmitter receptor properties or other ASM targets. (Tang, Hartz and Bauer, 2017). These mechanisms may contribute to the severity of epilepsy and also exacerbate resistance to ASMs.

2.7.3 Clinical features linked to ASM resistance

Although currently there is no dedicated protocol in the clinic to identify resistance to ASMs at the time of epilepsy diagnosis, some guidance on the ASM efficacy can be made based on some of the clinical features which are commonly recorded during diagnosis and treatment follow-ups. Of these, several studies have reported resistance to ASMs in patients with structural abnormalities on MRI scan, younger age of onset, symptomatic epilepsy and focal epilepsy with lesions, high frequency of tonic-clonic seizures, and failure to control seizures from the first ASM regime prescribed (Johnson *et al.*, 2003; Bonnett *et al.*, 2014; Assenza, 2020; Flores-Sobrecueva *et al.*, 2020). The abnormalities reported by Flores-Sobrecueva *et al.*, (2020) were hippocampal sclerosis and calcific neurocysticercosis lesions (CNLs) in the brain. However, the causal link between CNLs and ASM resistance are yet to be identified (Rathore *et al.*, 2013). Other clinical features derived from the attendance to medical care facilities, past medical prescriptions or patient' age are also reported to predict the response of ASMs (An *et al.*, 2018).

The clinical indicators of ASM resistance discussed so far were from studies that ran for a few years, but were much less than a decade. Therefore, to understand predictors that lead to resistance over an extended time period, Chen *et al.*, (2018) evaluated risks factors of resistance to ASMs in patients with epilepsy over a 30-year period. Their study observed that the history of recreational drug use and 'higher seizure frequency' prior to treatment were predictors of resistance to ASMs. Though the association of recreational drugs with resistance to ASMs is not established, one can speculate on structural changes in the brain caused in long term drug users (Hitiris *et al.*, 2007; Yuan *et al.*, 2009; Li *et al.*, 2014; Seifert *et al.*, 2015). The 'higher seizure frequency' could simply indicate the effect of the pathology as per the intrinsic hypothesis of ASM resistance, rather than an independent cause (Rogawski and Johnson, 2008; Rogawski, 2013).

Furthermore, several studies have also identified resistance to ASMs in a subset of patients with comorbidities such as neuropsychiatric disorders, epilepsy in the family, prolonged febrile seizure and distinct EEG patterns (Hitiris *et al.*, 2007; Xue-Ping *et al.*, 2019). The distinct EEG patterns in patients resistant to ASMs were 'diffuse slowing', greater asymmetries and asynchronous waveforms, as well as distinctive epileptiform discharges (Ko and Holmes, 1999; Wirrell *et al.*, 2012). Lastly, the mechanisms that lead to resistance to ASMs in conjunction with neuropsychiatric disorders, epilepsy in the family and febrile seizure are yet to be established (Hitiris *et al.*, 2007). In summary, while numerous studies have investigated various clinical variables in an effort to differentiate patients resistant to ASMs, a definitive solution has yet to be found.

2.8 Role of neuroimaging in identifying ASM resistant patients

As we've observed, neuroimaging methods can highlight epileptogenic regions within brain networks, as well as those regions affected by the ASM resistant pathology (Koepp and Woermann, 2005; Duncan, 2010; Bernhardt *et al.*, 2011; Bonilha *et al.*, 2014). Here, we delve into other neuroimaging techniques that have been employed in previous research to investigate distinctive lesions, as

well as structural or functional changes in the brain commonly observed in patients resistant to ASMs.

The positron emission tomography (PET) is a useful tool that can investigate changes in uptake of specific molecules in the brain. Using this approach, several studies have used PET scans to identify patients associated with changes in ASMs' target (Löscher and Potschka, 2005; Shin *et al.*, 2016). Images acquired from PET scans are usually co-registered with a MRI scan, as we cannot see anatomic details on the PET image. Co-registration plays a crucial role in pinpointing the concentration of specific molecular uptake within individual brain regions. Using PET imaging, several studies have detected an increased expression or function of the drug efflux transporter Pgp using [^{11}C]-verapamil in patients resistant to ASMs. (Löscher and Potschka, 2005; Shin *et al.*, 2016). Here, [^{11}C]-verapamil is a tracer that binds to Pgp. This increased Pgp concentrations is detected at the BBB, as well as the epileptogenic focus and is believed to lower ASMs' concentration in the brain networks.

Furthermore, the Blood Oxygen Level Dependent (BOLD) functional MRI (fMRI) also provides a means to explore various functional mechanisms of the brain. The BOLD signal, measured in fMRI, acts as an indicator of neural activity by reflecting changes in blood flow associated with activated neurons (Glover, 2011). A notable study by Szaflarski et al. (2013) compared groups of patients diagnosed with IGE that were either resistant or responsive to sodium valproate using resting state fMRI and EEG data. Their study also reported that the GSW generators seen on EEGs were concurrent with abnormality detected in the fMRI data. In patients resistant to sodium valproate, these abnormalities were widespread across various brain regions, including the medial frontal cortex, paracingulate gyrus, and bilateral anterior insula.

Within the mechanisms related to the changes in ASM target, seizures can specifically result from disruptions in GABA levels. A crucial player in this disruption process is glutamic acid decarboxylase (GAD) enzyme that is responsible for the decarboxylation of glutamate to GABA and carbon dioxide. Contrary to this knowledge, high levels of glutamic acid decarboxylase antibodies (GAD-ab) that work against GAD are reported to be prevalent in

about 10% of patients with MTLE who are resistant to ASMs (Giometto *et al.*, 1998; Peltola *et al.*, 2000; Sokol *et al.*, 2004; McKnight *et al.*, 2005; Falip *et al.*, 2012; Iorio *et al.*, 2015; Malter *et al.*, 2015).

The study by Iorio *et al.*, (2015) suggested that such patients with increased levels of GAD-ab can be identified from distinct T2W-hyperintense lesions on MRI scans and immunoglobulin levels in the CSF. Their study also provided evidence of a significant (>50%) reduction in seizure frequency among these patients when incorporating immunoglobulin G (IgG) into the treatment regimen. However, the exact mechanism by which GAD-ab influences treatment responsiveness is complex and may involve multiple factors. Therefore, the presence of elevated GAD-ab alone does not necessarily determine whether a patient will be responsive or resistant to ASMs. In order to translate these findings for clinical use, additional research and clinical studies are needed to fully understand the relationship between GAD-ab levels and the effectiveness of ASMs. In summary, previous research studies have helped us understand that resistant to ASMs is a complex process and have multiple factors or phenotypic traits that may be detected by neuroimaging methods.

2.9 Investigating the link between facial asymmetry and structural changes in the brain in epilepsy

A study by Chinthapalli *et al.*, (2012) reported a subset of PWE, particularly those detected with pathogenic structural variants exceeding 1 Mb or present in specific regions of the genome linked to epilepsy, exhibit subtle asymmetrical facial features compared to individuals lacking such variants. Moreover, their study found that facial asymmetry observed in these PWE was independent of factors like facial injury, intellectual disability, drug history among other patients analysed within the cohort. Additionally, our collaborators, Balestrini *et al.*, (2021), showed that facial asymmetry is prominent in people with lateralised focal epilepsies compared to people with IGE or controls without epilepsy.

However, the mechanisms underlying facial asymmetry and its link to structural changes in the brain remain poorly understood.

Furthermore, focal epilepsies discussed so far are considered to have network alterations in regions of the hemisphere ipsilateral to the seizure onset, whilst generalized epilepsies are considered to have bi-hemispheric network changes. We have also discussed epilepsies as a neurodevelopmental disease, with early changes in the brain underpinning seizure biology. As the development of the structure of the face is influenced by interactions in the developing forebrain, we hypothesize that facial asymmetry is associated with factors contributing to structural changes in the brain in PWE.

As outlined in Section 2.8, various neuroimaging methods have been utilized to study distinctive lesions, structural or functional changes in the brain commonly reported in PWE. Nonetheless, T1W MRI stands out as one of the most accessible neuroimaging modalities, offering a broad array of tools for pre-processing the brain scans. In our study, we utilized FreeSurfer to segment the MRI scans and extract regional brain measurements, a process detailed in Section 4.2.3.

Chapter 4 focuses on utilizing these regional brain measurements from T1W MRI scans to investigate whether people with lateralised focal epilepsies (i.e., asymmetric network changes) have an increased degree of facial asymmetry compared with people with generalized epilepsies or controls without epilepsy. This investigation will improve our understanding whether there is a shared pathology between the mechanisms responsible for phenotypic traits of facial asymmetry and those underlying lateralized structural changes in the brains of PWE.

2.10 Investigation of progressive changes in the brain in epilepsy

Structural changes in grey matter and white matter tracts of the brain have been documented in people with both focal and generalized epilepsies compared to healthy controls (Bernasconi, Natsume and Bernasconi, 2005; Bernhardt *et al.*,

2010; Coan and Cendes, 2013; Kim, 2017; Whelan *et al.*, 2018; Buksakowska *et al.*, 2019; Hatton *et al.*, 2020). It is noteworthy that these structural changes are detected in both ASM-resistant patients and those with well-controlled seizures (Bernhardt, Kim and Bernasconi, 2013; Asadi-Pooya *et al.*, 2016; Chipaux *et al.*, 2016; Kuzmanovski *et al.*, 2016). Understanding the progression of these structural changes in the brain is crucial as it may provide insights on clinical variables such as treatment outcomes or seizure type.

In an effort to unravel this progression of structural changes, Galovic *et al.*, (2019) investigated a longitudinal dataset of T1W MRI scans taken at least six months apart from people with focal epilepsy. Their findings revealed that the annualized rate of atrophy within brain regions structurally connected to the ipsilateral hippocampus exceeded the rate associated with healthy aging. Subsequent work by Galovic *et al.*, (2020) showed that resective surgery prevents further structural changes in the brain. While these previous studies demonstrated the progressive nature of the structural changes, their approach did not address whether there is an explicit sequence in which they occur in or whether this sequence can be used to stage epilepsy. Moreover, lower hippocampal volume has been reported in non-affected siblings and thus may reflect a genetic origin, (Kobayashi *et al.*, 2002; Tsai *et al.*, 2013; Vaughan *et al.*, 2017; Long *et al.*, 2020) predating any further changes such as cortical thinning, which was not observed in siblings (Alhusaini *et al.*, 2019). However, progress on deciphering how grey matter reductions unfold over time in epilepsy has been limited by the scarcity of longitudinal imaging cohorts.

Therefore, our objective is to first investigate whether structural changes in the brain in patients with MTLE-HS follow a distinct progression pattern using available cross-sectional data. This will be investigated by implementing the event-based modelling (EBM) in **Error! Reference source not found.** that infers a temporal progression of structural changes in the brain from cross-sectional data (Fonteijn *et al.*, 2012). For detailed insight into the EBM algorithm, please refer to Section 3.4.1. We will estimate the progression sequence based on regional brain measurements obtained from T1W MRI scans sourced from the ENIGMA-Epilepsy cohort (Whelan *et al.*, 2018).

Subsequently, we broaden the scope of uncovering disease progression of structural brain changes to a broader population of PWE using the Subtype and Stage Inference (SuStaIn) algorithm (Young *et al.*, 2018). SuStaIn, an extension of the EBM, identifies unique imaging-derived subtypes of diseases in the brain based on the unique progression of structural changes in the brain, a process detailed in Section 3.5. Previously, SuStaIn has been applied to model disease progression in Alzheimer's disease (AD) using features derived from a range of neuroimaging techniques, including T1W MRI (Young *et al.*, 2018), as well as PET and neuropathology data (Aksman *et al.*, 2023). The application of SuStaIn in multiple sclerosis uncovered subtypes where progression was led by cortical regions, white matter tracts, or lesions in the brain (Eshaghi *et al.*, 2021). Importantly, this study by Eshaghi *et al.*, (2021) identified clinical implications linked to these data-driven subtypes: subtype assignment predicted the progression of disability in MS patients as well as their treatment response.

Moreover, a recent study by Xiao *et al.,* (2022) used the SuStaIn algorithm to identify imaging-derived subtypes of epilepsy based on the progression of changes in grey matter regions in PWE. Their findings revealed a Hippocampal subtype for focal epilepsies, and Cortical and Basal Ganglia-led subtypes that were common in both focal and generalized epilepsy syndromes. This study by Xiao *et al.,* (2022) also reported most people (75%) in the limbic-led subtype had at least weekly seizures compared to 50% of PWE in the cortical and basal ganglia-led subtypes. However, the sequential changes in grey and white matter over time across epilepsy syndromes are not yet been explored in a single analysis due to the poor availability of longitudinal data. Uncovering this sequence would provide insights into the complex interaction between changes in grey matter and white matter tracts in epilepsy.

Here, we also use measures derived from DTI scans, as described in Section 2.5.1.2, which are used to quantify changes in white matter tracts. DTI has proven particularly valuable in tracking microstructural changes in people with non-lesional temporal lobe epilepsy (NL-TLE), with previous studies documenting changes in the ipsilateral uncinate and arcuate fasciculus

(Govindan *et al.*, 2008; Ahmadi *et al.*, 2009; Concha *et al.*, 2009). We therefore use the SuStaIn algorithm in Chapter 6 to investigate imaging-derived subtypes based on changes in changes in grey matter regions detected from T1W MRI and white matter tracts quantified from DTI scans from a cohort of common epilepsies facilitated by the ENIGMA-Epilepsy group.

Chapter 3 Machine learning techniques

3.1 Introduction to machine learning techniques

Machine learning techniques play a pivotal role in the analysis of medical imaging data among other applications. These methods are utilized to extract features that offer insights into disease pathology, adjust for confounding effects (such as age and sex), and categorize subjects as either having a disease or being in a healthy state. Over the past years several machine learning methods have been employed to extract features from neuroimaging that display a quantitative change linked to epilepsy (Petrovski *et al.*, 2010; Cantor-Rivera *et al.*, 2015; Takahashi *et al.*, 2020; Croce *et al.*, 2021; Drenthen *et al.*, 2021). Broadly speaking machine learning methods can be supervised or unsupervised. In supervised machine learning methods, an algorithm investigates the relationship or function between a set of observations (features) and some response variable (labels). This learned function can then be employed to make predictions on new, unseen data. Conversely, unsupervised methods operate without using labelled response variables, instead focusing on uncovering patterns or associations within the data itself.

Examples of supervised learning methods include the random forest and regression algorithms. These models are trained on labelled data to make predictions or infer relationships between features and responses. In contrast, K-Means is a widely used unsupervised method that clusters data into K distinct groups based on similarities in feature space, without the need for labelled responses.

When choosing a machine learning model, it's crucial to consider whether the response variable is continuous or categorical. Linear regression is suitable for datasets with continuous response variables, while logistic regression is more appropriate for datasets with categorical responses. Further details on these methods are provided in Section 3.2 and Section 3.3 respectively. In our analysis, we utilize the linear regression algorithm in **Error! Reference source**

not found., to remove confounding effects from regional brain measures. Conversely, logistic regression was chosen for classifying treatment outcomes in Chapter 6. In addition, regression-based techniques are prevalent in data analysis, and can easily be fine-tuned with regularization to minimize the prediction error.

In order to assess the generalizability of a model for any application, it's crucial to evaluate its performance on new out-of-sample data. One effective method for achieving this is k-fold cross-validation, which involves dividing the data into k subsets. The algorithm then iteratively holds out one of the subsets as the testing set, while the remaining form the training set. The prediction error is then computed based on the testing set. Similarly, in the next iteration, a new subset previously used in the training set is considered as the test set, and the previous test subset becomes part of the training set. The error is then averaged over all iterations to estimate the model's performance for real-world application. The cross-validation algorithm was used in several instances across the research reported here. For instance, in Chapter 6, it was utilized to determine the optimal number of imaging-derived subtypes in SuStaIn, that best described the given dataset.

3.2 Linear regression for continuous variables

3.2.1 Ordinary least squares (OLS)

The regression models commonly used for medical data analysis include the ordinary least squares (OLS) regression, Ridge regression and least absolute shrinkage and selection operator (LASSO) regression. These regression models assumes that the response is a linear combination of the input variables (Stigler, 1981). The coefficients (slopes and intercept) of their linear projections are estimated, such that the sum of squared difference between prediction and actual response is minimized on the training data. This is illustrated in Figure 3.1 for a single predictor or feature x_1 and response y with n samples.

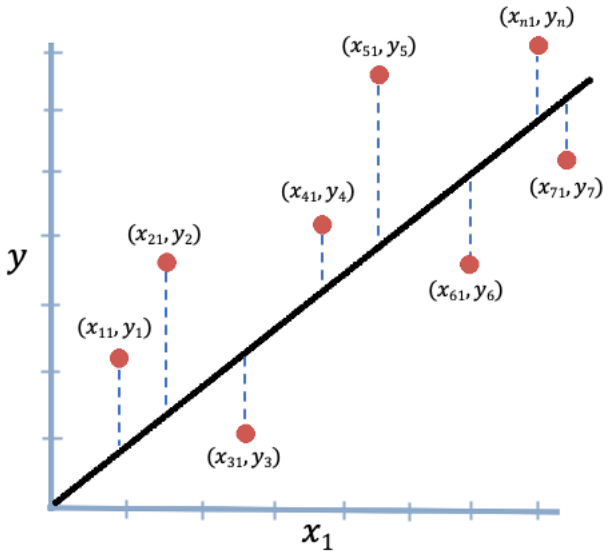

Figure 3.1 OLS regression estimation: The figure shows the OLS model built based on the linear projection between feature x_1 and response y. A new input on x_1 will predict the corresponding y from this (projection) regression line.

If we expand the number of predictors as $x_1, x_2 \ldots x_p$ where p is the total number of predictors, the linear regression (projection) of y can be represented by

$$y = \beta_0 + \sum_{j=1}^{p} \beta_j x_j + \varepsilon \qquad \text{Eq. 3.1}$$

OR $$\hat{y} = \hat{\beta}_0 + \sum_{j=1}^{p} \hat{\beta}_j x_j \qquad \text{Eq. 3.2}$$

Where β_0 is the y-intercept of the regression entity (line for 2D, plane for 3D or higher dimensions) projected, and β_j terms are the slopes or coefficients of each of the features considered in a model (Hastie et al., 2008). ε is the error term that represents the difference between y and $\hat{y}$. This error accounts for measurement noise and natural variations. The $\hat{\beta}$ are estimates of the 'true' β from the training data, and $\hat{y}$ are the estimated or predicted values. The equations and derivations

presented in this text are extracted from the sources referenced here (Stigler, 1981; T. Hastie, R. Tibshirani, 2008).

If we have n number of samples of the response $\hat{y}_i$ where $i = 1, 2 \ldots n$, the OLS regression is obtained by minimising the residual sum of squares (RSS) of the actual y_i and estimated responses $\hat{y}_i$, where we pick the coefficients β_j for each of x_{ij} $(j = 1, 2 \ldots p)$. The $RSS(\beta)$ below is a vector containing all β_0 to β_p.

$$RSS(\beta) = \sum_{i=1}^{n} (y_i - \hat{y}_i)^2 \qquad \text{Eq. 3.3}$$

$$\therefore\ RSS(\beta) = \sum_{i=1}^{n} (y_i - (\beta_0 + \sum_{j=1}^{p} \beta_j x_{ij}))^2 \qquad \text{Eq. 3.4}$$

As we are interested in finding the minimum value for RSS, we can differentiate Eq. 3.4 w.r.t β_0 and equate to 0 we get

$$\therefore\ RSS(\beta)_{min} = \hat{\beta} = \frac{\sum_{i=1}^{n} (x_i - \bar{x})(y_i - \bar{y})}{\sum_{i=1}^{n} (x_i - \bar{x})^2} \qquad \text{Eq. 3.5}$$

Where $\bar{x}$ and $\bar{y}$ is the mean of individual features and their response values, respectively.

We used OLS to statistically adjust features for the effects of covariates like age, sex and intracranial volume (ICV). It is important that number of samples n is greater than predictors p for estimating the regression solution. This is because when the number of predictors $p>n$, the inverse of $X X^T$ cannot be computed. In addition, while the model' performance is optimised with the lowest RSS, it does not distinguish informative features versus features independent of the response. The OLS is therefore considered as an unbiased algorithm. However, for machine learning applications, it is often required to distinguish informative versus non-informative features. We can address this issue by penalising and eliminating features that do not contribute towards the response variable. The Ridge and LASSO regression are the two main types of penalised regression discussed below.

3.2.2 Optimizing OLS and feature selection using Ridge and LASSO

The penalised/regularized regression, namely Ridge (L2 norm) (Hoerl and Kennard, 1970) and LASSO (L1 norm) (Tibshirani, 1996) creates a linear regression model along with a regularisation parameter that punishes features that are not informative of the response variable. This is achieved by applying a constraint on the RSS solutions as discussed below.

The Ridge regression can be represented as an extension of OLS such that

$$\hat{\beta}^{Ridge} = argmin_{\beta} \left\{ \sum_{i=1}^{n} (y_i - \beta_0 - \sum_{j=1}^{p} x_{ij}\, \beta_j)^2 + \lambda \sum_{j=1}^{p} {\beta_j}^2 \right\} \quad \text{Eq. 3.6}$$

Where $\lambda \geq 0$ is called the complexity (regularisation) parameter as it controls the amount of shrinkage against the corresponding RSS function. Thus, higher the value of λ greater the amount of shrinkage. We can express the Ridge problem as

We can rewrite Eq. 3.6 in matrix form

$$RSS^{Ridge}(\lambda) = (y - X\beta)^T (y - X\beta) + \lambda \beta^T \beta \quad \text{Eq. 3.7}$$

Where X is the matrix of nxp rather than (p+1). Differentiating Eq. 3.7 w.r.t β we get the optimum $\hat{\beta}^{Ridge}$ as

$$\hat{\beta}^{Ridge} = (X^T X + \lambda I)^{-1} X^T y \quad \text{Eq. 3.8}$$

Here I is the identity matrix of dimensions pxp, and therefore solves the OLS problem of computing the inverse of $X^T X$ in cases of p>n. The Ridge regression does not eliminate features. We can use LASSO regression to achieve this while optimising RSS.

The other penalised regression is the LASSO regression, which is similar to Ridge regression. However, instead of taking the square of the coefficients we use their magnitudes to constrain the RSS function. Thus, we have

$$\hat{\beta}^{Lasso} = argmin_{\beta} \left\{ \sum_{i=1}^{n} (y_i - \beta_0 - \sum_{j=1}^{p} x_{ij}\, \beta_j)^2 + \lambda \sum_{j=1}^{p} |\beta_j|^q \right\} \quad \text{Eq. 3.9}$$

Where $q > 0$. In the case of LASSO q=1, and for Ridge regression q=2. We can express the regularisation of L1 norm as

$$||\beta||_1 = \sqrt{\sum_{j=1}^{p} |\beta_j|}$$

Where $||\beta||_1$ is the LASSO regression or L1 norm. The $|\beta_j|$ term is not differentiable at $\beta_j = 0$, which complicates finding the solution to this optimization problem. We therefore use iterative optimization algorithms embedded in software packages that solves Eq. 3.9 up to some acceptable accuracy.

In graphical form, the Ridge and LASSO regression can be illustrated as in Figure 3.2. As shown in the figure, in the Ridge regression the coefficient values of the predictor whose contribution to the response is not substantial are shrunk close to zero (β_2 in this case), while in LASSO the coefficient values are set to zero. Hence, LASSO regression is best suited for tackling feature selection tasks, where the least contributing predictors are eliminated completely.

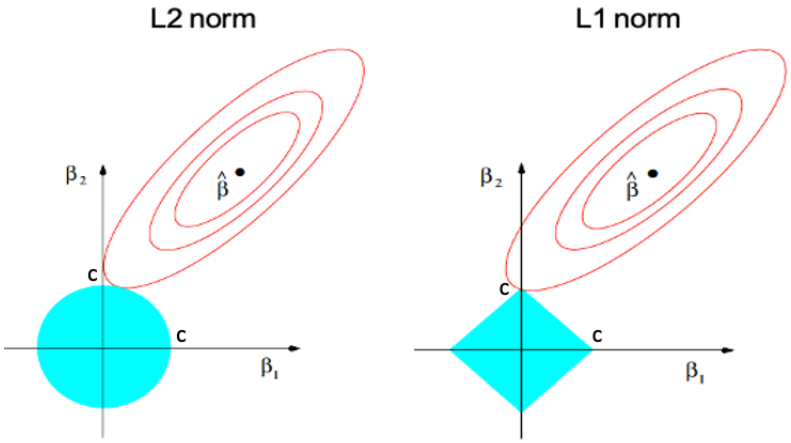

Figure 3.2 Regularization in L2 and L1 norms: The blue areas represent the constraint regions of the regularisation norms, whereas red ellipses are contours of the RSS for a set of βs. Here the RSS contours touch $\beta_1^2 + \beta_2^2 \leq$ c and $|\beta_1| + |\beta_2| \leq$ c close to zero and exactly zero at β_2, for the L2 and L1 norm respectively. Reproduced from (Hastie et al., 2008).

In order to acquire the best performing model corresponding to the optimal λ, we usually split the dataset into a training and test set and apply a series of λ values to the algorithm. The model's performance on the train set and test set are evaluated with a measurement such as 'Mean Square Error (MSE)' given below.

$$MSE = \frac{1}{n}\sum_{i=1}^{n}(y_i - \hat{y}_i)^2 \qquad \text{Eq. 3.10}$$

y_i is the actual response and $\hat{y}_i$ is the response predicted by the regression model. The model' parameter λ, is first optimised by applying the k-fold cross-validation on the training set of the data. During cross-validation, λ of the best average MSE of the k-fold test set is selected. The models' performance is then validated on the test dataset separated earlier, that was not used in the λ optimising process. The LASSO regression model utilized in Chapter 4 for identifying features associated with facial asymmetry in PWE, incorporated the use of MSE to estimate the best value of λ for optimal model performance on the given dataset.

3.3 Logistic regression for classification analysis

The regression methods described so far are mainly used for continuous response variables but face limitations for modelling discrete variables because they rely on applying linear projections to capture non-linear relationships. To overcome this, we use logistic regression which employs a sigmoid function to estimate probabilities of the response (outcomes) as shown in Figure 3.3 (Hastie et al., 2008).

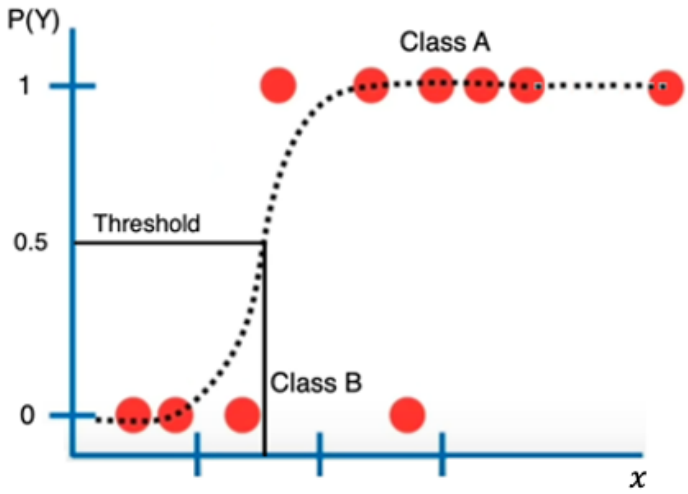

Figure 3.3 Logistic regression estimation: A sigmoid function provides a reliable estimation for classifying outcomes. Here for input variable x, the probability of the response Y in Class A ranges 0-1. The threshold typically from a point of 0.5 from the probability axis P(Y) projected on the sigmoid function assigns the class of each data point.

Here, for simplicity we have considered a variable response with two possible classes: class A and class B. The sigmoid shown in the figure acts as the decision curve, which is estimated by maximum likelihood, a statistical technique further described in Section 3.4.2.1. The projection of each datapoint onto the sigmoid determines the probability of belonging to one of the classes. Thus, the datapoints are classified into one of the classes from the response variable. Similar to linear regression, a regularisation term can be added with the

maximum likelihood to penalise features that are not informative of the response.

3.3.1 Evaluating the performance of classification models

While designing a classification model for any dataset, features' datapoint tend to overlap among the different response variables, and therefore inevitably some of the datapoints will be misclassified. Thus, in order to find the classifiers' optimal threshold and evaluate performance, we use the Receiver Operator Characteristic (ROC) graph shown Figure 3.4. The area under the curve (AUC) is simply a measure on how well the classes are separatable based on the classifier' prediction.

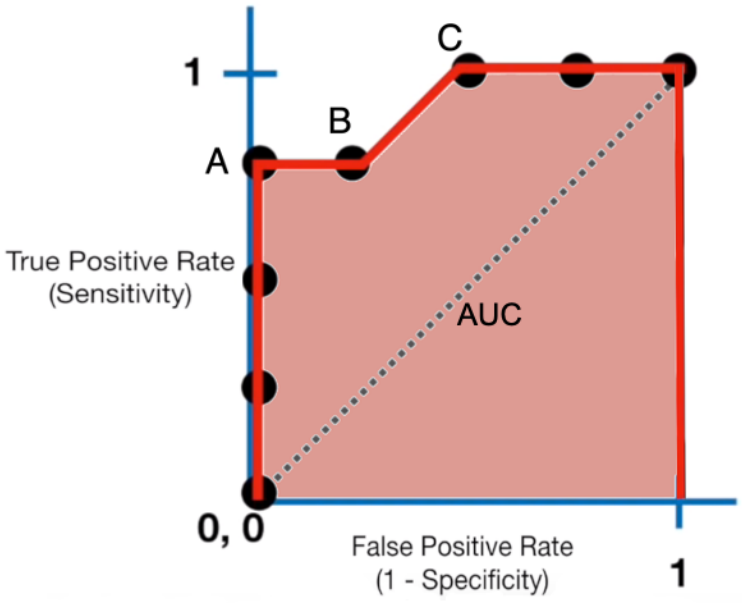

Figure 3.4 ROC-AUC graph for logistic regression: The ROC graph illustrates the true positive (TP) rate and false positive (FP) rate encountered by the model with the corresponding threshold. Here, point A has the highest TP rate at 0 FP rate while point C is the lowest FP rate at the highest TP rate. Point B achieves the same TP as A, but increases FP and therefore not considered an optimal threshold. AUC values can be 1 for best performance and 0.5 for random predictions. Adapted from (Zhu, Zeng and Wang, 2010).

To graph the ROC, we define the sensitivity as a ratio of true positive (TP) and total positives P, and specificity as a ratio of true negative (TN) and total negatives N. Table 3.1 shows the confusion matrix of the potential outcomes expected by the model, where FN and TN are false negative and true negative respectively. The TP rate and FP rate can be calculated from

$$TP\ rate = Sensitivity = \frac{TP}{P} = \frac{TP}{TP + FN}$$

$$FP\ rate = 1 - Specificity = 1 - \frac{TN}{N} = \frac{FP}{FP + TN}$$

Table 3.1 Confusion matrix of outcomes classified: Table shows the logistic regression classes predicted as positive (P) and negative (N) versus the actual class.

		Actual class	
		P	**N**
Predicted class	**P**	**TP**	FP
	N	FN	**TN**

We can also use the positive predictive value, error rate or accuracy to evaluate the model' performance. We use AUC in our analysis due to the advantage of being invariant to class-imbalances. Thus, the ROC graph and AUC values can be used to fine-tune, the logistic regression parameters of threshold, sensitivity and specificity. The AUC metric was employed in **Error! Reference source not found.** and Chapter 6 to assess the predictive power of the disease stages assigned to patients, in relation to their treatment response.

3.4 Statistical tools used in disease progression modelling

In Chapter 5, we utilize the EBM algorithm to estimate the sequence of structural changes in the brain, transitioning from normal to abnormal states, in PWE. An 'event' in this context could be hippocampal shrinkage to a certain

degree. For instance, we investigate whether the amygdala or the hippocampus shrinks first in PWE. The EBM algorithm can estimate this sequence from cross-sectional data, providing insights into disease progression over time. The estimated order of events is optimised using the Markov Chain Monte Carlo (MCMC) sampling algorithm discussed in Section 3.4.1. Furthermore, the probability in which the brain measure of a patient transitions from normal to abnormal is estimated using mixture models which are discussed in Section 3.4.2.

3.4.1 The Event-based model architecture

The overview of the EBM algorithm is depicted in Figure 3.5. The MCMC algorithm is the central component of the EBM, which plays a crucial role in determining the order of features that transition from normal to abnormal, such that the estimated order best explains our observed data. Here we assume the sequence of brain measures becoming abnormal cannot revert to a state where the brain measures are considered as normal. The Markov Chain also assumes that the future event state is independent of the past, given the present (Chung, 1967). In the EBM algorithm, we define a discreet set of random events that correspond to each feature becoming abnormal: $E_1, E_2 \dots E_k$ as a Markov Chain with k number of events. The Markov Chain is a system where an event moves consecutively to the next event, and the future event does not depend on the previous events.

We can express the sequence ordering that we aim to estimate as $\bar{S}$=(s(1), s(2)…s(k)). If for each feature, we have n subjects of patients and controls, and we have independent measurements X, then the likelihood of subject j at position t for a sequence S is

$$P(X_j|S,t) = \prod_{i=1}^{t} P(x_{ji}\,|E_{s(i)}) \prod_{i=t+1}^{k} P(x_{ji}\,|\neg E_{s(i)}) \qquad \text{Eq. 3.13}$$

Where at position t, events $E_{s(i)}$ representing structural changes in brain region 1,…,t have occurred, whereas events $E_{s(i)}$ t+1,…,k have not yet occurred, for the current sequence S. Subject j can belong to an alternative event across events $t = 0,\ldots,k$, where at $t = 0$, none of the events have occurred. We can reduce the unknown variable t in Eq. 3.13, by defining the equivalent posterior probability $P(X_j|S)$, for all possible events $t = 0,\ldots,k$, such that

$$P(X_j|S) = \sum_{t=0}^{k} P(t)P(X_j|S,t) \qquad \text{Eq. 3.14}$$

Where $P(t)$ is the prior probability of subject being at point t for subject j. Therefore, for all n subjects we can write

$$P(X|S) = \prod_{j=1}^{n} P(X_j\,|S) \qquad \text{Eq. 3.15}$$

Substituting Eq. 3.13 and Eq. 3.14 in Eq. 3.15 we get

$$P(X|S) = \prod_{j=1}^{n}\left[\sum_{t=0}^{k} P(t)\left(\prod_{i=1}^{t} P(x_{js(i)}|E_{s(i)})\right)\prod_{i=t+1}^{k} P(x_{js(i)}\,|\neg E_{s(i)})\right] \qquad \text{Eq. 3.16}$$

Hence, the likelihood function $P(X|S)$, describes how well our data X is represented by the given sequence S. The EBM therefore strives to maximise this likelihood function, which corresponds to a characteristic sequence $\bar{S}$. We can then use Bayes' theorem to obtain the posterior distribution $P(S|X)$

$$P(S|X) = \frac{P(S)P(X|S)}{P(X)} \qquad \text{Eq. 3.17}$$

Here the marginal distribution is analytically intractable. We therefore use a MCMC algorithm to sample from $P(S|X)$. Monte Carlo is a method of drawing a random sample from the probability distribution, such that the random sample is an approximate representation of that distribution (Metropolis *et al.*, 1953). The MCMC is used to draw random sequences of S and determines $P(X|S)$ for

each of these. A greedy ascent (GA) algorithm is used to find the best initial sequence S which maximises $P(X|S)$, to find the desired feature sequence $\bar{S}$. Depending on the distribution of the feature' measurements, we can use a gaussian distribution or kernel density to approximate the required likelihood function. The bootstrap samples provide a robust estimate uncertainty or variation of the maximum likelihood sequence.

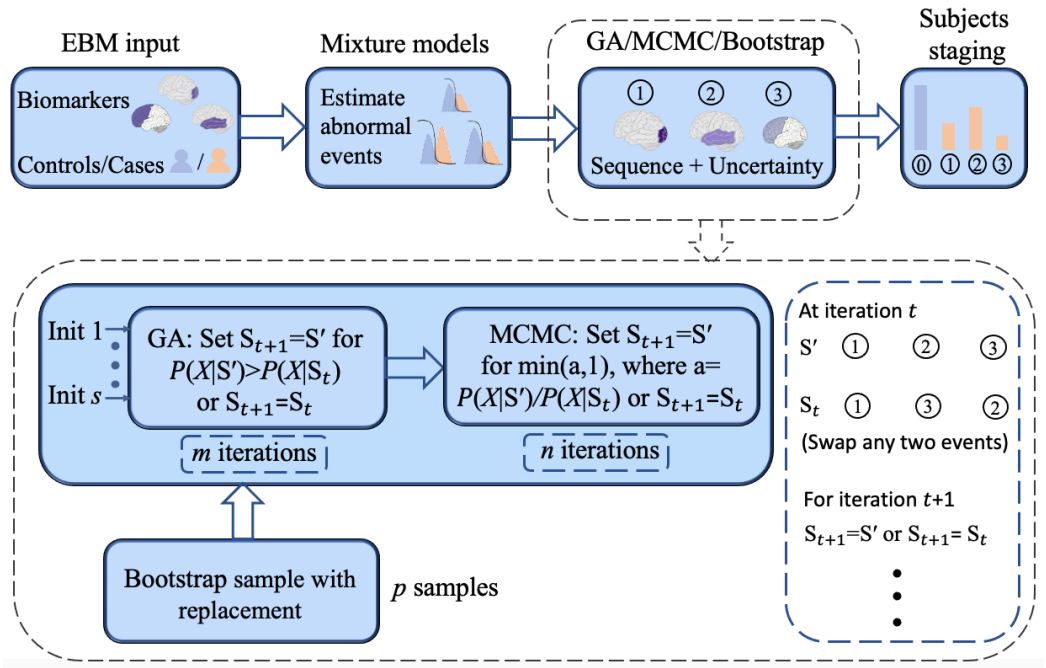

Figure 3.5 EBM architecture: Measures of brain regions from patients and controls are input into the EBM. Using mixture models and expectation-maximisation, datapoints are assigned probability values (0-1) for each of the events. A GA algorithm run for *m* iterations, which gives the best sequence for the MCMC to start on, and is repeated for s different initialisation points. MCMC procedure run for n iterations, retains S_{t+1}= S′ for a<1, thus preventing the algorithm being adhered in a local maxima state. Finally, the uncertainty of the estimated sequence is computed from variance of the MCMC iterations. A bootstrap algorithm of *p* samples of the data can be used for a robust estimate of the uncertainty. Brain region measures that best describe the sequence, are used to place subjects in their respective stages.

3.4.2 Mixture Models

3.4.2.1 Normal distributed data likelihood using maximum likelihood

For a given dataset $Z \in z_i$ with i =1,…,n, we have a probability function $P(Z|\theta)$ that represents the probability of observing datapoints of Z, given the parameters θ. Maximum Likelihood is simply the process by which we estimate parameters θ, so that observing datapoints z_1, z_2,…, z_n, (probability of $P(z_1|\theta)$, $P(z_2|\theta)$,… ,$P(z_n|\theta)$) is maximized (Fisher, 1912). For a normal distribution, θ is simply the mean (μ) and standard deviation (σ) of the dataset. We can represent the probability density function of Z as

$$z_i \sim g_\theta(Z) \qquad \text{Eq. 3.18}$$

Where θ represents one or more unknown parameters of the distribution of Z. For a normal distributed data, we use a gaussian function represented as

$$g_\theta(Z) = \frac{1}{\sqrt{2\pi\sigma}} e^{-\frac{1}{2}(z-\mu)^2/\sigma^2} \qquad \text{Eq. 3.19}$$

$$Here\ \theta = (\mu, \sigma)$$

The likelihood function can be evaluated by computing the probability observed for all datapoints. If we have n samples, we can compute this as

$$L(\theta; Z) = \prod_{i=1}^{n} g_\theta(Z) \qquad \text{Eq. 3.20}$$

To find the maximum $L(\theta; Z)$, we differentiate w.r.t θ components and equate to zero. As the derivative of log of $L(\theta; Z)$ is easier to compute we write

$$l(\theta; Z) = \sum_{i=1}^{n} l(\theta; z_i) \qquad \text{Eq. 3.21}$$

$$= \sum_{i=1}^{n} log\ g_\theta(z_i) \qquad \text{Eq. 3.22}$$

$$l(\theta; Z) = \sum_{i=1}^{n} log(\frac{1}{\sqrt{2\pi\sigma}} e^{-\frac{1}{2}(z_i - \mu)^2/\sigma^2}) \qquad \text{Eq. 3.23}$$

Solving for μ and σ we get

$$\mu = \sum_{i=1}^{n} \frac{z_i}{n} \qquad \text{Eq. 3.24}$$

And

$$\sigma = \sqrt{\frac{1}{n}\sum_{i=1}^{n}(z_i - \mu)^2} \qquad \text{Eq. 3.25}$$

The standard EBM developed by Fonteijn *et al.* (2012) uses gaussian mixtures, i.e., one gaussian representing event (abnormal) and the other non-event (normal). These are estimated using the Expectation Maximization algorithm (Dempster, Laird and Rubin, 1977) which assigns values for $P(x_{js(i)}|E_{s(i)})$ from Eq. 3.16, as shown in Figure 3.6.

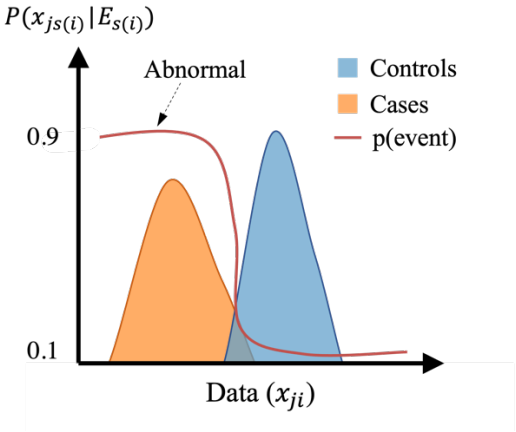

Figure 3.6 Estimate abnormal events using mixture modelling: A Expectation Maximization algorithm is used to model the brain measures as abnormal and normal. This technique assigns probability values between 0.1-0.9 of being abnormal for each subject.

3.4.2.2 Skewed or multimodal data's likelihood using kernel density

In some cases, neuroimaging data may not have a normal distribution and can be misrepresented by the maximum likelihood function we discussed in the previous section. The kernel density estimation (KDE) (Hall, 1982) is a non-parametric way to estimate a smooth likelihood function of the observed data. This is done by taking the average of kernel functions centred at each data point. The kernel function should ideally be symmetric around data point x such that $K(x) = K(-x)$, likelihood decrease away from datapoint such that $K'(x) \leq 0$ for every $x > 0$, and non-negative $K(x) \geq 0$ for every x. Normally we use a gaussian, box or triangular function, as these satisfy the above criteria. A gaussian function being used to estimate the data likelihood is shown in Figure 3.7. If we have n samples, we can represent the KDE estimate $\hat{f}(x)$ from a likelihood function $f(x)$ as

$$\hat{f}(x) = \frac{1}{nh}\sum_{i=1}^{n}\frac{(x - x_i)}{h} \qquad \text{Eq. 3.26}$$

Here h is called the bandwidth of $\hat{f}(x)$, and is used to control the width of each kernel. The mean integrated squared error (MISE) can be used to express the expected loss incurred by the choice h such that

$$MISE(h) = E\left[\int (\hat{f}(x) - f(x))^2 dx\right] \qquad \text{Eq. 3.27}$$

The optimal bandwidth h for Eq. 3.27 can be solved using Silverman's rule of thumb (Silverman, 1982) expressed in Eq. 3.28, with the assumption that the data is univariate.

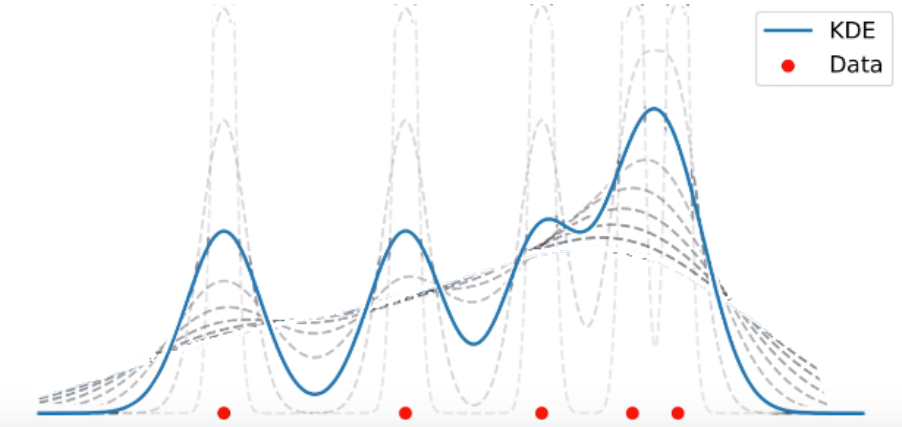

Figure 3.7 KDE for non-parametric distributions: The likelihood function is computed by taking the average of the gaussian functions imposed at each datapoint. The choice of bandwidth h determines the smoothness of the likelihood function. Here we represent probability density in blue and grey for the optimal h, and values of h higher or lower the optimal respectively.

$$h = \left(\frac{4\hat{\sigma}^5}{3n}\right)^{\frac{1}{5}} = 1.06\hat{\sigma}n^{-1/5} \qquad \text{Eq. 3.28}$$

The equation above in a nutshell is a function of sample size n, and the data spread $\hat{\sigma}$.

Often in a dataset some feature' distributions may be single skewed, and others have multiple peaks. In order to make the h value robust for long-tailed skewed distribution, as well as bimodal mixture distribution, it is better to substitute the value of $\hat{\sigma}$ with another parameter A, which is given by:

$$A = min(\hat{\sigma}, IQR/1.34) \quad \text{Eq. 3.29}$$

Where IQR is the interquartile range of the data.

The above non-parametric mixture model was first incorporated into the EBM by Firth *et al.*, (2020), and was used to determine the sequence of cortical atrophy in Alzheimer's disease patients.

3.5 The Subtyping and Staging Inference (SuStaIn) algorithm

The SuStaIn algorithm, an extension of the EBM, addresses a limitation of the EBM assumption, which assumes that all individuals follow the same sequence of structural changes in neurodegenerative diseases. SuStaIn overcomes this limitation by revealing distinct imaging-derived subtypes, each characterized by unique patterns of structural brain changes. These different sequences within each imaging-derived subtypes identified by SuStaIn, allow for a more nuanced understanding of disease progression. A basic overview of the SuStaIn algorithm architecture is shown in Figure 3.8. The progression of these changes in brain measures within each imaging-derived subtype can be elucidated through a linear z-score model, depicting a piecewise linear trajectory across a temporal space. This z-score model within SuStaIn algorithm helps uncover the gradual and continuous linear accumulation of changes in brain measures, as opposed to an abrupt transition from a normal to an abnormal level in the EBM algorithm. The equation that the SuStaIn algorithm follows can be written as

$$P(X|M) = \sum_{c=1}^{C} f_c P(X|S_c)$$

Here, the algorithm aims to maximise $P(X|M)$ which represents the probability of observing the data X for a given model M. The $P(X|S_c)$ is estimated similar to Eq. 3.16 in the EBM algorithm. The SuStaIn algorithm considers the number of image-derived subtypes C specified by the user for which it estimates the proportion of subjects f_c that belong to each subtype, and the order S_c in which brain measures reach each z-score for each subtype $c = 1 \ldots C$. We determine the optimal number of image-derived subtypes C for a particular data using cross-validation-based information criterion (CVIC) (Gelman, Hwang and Vehtari, 2014) as discussed in Section 6.2.3.

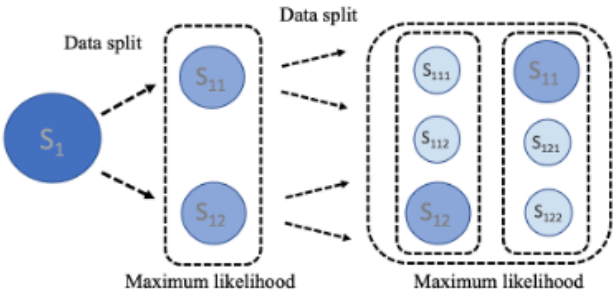

Figure 3.8 Core architecture of the SuStaIn algorithm: At first the algorithm estimates the S_1 sequence that can best describe the entire dataset using a maximum likelihood approach as described in the EBM algorithm. The algorithm then splits the dataset into two subtypes (S_{11} and S_{12}) with a random set of subjects in each subtype, then swaps patients between subtypes and retains the set that demonstrates maximum likelihood for a sequence of 'events'. Depending on the number of subtypes specified, the algorithm continues to split the newly determined subtype, into additional two subtypes as shown. Similar to the previous step, the algorithm selects the set of subtypes (split and previous unsplit subtype) with sequences that demonstrate maximum likelihood.

Chapter 4 Investigating the association between facial asymmetry and brain asymmetry in epilepsy

Parts of the following chapter have been published in Balestrini *et al.*, (2021). My part was to investigate if asymmetry of regional brain measures observed in PWE are associated with their facial asymmetry. In particular, I processed the patients MRI scans, and developed the machine learning pipeline (Section 4.2.5) that predicted facial asymmetry from the asymmetry of regional measures in the brain caused by pathological mechanisms of epilepsy. I also investigated the association between these structural changes in the brain and duration of illness.

4.1 Introduction

Neurological disorders often do not affect brain regions bilaterally, thus, creating a disease-associated asymmetry. For instance, in autism, structural brain asymmetry has been found along with increased facial asymmetry (Hammond *et al.*, 2008; Postema *et al.*, 2019). Moreover, in Down syndrome a typical face shape can arise from pathogenic genetic variation along with increased structural brain asymmetry (Allanson *et al.* 1993; Fu *et al.*, 2020).

Previous studies using data derived from neuroimaging have identified cortical thinning, predominantly in the ipsilateral structures in people with focal epilepsies (Bernasconi *et al.*, 2004; Thom *et al.*, 2012; Bernhardt, Bonilha and Gross, 2015; Whelan *et al.*, 2018). Therefore, in the context of focal epilepsy, it can be observed that patients exhibit an increase in asymmetry between the left and right brain regions that arise from lateralized structural changes (Alhusaini *et al.*, 2012; Galovic *et al.*, 2019; Hatton *et al.*, 2020). We've also discussed in the introduction that PWE have subtle asymmetric facial features. Discreet points of facial features obtained from 3D models using the 3D

stereophotogrammetry technique can be used to quantify facial asymmetry in individuals (Hammond, 2007).

Thus, using the asymmetric facial measures derived from 3D models, we investigate if unilateral changes in focal epilepsy leading to asymmetry brain measures are associated with a higher degree of facial asymmetry, compared to people with IGE (that tend to have lower degree of unilateral changes) or controls without epilepsy. We subsequently investigate whether the facial asymmetry is predominantly associated with focal symptomatic cases with noted brain lesions, as opposed to focal cryptogenic cases without detectable or identified lesions on the MRI scans.

4.2 Methods

4.2.1 Patients and controls

PWE were consecutively recruited at the National Hospital for Neurology and Neurosurgery (UK). Controls were recruited as volunteers, unaffected relatives of PWE, from the UCL Institute of Child Health (London, UK). The data gathered included age, sex, epilepsy diagnosis (Commission on Classification and Terminology of the ILAE, 1989), MRI brain scans and history of facial injury or surgery. In brief, PWE were grouped according to their syndrome: focal cryptogenic, focal symptomatic, and IGE. In total we had 307 PWE with recorded measures of facial asymmetry. We also had MRI scans for 234 of the PWE. Data on duration of illness was available for 194 of these 234 PWE, including focal epilepsies classified as cryptogenic (n=97), symptomatic (n=70) and IGE (n=27).

4.2.2 Signature asymmetry index (SAI)

The signature asymmetry index (SAI) was acquired by collaborators at the UCL Institute of Neurology (Balestrini *et al.*, 2021). The steps used for computing the SAI are illustrated in Figure 4.1. In brief, 3D face images were captured with a single device (Vectra CR 3D; Canfield Scientific Inc.), and landmarks

previously described by Toma *et al.*, (2009) were manually annotated for each subject. Principal component analysis was used to reduce the number of points on the 3D face and construct the dense surface models (DSMs) that represented 99% of the facial features.

The 'signature' of a face surface is the set of differences between the points position on the DSM of PWE and controls, where the average of the controls across age and sex are compared to individual PWE. A signature heat map of the difference between the original face and its mirrored form (usually in the plane x=0) can be used to demonstrate the facial asymmetry compared to that of controls. Thus, the signature weight of this difference, also called the SAI, is used to quantify the degree of facial asymmetry (Balestrini *et al.*, 2021).

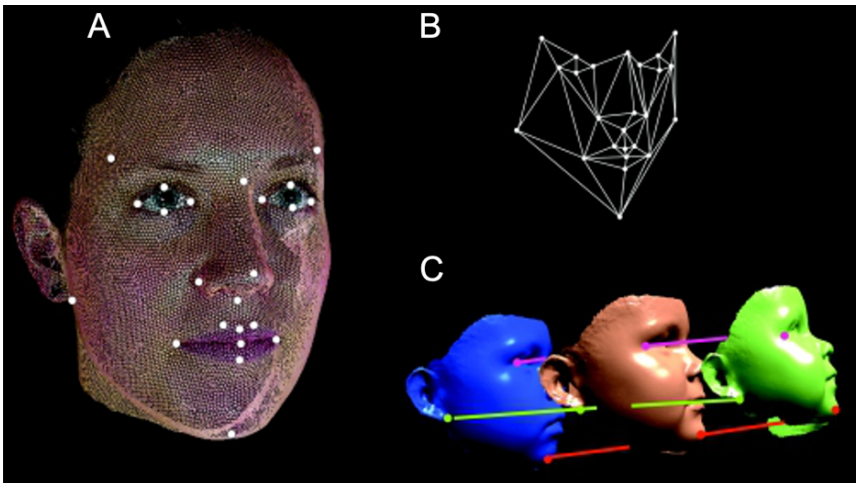

Figure 4.1 Dense surface model (DSM): PCA is applied on (A) DSM model with morphometric points of the face (measured in milli-meters (mm)). The principal components or modes of shape variation are extracted, which reduces the data dimensions (B). Sparse anatomical points extracted are projected on subjects individually (C), which is used to compute facial asymmetry. Adapted from (Hammond, 2007).

4.2.3 Brain MRI imaging and processing

SAI measures were obtained from 307 PWE, attending the clinics at the National Hospital for Neurology and Neurosurgery, London (UK). Of these we had T1W MRI scans for 239 PWE were acquired within a period of two years of measuring the respective SAI. In total, three different 3D-T1W MRI sequences were used: 1) a coronal T1W 3D inversion-recovery fast spoiled gradient echo (IR-FSPGR) with repetition time / echo time / inversion time = 8.1 / 3.1 / 450 ms; field-of-view (FOV) 187x240x240 mm; matrix 170x256x256 (176 scans); 2) an axial T1W 3D (FSPGR BRAVO) with TE/TR/TI 3.6/0.2/400 ms, FOV 240×240×183 mm, matrix 256×256×166, parallel imaging acceleration factor 2 (43 scans); and 3) a three-dimensional (3D) T1W inversion-recovery fast spoiled gradient recalled echo (TE/TR/TI 3.1/7.4/400 ms, FOV 224×256×256 mm, matrix 224×256×256, parallel imaging acceleration factor 2 (20 scans). Sequences 1 and 2 were used for data acquired between August 2004 and March 2013 on a single 3T MRI GE Signa HDx scanner (GE, Milwaukee, WI, USA) using an 8-channel head coil. Sequence 3 was used for data acquired from September 2013 onwards, on a 3T GE Discovery MR750 (GE, Milwaukee, WI, USA) with a 32-channel head coil.

Following a visual inspection, MRI scans with resections were excluded before using FreeSurfer 6.0 (Dale, Fischl and Sereno, 1999) for the automated segmentation of brain regions. A brief pipeline used in FreeSurfer to extract cortical thickness, surface area and subcortical volumes is shown in Figure 4.2. From the FreeSurfer processed images, we extracted information on 156 features from the left and right brain regions, which are defined in the Desikan-Killiany atlas (Desikan et al., 2006). We had 57 measures of the brain asymmetry index (BASI) which were computed (as described further and expressed in Eq. 4.1.) from: 70 (left and right hemisphere together) regional measures of cortical thickness, including average hemisphere cortical thickness and average hemisphere surface area; 16 subcortical volumes; and 26 measures were for hippocampus subfields. The BASI measures used in the analysis are listed in Supplementary Table S1.

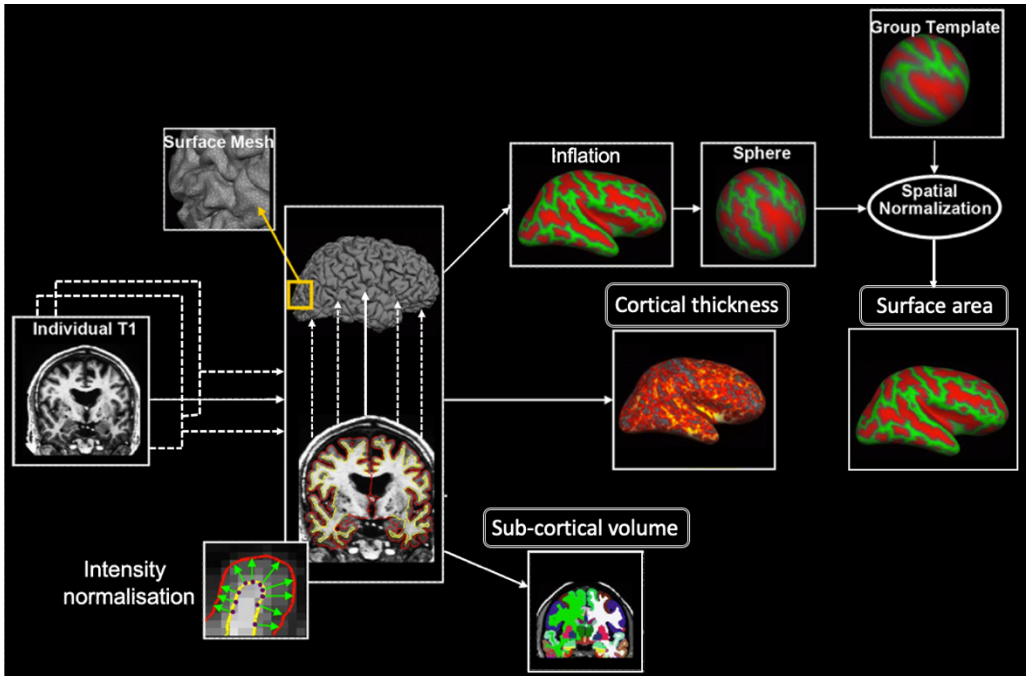

Figure 4.2 FreeSurfer pipeline for segmentation and feature extraction: In the first step FreeSurfer uses a skull stripping algorithm to remove nonbrain tissue. To account for artifacts and RF-field inhomogeneities, the highest intensity of white matter is used to center the mean of every x-y white matter pixels. An image processing algorithm determines the grey-white matter boundary for each slice, and subsequently computes cortical and subcortical measures. This is followed by deformation of grey-white matter boundary outward, to generate the pial surface mesh. The cortical surfaces are inflated to a smooth surface where sulci are red and gyri are green. Each vertex on the inflated surface is registered to a template sphere, that is derived from a group of healthy and disease state scans. Adapted from Dale, Fischl and Sereno, (1999) and (Gao *et al.*, 2020).

For an automated quality control step, we employed a script developed by the ENIGMA consortium (http://enigma.ini.usc.edu/protocols), which, for every brain region, identifies potential outliers based on the distribution in the cohort. We tested for outliers for a range of z-scores and reviewed the FreeSurfer segmentation on MRI scans, for corresponding brain region indicated as outlier. Following this we found scan values showing a z-score of ≥4.7 in either direction marked as outliers were best in identifying mis-segmented regions.

This automated quality control highlighted five patients whose segmented brain scans were manually inspected and excluded as outliers. Using the resulting 234 scans, regional measures were adjusted for ICV, age, sex and scanner using linear regression. We computed the absolute BASI between contralateral regions, where the BASI of each brain region (57 in total) was defined as the difference between the left (57) and right (57) brain regions, divided by their average as shown in Eq. 4.1

$$BASI_{BR} = \frac{BR_L - BR_R}{(BR_L + BR_R)/2} \qquad \text{Eq. 4.1}$$

4.2.4 Correlation analysis

We computed Pearson's correlation between duration of illness and the BASI of average thickness and surface area of cortical brain regions to investigate the effect duration of illness has on the brain. In order to investigate if face asymmetry is associated with increased brain asymmetry, we also computed Pearson's correlation between SAI and the BASI of average thickness and surface area of cortical brain regions.

4.2.5 Machine learning approach

The automated segmentation of brain regions by FreeSurfer enables us to investigate the association between structural changes in the brain and facial asymmetry. In pursuit of this, we constructed a regression model utilizing sample data from our cohort and assessed the model's predictions.

We chose the LASSO regression model, as outlined in Section 3.2.2, due to its ability to provide a transparent interpretation of the BASI measures that predict the SAI values. Our objective was to predict patient' SAI (response variable), from the 57 BASI brain regions (features) computed. Before incorporating them into the learning algorithm, BASI values underwent normalization, where each feature had the dataset mean subtracted, and the values were divided by the Euclidean norm. This ensured a comparable range for each BASI value,

facilitating a fair estimation of their corresponding LASSO coefficients. Figure 4.3 illustrates the flow chart used to build and train the LASSO model. In brief we split the data into a training and testing set to ensure our predictions are not biased or overfitted to the data. We optimized the regularization parameter λ, and compared the predicted SAI and measured SAI on the test set. This process was repeated 1000 times to introduce randomness in splitting train and test data and to better evaluate the trained model' performance.

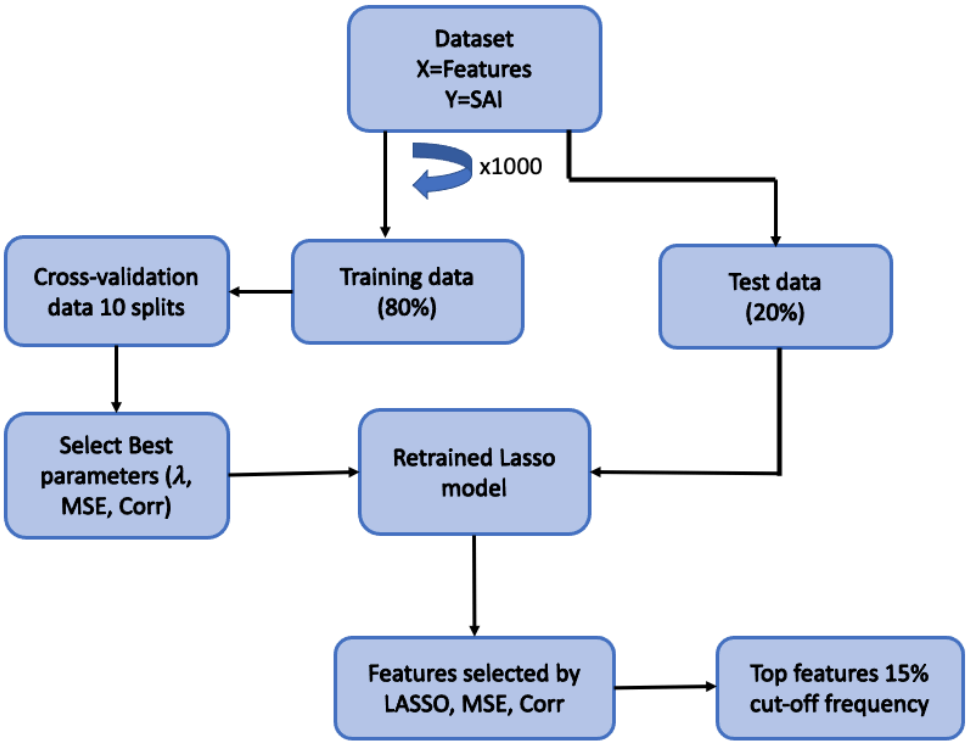

Figure 4.3 Machine learning flow chart: The dataset is split into random 80% for training and 20% test. λ is optimised through a 10-fold cross-validation, (λ values 2^{-16} to 2^{-4}) on the train set. Features selected by LASSO are noted along with the performance evaluation parameters of MSE and correlation between measured SAI and predicted SAI. This process was repeated 1000 times, and a 15% frequency cut-off of features selected by LASSO model was used to extract the top five features to be interpreted.

A similar LASSO model was analysed with added features of lesion laterality observed on MRI scan, and the type of focal epilepsy determined for each patient. Thus, we investigated these additional clinical variables effect on SAI, of PWE. The BrainPainter software was used to visualise the frequency of the brain regions selected across the 1000 repetitions (https://brainpainter.csail.mit.edu) (Marinescu *et al.*, 2019). Moreover, we analysed only people with focal cryptogenic (sample size (n)=109) and focal symptomatic (n=96) separately to investigate if the prediction accuracy of SAI is improved with LASSO model trained on BASI of brain regions and laterality of the lesion in an MRI scan as additional feature.

4.3 Results

Table 4.1 shows demographics of the 307 PWE with SAI measures, and the 194 PWE with MRI scans available. The cohort had a fairly balanced proportion of sex ratio, with slightly more females. The duration of illness recorded for some PWE extended to over 50 years. PWE with lesions detected on left and right hemisphere were also well balanced. Sample size for people with focal symptomatic, focal cryptogenic and IGE and MRI sequences used in the acquisition process is also shown in Table 4.1.

4.3.1 Duration of illness relation with SAI and BASI

Duration of illness was significantly correlated with BASI of average cortical thickness (r=-0.19 p=0.0075) but not with BASI of surface area (r=0.06 p=0.3968) (see Figure 4.4). In the case of SAI and BASI of cortical measures, the correlation was r=-0.01 (p=0.9306) and r= -0.05 (p=0.4820) for BASI of average thickness and BASI of surface area, respectively (Figure 4.4).

Table 4.1 Patient demographics: Table shows sex, duration illness, lesion side detected on MRI for people with focal symptomatic, focal cryptogenic and generalized epilepsy.

	Focal symptomatic cases	Focal cryptogenic cases	Generalized cases	Total (Focal + Generalized) cases
Sex				
Male	55	61	17	133
Female	71	82	21	174
Total SAI measures	126	143	38	307
Age at SAI				
Mean/±SD	41.63 ±11.64	38.10 ± 12.51	34.75 ±10.71	39.33 ±12.10
Duration of illness				
Mean/±SD	27.73 ±13.21	22.30 ±12.45	21.37±12.46	24.61±13.06
Lesion on MRI scan				
Left	34	N/A	N/A	34
Right	36	N/A	N/A	36
Unknown	N/A	97	27	124
Total MRI scans	70	97	27	194
MRI sequence				
FSPGR_3D	53	69	17	139
FSPGR_BRAVO	12	19	8	39
1mm_Cor_MPRAGE	5	9	2	16

4.3.2 Facial and brain asymmetries in PWE

The LASSO model was trained on patients of all epilepsy syndromes using the BASI of brain regions, along with additional features of epilepsy syndrome, side of lesion present on MRI scan, in separate analysis as predictors, with SAI as the response variable. The main analysis involving all 234 patients using only brain regions yielded an average correlation of -0.022 and an average MSE of 0.099 (Figure 4.5). Based on this correlation result, we can infer the model would not be able to make any useful predictions.

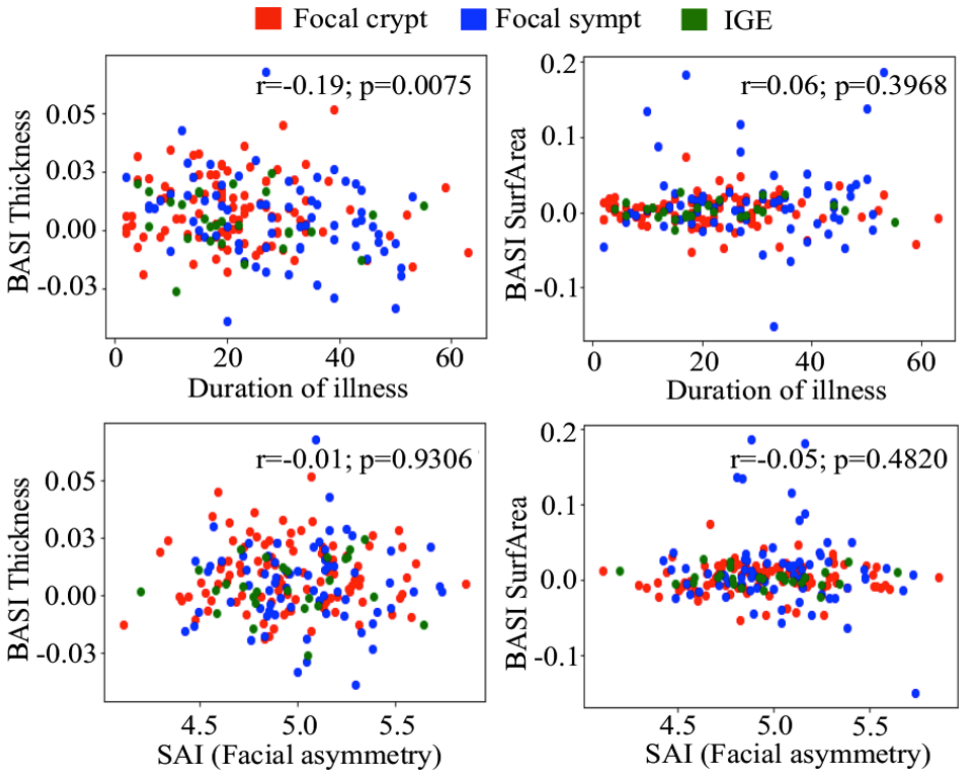

Figure 4.4 Correlation analysis of duration of illness and SAI vs BASI average cortical thickness and BASI average surface area: The strength of relationship shows BASI thickness decreases for longer duration of illness, whereas no such relationship is observed in the case of BASI average surface area and duration of illness. The facial asymmetry measures appear to be independent of the BASI measures as illustrated in the figure.

Furthermore, adding the information on epilepsy syndrome and lesion laterality as features, yielded a mean correlation of -0.024 and mean MSE of 0.099. Thus, there was no notable difference in the average correlation and MSE of the two models. Of the 1000 iterations, in 683 models LASSO did not select any features besides the intercept (indicated by correlation values of exactly 0). However, in the remaining models, the frequency at which the features were selected are listed in Supplementary Table S1. Here, the most frequently selected features were the entorhinal gyrus (25.8%), fimbria (25.6%), the pallidum (25.2%), the frontal pole (16.8%) and the caudal anterior cingulate (16.2%), which span the frontal and anterior regions of the brain and are shown in Figure 4.6. The model

that included the two clinical variables also selected the side of lesion on MRI scan among these.

The final analysis was to determine the association between increased SAI and focal epilepsies. We analysed only people with focal cryptogenic and focal symptomatic separately. Here we found the focal cryptogenic model performed slightly better compared to focal symptomatic cases, with average correlation (n=109) of 0.095 (average MSE of 0.11) and average correlation (n=96) of -0.03 (average MSE of 0.09), respectively.

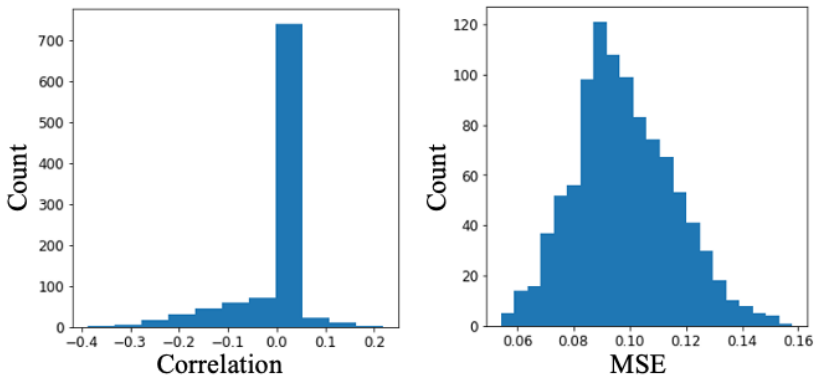

Figure 4.5 Correlation and MSE distribution of predicted vs actual SAI: Average correlation of predicted vs actual SAI with LASSO model trained on BASI of brain regions.

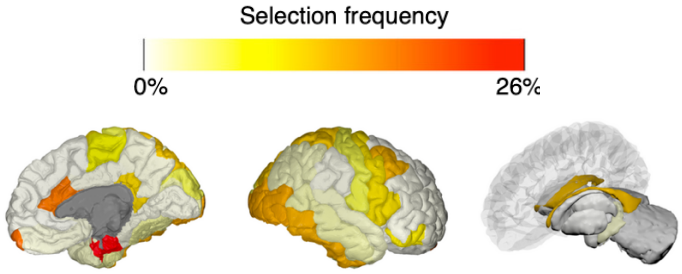

Figure 4.6 Brain region selection frequency: Patients from all categories included, model trained on BASI brain regions, epilepsy classification and lesion laterality on MRI scan. The entorhinal gyrus (dark red), fimbria (dark orange), pallidum, frontal pole, caudal anterior cingulate (yellow) were the top brain regions selected in the LASSO model to predict SAI across the 1000 iterations.

4.4 Conclusion

Our collaborators, Balestrini *et al.*, (2021), showed that people with lateralised focal epilepsies have an increased degree of facial asymmetry, compared to individuals with IGE or controls without epilepsy. Evident from the correlation result of BASI regional thickness and surface area measures, versus SAI, the performance of the LASSO model would indicate minimal relationship between these measures. This suggests that pathological mechanisms that cause structural changes in the brain in PWE are independent to those responsible for increased facial asymmetry. In addition, the actual sidedness of lesion included in the analysis did not appear to increase the model performance of predicting the SAI. This performance was maintained after excluding PWE with unilateral lesions of established acquired aetiology. Although the size of the lesions was not systematically measured, in most cases the brain structural lesion was not extensive. Whilst there was a significant effect of disease duration on both brain and facial asymmetries, there was no association between brain asymmetry and facial asymmetry.

We found that disease duration is associated with increased asymmetry of cortical thickness as previously demonstrated (Bernasconi, Natsume and Bernasconi, 2005; Bonilha *et al.*, 2006; B. C. Bernhardt *et al.*, 2009; Whelan *et al.*, 2018), and with increased facial asymmetry (Balestrini *et al.*, 2021). In addition, studies using magnetoencephalography (MEG) have shown focal epilepsies with altered connectome profiles of the brain are also associated with disease duration (Martire *et al.*, 2020; Ramaraju *et al.*, 2020). This indicates structural changes in the brain affect networks in the brain and not confined to specific regions. Structural brain asymmetry and increased facial asymmetry has also been described in other neurological diseases, including autism spectrum disorder (Hammond *et al.*, 2008; Postema *et al.*, 2019). The findings from these studies suggests altered neurodevelopment may lead to structural changes in the brain. Our collaborators, Balestrini *et al.*, (2021) proposed that the greater facial asymmetry may be explained by aberrant mechanisms between the brain and facial structures.

These findings published in Balestrini *et al.*, (2021) suggest that the DSM model provides distinguishing features between focal and generalised epilepsy, warranting further research to explore its potential clinical implications. However, for future consideration, it's crucial to note that alterations these in facial features resulting from pathological factors tend to be subtle in PWE. Such subtleties may escape detection by clinicians and necessitate specific training for accurate identification. (Chinthapalli *et al.*, 2012; Galizia *et al.*, 2012). Moreover, atypical facial features can result from injuries or conditions other than epilepsy. Additionally, the accuracy of identifying facial landmarks by operators in research may be compromised by the diverse facial structures across the population (Chinthapalli *et al.*, 2012).

In summary, appropriate measures would need to be considered for adopting the use of facial asymmetry for clinical applications and research for PWE. Future studies, incorporating data on seizure semiology and a larger sample size, can contribute to a better understanding of the utility of facial asymmetry. Furthermore, longitudinal data acquisition in future research can provide insights into the progression of facial feature asymmetry and epileptogenesis.

Chapter 5 A novel disease staging of PWE based on structural changes in the brain

5.1 Background

The investigation into structural changes in the brain in epilepsy has gathered significant interest in recent decades, aiming to enhance our understanding of disease progression and its implications for clinical management. Here we investigated whether staging people with MTLE-HS based on the progression of structural changes, from one region to another are associated with clinical features of disease duration and treatment response. This work has been published in Lopez *et al.*, (2022).

In a recent study conducted by Zhang et al. (2017), researchers aimed to elucidate a progression pattern comparable to our work by utilizing Granger causality analysis. Their analytical approach aimed to determine whether a previously affected brain region or a group of brain regions with structural changes could predict the subsequent abnormal brain region. Thus, their method attempts to make a "causal" inference from linear relationships. Zhang et al., (2017) found that subcortical regions such as the hippocampus and thalamus "causally" affected other regions, most prominently the prefrontal cortex and cerebellum. Their approach however does not allow direct inference of a temporal sequence. A major step towards addressing the question of progression was provided by previous longitudinal studies that assessed progressive atrophy in people with MTLE-HS (B. C. Bernhardt *et al.*, 2009; Coan *et al.*, 2009; Bernhardt, Kim and Bernasconi, 2013; Keller *et al.*, 2014). The findings from these studies indicated structural changes in the subcortical regions, predominantly the ipsilateral hippocampus, thalamus, amygdala and were also widespread across cortical structures including those of the temporal and frontal lobe structures.

Here, we investigate the sequence in which structural changes in the brain occur in people with left and right MTLE-HS using the EBM described in Section 3.4. Since its inception the EBM has been used across a wide range of neurological diseases including Alzheimer's disease (Fonteijn *et al.*, 2012), multiple sclerosis (Dekker *et al.*, 2021), amyotrophic lateral sclerosis (Gabel *et al.*, 2020) and Parkinson's disease (Oxtoby *et al.*, 2021). The findings from these studies have helped map the early pathological changes in the brain in each of the respective diseases and the sequential progression of changes in other parts of the brain. Please see Young *et al.*, (2024) for a recent review.

Patients resistant to ASMs are reported to have a better outcome following surgery if the epileptogenic region is resected within 5 years (Simasathien *et al.*, 2013; Jehi and Mathern, 2014). However, the current referral process for surgery can take up to a decade or longer, which can seriously impact the quality of life for these patients. Early identification of patients resistant to ASMs and their causes at the time of epilepsy diagnosis would be highly advantageous. Moreover, resistance to ASMs has been suggested to be associated with the severity of the disease in the intrinsic hypothesis (Rogawski and Johnson, 2008; Rogawski, 2013). While severity primarily refers to frequency of seizures, it could also imply the extent of progressive structural changes in the brain. The EBM algorithm assigns ordinal stages to patients based on the estimated sequence that correspond to the extent of abnormality in brain regions. We can therefore investigate whether patients assigned in the early EBM stages are ASM responsive and those assigned in the later stages are resistant to ASMs. This will help assess if mechanisms of epileptogenesis accompanied with ASM resistance is associated with the structural changes of specific brain regions.

5.2 Materials and methods

5.2.1 Data analysis and feature selection

We analysed data from the ENIGMA-Epilepsy working group (Sisodiya *et al.*, 2020) comprising of neuroimaging data from subjects, namely patients with MTLE-HS and controls from 25 centres (Table 5.1). As previously described in

Whelan *et al.*, (2018), T1W brain MRI scans were acquired using 1.5T or 3T MRI scanners from different manufacturers and different imaging sequences. Brain scans were processed at each contributing centre using the same pipeline based on FreeSurfer Version 5.3.0 (Dale, Fischl and Sereno, 1999; Fischl, 2012). Diagnosis of left and right MTLE-HS were made by an epilepsy specialist at each centre, based on seizure semiology and EEG findings. Presumed sclerosis of the hippocampus or the mesial temporal lobe was diagnosed according to established features on MRI [i.e., a T1W, T2W or fluid-attenuated inversion recovery (FLAIR) scan].

A common set of 156 regional features was extracted based on the Desikan-Killiany atlas (Desikan *et al.*, 2006): 68 measures for regional cortical thickness (CT), 68 measures of regional surface area (SA), two measures of hemispheric average CT, two measures of hemispheric SA, and 16 subcortical brain volumes as previously described in detail (Whelan *et al.*, 2018). Since the initial study (Whelan *et al.*, 2018), five new centres were added, providing an additional 244 subjects. Overall, the ENIGMA-Epilepsy dataset features pre-processed MRI scans from 1,625 controls as well as 446 left MTLE-HS and 358 right MTLE-HS patients. After segmentation quality assurance, certain regional brain measures were removed for some subjects in the acquired dataset (about 0.02% of the values). We removed subjects with more than ten missing values (66 subjects). Missing measures in the remaining subjects were imputed within each centre using a singular value decomposition (SVD)-based approach (Troyanskaya *et al.*, 2001). Additionally, age, sex, case-control status, lateralization (left or right MTLE-HS), age at onset and duration of illness were available. Furthermore, ASMs response status (defined as one or more seizures in the 12 months before MRI) was obtained for 408 MTLE-HS cases.

5.2.2 Data harmonization and confound adjustment

ENIGMA-Epilepsy is a multi-centric study and therefore the data are subject to centre-specific biases arising from various factors. To mitigate this, the regional measures were harmonized across centres using NeuroCombat (Fortin *et al.*, 2018). NeuroCombat posits a linear model within a Bayesian framework to

improve the estimation of the site parameters. It models the location and scale on the features, where each centre is assumed to have additive and multiplicative factors (Johnson, Li and Rabinovic, 2007; Fortin *et al.*, 2018). Following the harmonization, the regional measures were adjusted for ICV, age at imaging and sex using linear regression. The residuals for each regional measure plus the intercept of the model were used for further analysis.

5.2.3 Ipsilateral and contralateral features

Studies have shown unilateral and bilateral changes in structural connectivity and cortical thinning in people with left and right MTLE-HS, with the ipsilateral regions being strongly affected (Bernasconi, Natsume and Bernasconi, 2005; Pereira *et al.*, 2010; Caciagli *et al.*, 2014; Whelan *et al.*, 2018; Galovic *et al.*, 2019). In order to jointly analyse people with left and right MTLE-HS, we assembled the regional cortical thickness, surface area and volume measures by defining the ipsilateral regions as those on the same hemisphere as seizure onset (e.g., left hemisphere in left MTLE-HS), with regions in the other hemisphere defined as contralateral, effectively yielding a set of 156 imaging-derived features, where 78 were ipsilateral (34 cortical thickness (CT), 34 surface area (SA), 8 subcortical volumes (V), hemisphere CT and hemisphere SA and similarly 78 contralateral regions. For the controls, we randomly sampled half as controls for left MTLE-HS, where left and right hemispheres were defined as ipsilateral and contralateral regions, respectively. Similarly, the remaining half acted as controls for right MTLE-HS with the hemispheres swapped. Overall, this enabled us to analyse the lateralizing effect of structural changes in the brain in people with MTLE-HS.

5.2.4 Brain asymmetry index features

Previous studies have used the asymmetry of brain regions to model cortical thinning in people with MTLE-HS when compared with healthy controls, where regions ipsilateral to the side of seizure onset were found to be largely affected (Shah et al., 2019). Thus, to emphasize regions with increased brain asymmetry that is observed in people with MTLE-HS, we computed the BASI between

ipsilateral and contralateral brain regions. Here contralateral brain regions of each subject act as a personalized healthy reference region. We defined the BASI of regional cortical thickness, surface area and volume as ratio given in equation below

$$\text{BASI} = \frac{(\text{ipsilateral} - \text{contralateral})}{(\text{ipsilateral} + \text{contralateral})/2} \quad \text{Eq. 5.1}$$

5.2.5 Feature selection

The EBM requires selection of features, i.e., regional ipsilateral, contralateral and BASI measures, that differ to some degree between patients and controls. As our dataset had additional subjects compared to Whelan et al. (2018), we sought to identify relevant brain regions among these subjects. We combined the controls, people with left and right MTLE-HS and computed Cohen's d of the 234 features (78 ipsilateral, 78 contralateral and 78 BASI). That is, for each regional measure we divided the difference between the mean of patients and controls by the joint standard deviation (Cohen, 1966). In order to ensure that results were not driven by outliers, we additionally computed robust Cohen's d which uses the median and mean absolute deviation in place of the mean and standard deviation, respectively (Hampel, 1974). A cut-off of the absolute Cohen's d of >= 0.5 for a feature was specified as a sufficient distinct separation between patients and controls to be considered for disease progression modelling. We also evaluated a more lenient threshold (robust Cohen's $|d| \geq 0.4$).

5.2.6 Event based modelling

The EBM algorithm assumes that for any given dataset a greater proportion of patients across the cohort will show abnormality for the early-stage features and a decreasing proportion for brain regions that undergo structural changes at later stages. The overall EBM architecture is described in Section 3.4. After we evaluate the features required for the analysis, the first step of the EBM computes distributions which define what normal and abnormal measures look like for every brain region. In practice, these distributions are estimated for every

feature by fitting a mixture model (see Section 3.4.2) to patients and controls. In our case, we used a KDE mixture model that smooths the probability density function to provide more accurate estimations for the patients and controls (Cao, Cuevas and González Manteiga, 1994; Firth et al., 2020). In the second step, the EBM determines the best ordering of features for the given dataset. Here, 'best' means that the ordering agrees with the brain measures' profile of as many subjects as possible in the dataset.

We initialized the MCMC step (see Section 3.4.1) using the greedy ascent algorithm described in (Fonteijn *et al.*, 2012) for 10,000 iterations. Next, we run the MCMC procedure for 500,000 iterations, which yields one possible arrangements of features. However, changes to the training set (e.g., removing or adding some subjects) may lead to slightly different orderings. Lastly, the third step of the EBM determines the uncertainty and variability of the sequence using a bootstrap algorithm, which draws a random set of samples with replacement while maintaining the original sample size. Here, the maximum likelihood sequence was computed for 100 bootstrap samples of the data. Using the above bootstrapped sequence, we can create a positional variance diagram that shows the proportion of event uncertainty.

The trained EBM model can then be applied to assign each of the patients and controls to a distinct disease stage. These stages range from 0, indicating no detected abnormality to stage N, representing all N features considered in the model are abnormal. To investigate whether the sequence is consistent in people with left and right MTLE-HS, we re-ran the analysis for these two types of syndromes separately.

5.2.7 Association of EBM stages with duration of illness, age of onset, treatment response, and surgical outcome

To determine whether individual EBM stage is related to illness duration or age of onset, we computed Spearman's rank correlations between EBM stage and the duration of illness (in years) at the time of imaging and age of onset, respectively. We hypothesized that patients with advanced EBM-stages were

more likely to have a longer duration of illness, earlier disease onset, and are more likely to be ASM resistant. To investigate this, we used the Mann-Whitney U test to test for a difference in EBM-assigned stage regarding ASM response status.

5.3 Results

Table 5.1 and Supplementary Table S2 displays the overall cohort split by centre. On average, each centre contributed a range of subjects, ranging from young adults in their 20s to adults over 60 years (median 33.0 years; IQR 18.08 years). The binary sex distribution within the dataset was well balanced with a slight majority of women (56.0% of people with MTLE-HS and 55.9% of healthy controls). The duration of illness ranged from recently diagnosed to 68 years (median 20.0 years; IQR 24.0 years).

5.3.1 Effect sizes of selected features

The seven selected features (robust Cohen's $|d| \geq 0.5$) were ipsilateral hippocampal volume and its BASI, ipsilateral thalamic volume, cortical thickness of bilateral superior parietal gyrus, ipsilateral precuneus and ipsilateral lateral ventricle volume (Supplementary Table S3). Supplementary Figure S1 provides a visual representation of the effect sizes rendered using the ENIGMA toolbox (Larivière et al., 2021). Our effect sizes matched the findings of the original ENIGMA-Epilepsy multi-centric analysis (Whelan et al., 2018). In short, effect sizes (robust Cohen's d) ipsilateral to the seizure focus were stronger than those in the corresponding contralateral region for the surface area ($t=4.01$; $p=0.00033$; $df=33$; paired t-test) but not for cortical thickness ($t=1.95$, $p=0.06$; $df=33$, paired t-test) nor for subcortical volumes ($t=1.60$; $p=0.15$; $df=7$; paired t-test). Furthermore, effect sizes for cortical thickness were stronger than effect sizes for surface area ($t=8.08$; $p=1.09 \times 10^{-11}$; $df=67$; paired t-test). Use of the lower Cohen's d cut-off of 0.4 produced 12 additional features for EBM modelling (Supplementary Table S3).

Table 5.1 Demographics table: Table showing individual sites demographics including age, number of people with left and right MTLE-HS, controls and duration of illness of MTLE-HS cases. (Na= Not applicable)

Centre	Age controls (Mean ± SD)	Age cases (Mean ± SD)	Age of onset (Mean ± SD)	Duration of illness (Mean ± SD)	Total controls	Total cases	L MTLE-HS cases	R MTLE-HS cases	Total *n*
Bern	32.5± 9.39	31.3 ± 9.09	N/A	N/A	78	18	10	8	96
Bonn	40.4± 13.79	40.2 ± 13.37	17.1 ± 12.14	23 ± 14.16	80	112	74	38	192
CUBRIC	28± 8.17	N/A	N/A	N/A	48	0	0	0	48
EKUT	35.3± 12.33	N/A	N/A	N/A	18	0	0	0	18
EPICZ	38.8± 11.08	39.7 ± 9.11	18.1 ± 14.15	21.6 ± 13.48	116	46	19	27	162
EPIGEN_3T	34.7± 9.37	40.4 ± 6.28	21.8 ± 13.16	18.5 ± 11.98	70	13	8	5	83
Florence	32.2± 8.84	N/A	N/A	N/A	30	0	0	0	30
Genova	25.2± 8.23	N/A	N/A	N/A	20	1	0	1	21
Greifswald	26.3± 7.48	N/A	N/A	N/A	99	0	0	0	99
HFHS	N/A	40.4 ± 14.85	10.4 ± 12.96	25.4 ± 14.44	0	20	9	11	20
IDIBAPS	33.1± 5.99	37.4 ± 9.94	17.7 ± 12.79	18.8 ± 9.97	52	53	17	36	105
KCL_CNS	31.7± 8.4	41 ± 9.57	17.5 ± 14.16	25.2 ± 16.97	101	15	6	9	116
KCL_CRF	28.7± 8.29	37.8± 11.52	22.6 ± 12.34	15.2 ± 8.04	26	5	3	2	31
KUOPIO	25.2± 1.55	41.1± 11.06	23.3 ± 18.23	17.8 ± 17.02	67	9	0	9	76
MICA	31.9± 4.77	38.9± 13.12	23.4 ± 11.71	15.7 ± 14.58	38	14	12	2	52
MNI	30.7± 7.38	33.6± 9.53	17.3 ± 10.57	16.3 ± 11.4	46	83	45	38	129
MUSC	54.9± 8.4	33.5± 12.73	15.4 ± 12.34	18.2 ± 12.79	58	27	21	6	85
NYU	30.1± 10.36	33.8± 9.31	14.1 ± 8.04	20.2 ± 14.44	118	19	8	11	137
RMH	38.8± 20.44	39.6± 15.59	27.1 ± 17.69	12.4 ± 13.23	27	35	22	13	62
UCL	37.7± 12.4	39.5± 11.29	11.8 ± 8.72	27.7 ± 15.12	29	37	24	13	66
UCSD	36.9± 15.1	39.2± 12.53	15.6 ± 12.44	24.3 ± 17.82	37	26	16	10	63
UMG	34.7± 10.26	40.6± 12.49	15.4 ± 14.04	23.9 ± 18.49	21	20	10	10	41
UNAM	33.2± 12.29	34.4± 12.47	15.5 ± 13.84	18.8 ± 13.16	35	20	10	10	55
UNICAMP	34.4± 10.47	42.7± 8.33	11.4 ± 9.6	31.3 ± 12.13	398	191	107	84	589
XMU	31.5± 7	28.2± 8.45	17.2 ± 12.06	11.3 ± 8.02	13	40	25	15	53
Total	**33.8 ± 11.45**	**38.5 ± 11.44**	**15.9 ± 12.4**	**22.7 ± 14.39**	**1625**	**804**	**446**	**358**	**2429**

5.3.2 Sequence of abnormal features in people with left and right MTLE-HS

The EBM estimated the sequence for the seven selected features using the KDE mixture models (Supplementary Figure S2) and placed them in stages 0 to 7 (Figure 5.1). The bootstrapped version of the EBM placed the reduced ipsilateral hippocampal volume and increased asymmetry in hippocampal volume at the beginning of the sequence. This was followed by decreased cortical thickness and decreased ipsilateral thalamic volume in the sequence (Figure 5.1). We analysed people with left and right MTLE-HS separately, with similar progression patterns in both syndromes (Supplementary Figure S3). Reducing the inclusion threshold to Cohen's $|d| \geq 0.4$ led to 19 features and provided a more fine-grained staging, but with essentially the same progression sequence as in the original analysis (Supplementary Figure S4).

5.3.3 Cross-sectional distribution of disease stages as defined by EBM

We used the trained EBM to stage subjects based on structural changes in regional brain measures (Young *et al.*, 2014): PWE and controls were assigned to stages zero to seven. Most of the people with MTLE-HS (68.1%) were staged at stage one or greater (Figure 5.2). However, a large proportion of these patients (31.9%) were staged at zero, indicating mild or non-detectable abnormality on T1W MRI. About 49.3% were assigned to stages one and two, reflecting reduced volume of the ipsilateral hippocampus and abnormal asymmetry in the hippocampus. The other 18.8% of people with MTLE-HS were staged beyond stage two, suggesting neocortical involvement, reduction of ipsilateral thalamic volume and increase in ipsilateral lateral ventricle volume. The distribution of stages did not differ between people with left and right MTLE-HS ($H = 0.08$, p-value = 0.78; Kruskal-Wallis test).

Ipsilateral hippocampal volumes in cases at stage zero were significantly larger than in patients assigned to later stages (t= 31.15, p =1.11x10^{-138}, t-test; Supplementary Figure S5). Consequently, effect size of ipsilateral hippocampal volume was d=-0.42 and d=-2.16 for patients at stage zero and non-zero stages, respectively.

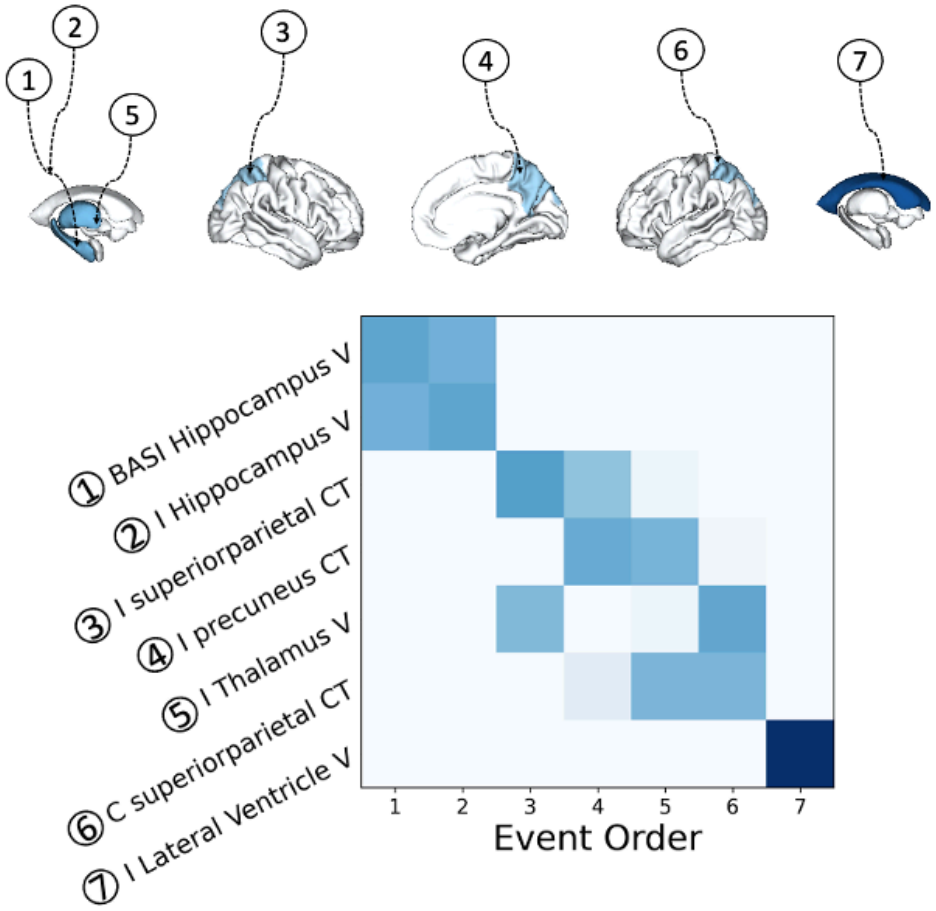

Figure 5.1 Sequential Accumulation of Pathology in people with MTLE-HS: Data-driven sequence of atrophy or increased asymmetry of brain regions: Colour intensity in the positional variance diagram (PVD) represents the proportion of certainty (0,0 in white to 1.0 in dark blue) in which features (y-axis) appear in a particular position (x-axis) in the event order obtained through bootstrapping. CT=cortical thickness, V=Volume, BASI=Brain Asymmetry Index, I=ipsilateral, C=contralateral.

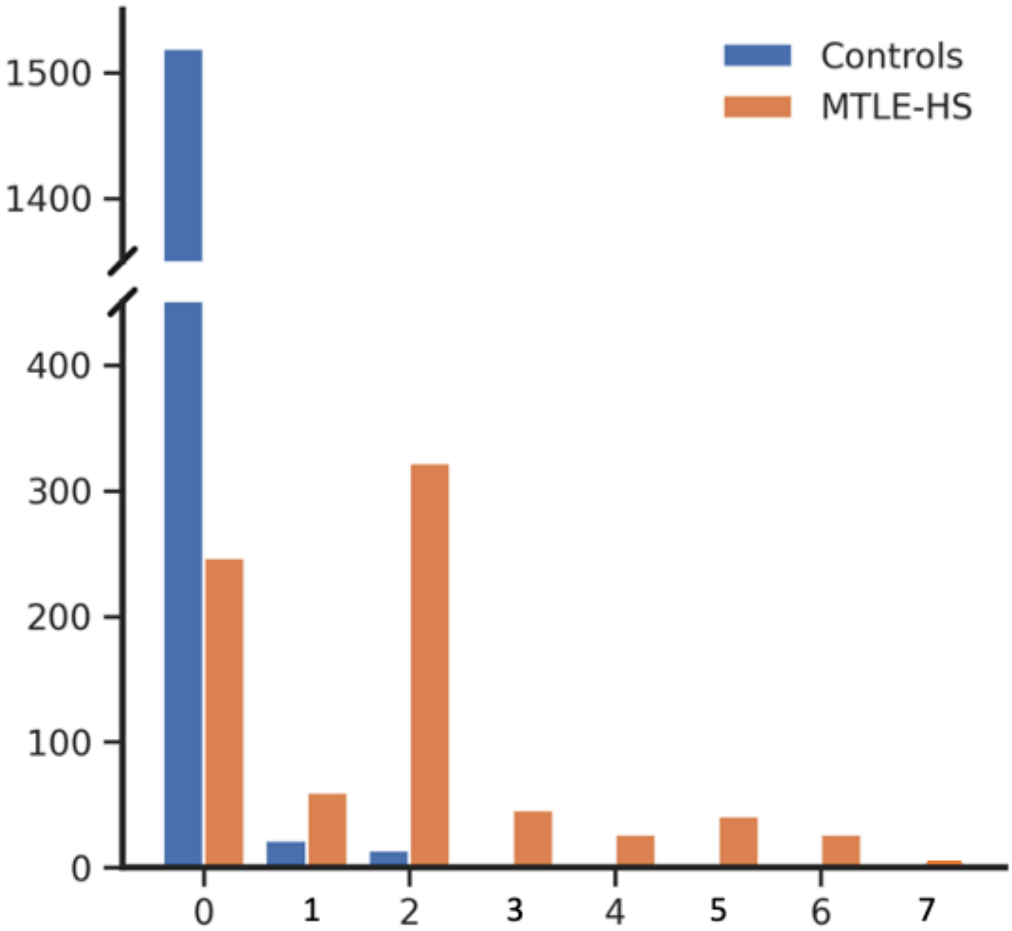

Figure 5.2 EBM Stage Distribution: Histogram showing stages (*x*-axis) assigned to people with MTLE-HS and controls and the corresponding count (*y*-axis). Stage 0 is assigned to subjects with no statistically detectable abnormal regional brain measure based on the T1W MRI scans. EBM places subjects with abnormal features progressively, such that subjects in stage 7 exhibit abnormality in all seven features.

5.3.4 EBM stage is associated with duration of illness and with response to ASMs in people with MTLE-HS.

People with MTLE-HS assigned to early EBM stages showed a relatively shorter illness duration than those in later stages (Figure 5.3). Duration of illness and stages 0-7 were significantly correlated in all people with MTLE-HS (Spearman's ρ=0.276, p=2.22x10^{-9}). After excluding patients at stage zero, the correlation was no longer significant (Spearman's ρ=0.046, p=0.42). Thus, the correlation was driven by the significant difference in duration of illness between EBM stage zero and non-zero (t=-6.61, p=1.09x10^{-10}). The same pattern was observed for age of onset: EBM stage and age of onset were negatively

correlated (ρ=-0.17, p=9.76x10^{-5}), but the effect vanished in the subset of patients at stages 1-7 (ρ=0.01, p=0.85). Age at onset was significantly later for patients in stage zero compared to those in non-zero stages (t=4.52, p=7.84x10^{-6}). EBM stages did differ between people with MTLE-HS who were resistant (N=336) or responsive (N=45) to ASMs in the 12 months prior to MRI (AUC=0.62, p=0.006, Mann-Whitney U test).

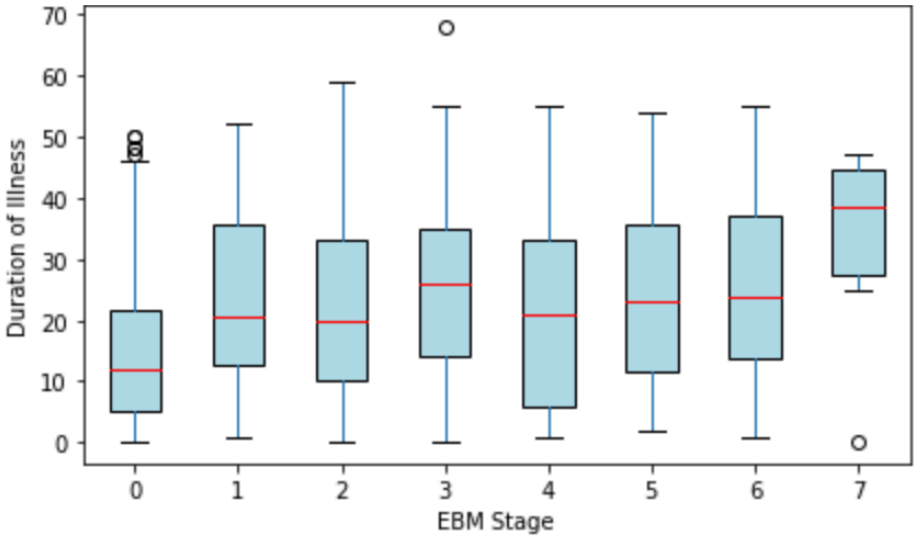

Figure 5.3 Distribution of duration of illness per EBM stage: Box plots showing distribution of duration of illness (in years) of corresponding EBM stages 0-7 assigned to people with MTLE-HS. Patients assigned to EBM stage 0 showed a shorter duration of illness compared to those assigned to the remaining EBM stages.

5.4 Discussion

In this multi-centre ENIGMA-Epilepsy consortium dataset we compared regional brain measures of surface area, cortical thickness, subcortical volumes as well as asymmetry measures for all brain regions between people with MTLE-HS and controls to identify features for the disease progression modelling. Main observations were volume reductions (and ventricular expansion) in nearly all subcortical regions ipsilateral as well as contralateral to the seizure focus. As expected in people with MTLE with hippocampal sclerosis, the strongest effect appeared in the ipsilateral hippocampus. Moreover, the

comparison with controls confirmed thinner cortices and reduced surface area in people with MTLE-HS, with effects being more pronounced in ipsilateral regions. Notably, measures of cortical thickness exhibited very pronounced distinction between people with MTLE-HS and controls, compared to measures of surface area. Here, the measured surface area depends on the number of columns containing neurons that run perpendicular to the cerebral surface, while cortical thickness is influenced by the number of cells within these columns (Rakic, 1995; Mountcastle, 1997). Moreover, previous studies have reported distinctive genetic influence on cortical thickness measures compared with measures of surface area (Panizzon *et al.*, 2009; Eyler *et al.*, 2012; Chen *et al.*, 2013; Hofer *et al.*, 2020; Schmitt *et al.*, 2020). Thus, the distinction in cortical thickness and surface area we report on, may reflect the distinct interplay of genetic factors influencing these neuroanatomical measures.

For the progression modelling we retained only features exhibiting a strong effect size between people with MTLE-HS and controls ($|d| \geq 0.5$;Figure 5.1; and 0.4 for a sensitivity analysis (Supplementary Table S3). The EBM applied to these data estimated an ordering of increasing pathological differences in the ipsilateral, contralateral brain regions and increased asymmetry in the hippocampal volume for people with left and right MTLE-HS analysed together, along with a measure of certainty of the acquired ordering (Figure 5.1). Furthermore, people with left and right MTLE-HS when analysed separately, had a similar progression pattern as when analysed together. However, for people with right MTLE-HS, the thalamus proceeded the cortical regions compared to the sequence of regions in people with left MTLE-HS. As expected for $|d| \geq 0.4$ patients with hippocampal sclerosis, measures quantified from the hippocampus were placed earlier compared to other brain regions: bilateral neocortical regions (e.g., precuneus and superior parietal lobule), the bilateral thalamus as well as the bilateral lateral ventricles (Supplementary Figure S4). Despite cortical regions having lower effect sizes compared with lateral ventricle measures, cortical and subcortical regions were staged before the lateral ventricles. Thus, EBM does not stage features based on effect sizes of the brain measures.

Besides the underlying mechanisms of epileptogenesis, hippocampal volume reduction and increased asymmetry may also be caused by a genetic predisposition to hippocampal sclerosis. Evidence supporting this comes from frequent observations of hippocampal abnormalities in healthy siblings of people with MTLE (Kobayashi *et al.*, 2002; Tsai *et al.*, 2013; Vaughan *et al.*, 2017; Long *et al.*, 2020), along with an association identified in a GWAS (Kasperavičiute *et al.*, 2013). However, cortical thinning likely represents disease-related effects since these changes have not been reported in healthy siblings (Alhusaini *et al.*, 2019). Furthermore, the progression pattern included decline in thalamic volume, which is a common feature in MTLE-HS (Bernhardt et al., 2012; Keller et al., 2008; Pulsipher et al., 2007; Seidenberg et al., 2008) and may be linked to the strong structural connectivity between the hippocampus and the thalamus (Bernasconi et al., 2004; Keller et al., 2008; Maller et al., 2019).

At first glance, it appears surprising that many people with MTLE-HS were assigned stage 0 despite the loss of hippocampal volume being considered as one of the hallmark signs of MTLE-HS. Two factors contribute to this discrepancy. Firstly, the radiologic diagnosis of hippocampal sclerosis is based on multiple imaging sequences, whereas hippocampal atrophy, as defined on T1W images is only one component of hippocampal sclerosis (Jin *et al.*, 2018). This is supported by our observation that the fraction of stage 0 MTLE-HS varied across centres (Supplementary Figure S6) and may therefore reflect differences between regional practices and capabilities to detect and diagnose hippocampal sclerosis in imaging data. For instance, the MNI centre and UNICAMP, which contributed ~30% of stage 0 of people with MTLE-HS, were diagnosed from detecting hippocampal sclerosis on T2W MRI scans as reported in Bernasconi *et al.*, (2019) and Coan *et al.*, (2015) respectively. Secondly, even though we observed a large group effect size for hippocampal volume difference in the whole cohort (d=-1.76), there is significant variability in volume loss at the individual level. In fact, about half the patients with hippocampal sclerosis exhibit measures of hippocampal volume that is within the normal range (Coan *et al.*, 2014); this is also the case in the ENIGMA-Epilepsy cohort (Supplementary Figures S2 and S5).

A study by Kong *et al.*, (2018) concluded that in regions of the left hemisphere, healthy people have thicker cortical thickness and smaller surface areas. Therefore, the BASI measures computed here were not able to factor in the innate asymmetry of brain regions. Moreover, the BASI measures of brain regions with bilateral changes would not be easily distinguishable from those not affected. As we analysed people with left and right MTLE-HS, the BASI measures were employed to detect unilateral changes caused by pathological mechanisms of MTLE-HS.

Longitudinal studies of PWE reveal cortical atrophy beyond the expected range of normal aging (Alvim et al., 2016; Bernhardt et al., 2009; Coan et al., 2009; Liu et al., 2003). Moreover, recent longitudinal studies of people with focal epilepsy (Galovic et al., 2019, 2020) found progressive atrophy in the contralateral regions of the parietal and frontal lobes, which was also featured in our study when using the more lenient cut-off (Supplementary Figure S4). Overall, we find that our regional disease progression sequence, which is based on cross-sectional data, agrees with previous findings in longitudinal cohorts that show the progressive nature of structural changes in MTLE-HS (Bernhardt et al., 2009; Bernhardt et al., 2013; Caciagli et al., 2017). The contralateral hippocampal volume (d =−0.14) missed the inclusion threshold for the EBM. Thus, the analysis could not provide further insights on whether untreated unilateral hippocampal sclerosis will lead to bilateral hippocampal sclerosis. However, PWE assigned to later EBM stages did present with reduced volume in the contralateral hippocampus, whereas this was not the case for PWE assigned to earlier stages (Supplementary Figure S5), illustrating the potential of EBM.

There are only few longitudinal imaging studies up to date detailing the long-term effect of MTLE-HS on the cortex. However, duration of illness has been used as a proxy for progression in various cross-sectional studies (Bernasconi, Natsume and Bernasconi, 2005; McDonald *et al.*, 2008; Caciagli *et al.*, 2017; Whelan *et al.*, 2018). Moreover, within study by Whelan et al., (2018), changes in numerous neocortical regions and subcortical volumes were negatively

correlated with duration of illness. However, these results were driven by epilepsies without hippocampal sclerosis; no correlations within the left MTLE-HS subgroup were found to be statistically significant, and within the right MTLE-HS group significant correlations were limited to the ipsilateral hippocampus, putamen, thalamus, contralateral transverse temporal gyrus, and ipsilateral caudal middle frontal gyrus. Therefore, the marginal correlations between EBM Stages 1–7 and duration of illness in people with MTLE-HS agree with these earlier observations.

The study by Zhang et al., (2017) suggested that in addition to the ipsilateral hippocampal volume, the grey matter volumes of the bilateral frontal lobes and cerebellar hemispheres were negatively correlated with duration of illness. However, in the same study, the lifetime number of seizures, another proxy for disease severity, was investigated and was correlated with structural changes in a different set of brain regions. Thus, either measure may capture different aspects of disease severity, and the relationship between disease duration and structural changes of the brain may be more complex. In our study, while disease duration and response to ASMs were the most apparent and plausible factors to investigate, they may not be the primary variables influencing the sequence of changes detected by the EBM.

In addition, Thom et al. (2011) applied the Braak staging (Braak *et al.*, 2006) for the progression of neurofibrillary tangle pathology in people with Alzheimer's disease and MTLE-HS. Their study reported neurofibrillary tangles in the hippocampus as an early event, followed by changes in brain regions structurally connected with the hippocampus. However, their study found no association between the Braak stages and the duration of illness or age of onset of epilepsy. This emphasizes the intricate and complex nature of the progression of pathological mechanisms involved in epilepsy and the duration of illness.

In summary, the EBM inferred the most likely sequence of structural changes in the brain from cross-sectional data derived from T1W MRI. The model could be further improved by considering measures from diffusion MRI scans to include

the role of white matter abnormalities in disease progression (Hatton et al., 2020; Sisodiya et al., 2020).

There were several limitations in our study. First, this ENIGMA-Epilepsy cohort is not a population-based cohort but represents data mostly from tertiary epilepsy centres and therefore the findings may not be generalisable to the overall epilepsy population. Also, within the ENIGMA-Epilepsy cohort, we observed sampling bias regarding availability of ASM response data (Supplementary Table S4); PWE with missing response data were younger, diagnosed more recently, and had later age at onset. Second, although the results were robust under bootstrap validation, they would benefit from a validation in a longitudinal cohort. Once validated, the EBM can be used to stage people with MTLE-HS in other cohorts and help establish machine learning-based disease staging as a potential tool in a clinical setting. However, designing well-powered longitudinal studies in patients and controls is challenging, especially since people with MTLE-HS who are AMS resistant may eventually undergo epilepsy surgery (Caciagli *et al.*, 2017). Third, clinical features such as frequency of seizure, pattern of ASM resistance and lifelong ASM exposure were not available in the ENIGMA-Epilepsy dataset. This would prove difficult to ascertain retrospectively but should be considered in future work. Finally, the use of specific ASMs may affect disease progression and, in some cases, even amplify tissue loss in epilepsy and should be considered in future analysis (Tondelli *et al.*, 2020).

In conclusion, we compared people with MTLE-HS to controls on range of cortical and subcortical features for surface area, cortical thickness, volume and their asymmetry between hemispheres, and used this information to produce a sequence of progressive pathology. The work indicated that the predicted disease stages may be associated with duration of illness. Further work is needed to investigate the link between disease progression stages and clinically relevant information such as ASM resistance, seizure frequency or severity.

Chapter 6 Novel imaging-derived subtypes of epilepsy based on structural changes in the brain

6.1 Introduction

In the previous chapter we have looked at estimating the progression sequence and staging of people with MTLE-HS based on structural changes of grey matter regions. Here, we aim to extend our analysis to a broader cohort of individuals with common epilepsies, with the goal of generalizing disease staging across a wider population. Additionally, numerous research studies have reported PWE have microstructural changes in white matter tracts compared to healthy controls, which are also considered to be of a progressive nature (Yasuda *et al.*, 2010; Winston *et al.*, 2014; Vaughan *et al.*, 2016; Buksakowska *et al.*, 2019; Hatton *et al.*, 2020). These regional changes in the brain among PWE vary across different epilepsy syndromes.

Hence, we hypothesise that subtypes of epilepsies exist based on unique progression of structural changes in both grey matter regions and white matter tracts. To investigate this, we apply SuStaIn to investigate progression patterns of changes detected on T1W MRI and DTI scans, which were obtained from the ENIGMA consortium (Whelan *et al.*, 2018; Hatton *et al.*, 2020), consisting of people with common epilepsies. Identifying these novel imaging-derived subtypes of epilepsy will allow us to explore the association between structural changes of the brain and clinical variables from a fresh perspective.

We know that resistance to ASMs is not specific to any of the epilepsy syndromes. Therefore, we aim to investigate whether the response to ASMs differs among the imaging-derived subtypes estimated by SuStaIn. Furthermore, from previous studies we know that patients with initial precipitating injury (IPI) develop mesial temporal sclerosis (MTS), where the extent of atrophy is believed to be progressive (Mathern, Pretorius and Babb, 1995). However, little is known about the impact of IPI on the progression of structural changes in

other brain regions. Similar to EBM, SuStaIn assigns each patient within the imaging-derived subtypes with a disease stage based on the estimated sequence of structural changes in the brain. Consequently, we aim to investigate whether disease stages estimated by our model are related to clinical markers of disease duration, response to ASMs or presence of IPI. Exploring these relationships will enhance our current understanding of the mechanisms underlying structural brain changes and provide deeper insights into the pathology of epilepsy.

6.2 Methods

6.2.1 Data

We used data previously collected and analyzed by the ENIGMA-Epilepsy working group (Whelan *et al.*, 2018; Hatton *et al.*, 2020; Sisodiya *et al.*, 2020). The data features subcortical volumes and cortical morphometrics extracted from T1W MRIs using FreeSurfer Version 5.3.0 (Dale, Fischl and Sereno, 1999; Fischl, 2012) as well as Tract-Based Spatial Statistics extracted from DTI MRI following the ENIGMA-DTI protocol (http://enigma.ini.usc.edu/ongoing/dti-working-group/). Additional information on the collection, quality control, and processing of T1W and DTI MRI can be found in Whelan *et al.*, (2018) and Hatton *et al.*, (2020), respectively. The combined data comprises of subjects, namely PWE and healthy controls from 15 centres. All PWE were assessed by a specialist at each centre, using the International League Against Epilepsy (ILAE) criteria for diagnosis (Berg *et al.*, 2010).

For this study we retained only PWE where both T1W and DTI MRI were available. Following the processing with FreeSurfer based on the Desikan-Killiany atlas (Desikan *et al.*, 2006), we extracted eight subcortical volumes and 34 cortical volumes per hemisphere. Missing regional values were imputed using a singular value decomposition (SVD)-based approach (Troyanskaya *et al.*, 2001; Lopez *et al.*, 2022). To further reduce the dimensionality for the down-steam analyses, the cortical volume features were grouped into left and right temporal, occipital, parietal and frontal lobes as well as the left and right cingulate, resulting in ten cortical features. From DTI scans, FA was extracted

for 39 tract bundles using the Johns Hopkins University (JHU) atlas as detailed previously (Hatton et al., 2020). We aggregated measures of 39 tracts from the left and right hemispheres following recommendations by Kochunov *et al.*, (2014), resulting in a total of 23 tracts. FA values were shown to exhibit stronger effect sizes than MD values in the same cohort (Hatton *et al.*, 2020), hence, this analysis focused on FA rather than MD. Thus, the features comprise 16 subcortical volumes, 10 cortical volumes and the average FA of 23 white matter tracts.

In addition to the features, sex and age at MRI were available for all subjects. For PWE a sub-diagnosis was available (left/right MTLE-HS, left/right NL-TLE, GEE, extra-temporal lobe epilepsy (ETLE), or unspecified). Moreover, for PWE, duration of illness, age of disease onset, and seizure frequency in the 12 months prior to the MRI were recorded. Here, ASM responsive status was defined as complete seizure freedom and ASM resistance defined as one or more seizures in the 12 months before MRI. Records of IPI for 50 PWE were available from one contributing centre.

6.2.2 Data Harmonization and confound adjustment

By design, the ENIGMA-Epilepsy dataset is a multi-centric cohort and therefore the data are subject to centre-specific biases arising from various factors. To harmonize the imaging data across centres NeuroCombat (Fortin *et al.*, 2018) was applied. NeuroCombat (v0.2.12 in Python) was executed separately for the 26 regional brain volumes extracted from T1W MRI and for the 23 tract level FA measures extracted from DTI MRI. The individual centre was used as the batch effect and ICV, diagnosis (controls versus epilepsy subtype), age at imaging and sex were used as the biological co-variates of interest to be retained.

To convert the regional measures to z-scores that reflect the deviation from the expected value, given a subjects' age and ICV we built normative models for each brain region (Marquand *et al.*, 2016; Janahi *et al.*, 2022) . In brief, we used Gaussian Process Regression (GPR) with a radial basis function (RBF) kernel

and white noise implemented in the sklearn python library (Pedregosa *et al.*, 2011) to estimate the regional measures in dependence of age and ICV. Next, using the trained GPRs, for a given subject we computed the expected mean and standard deviation of the regional measure and used these to convert the subject' measure into a z-score. These z-scores were then used for disease progression modelling in the SuStaIn algorithm.

6.2.3 Subtype and Stage Inference (SuStaIn) algorithm

The SuStaIn algorithm which is used to estimate the imaging-derived subtypes is previously described in Section 3.5. Here, we used z-score SuStaIn implemented in pySuStaIn (Aksman *et al.*, 2021), where abnormality of a measurement is expressed by exceeding a series of z-score cut-offs. The number of cut-offs and the exact values can be set for each of the brain regional measures. For this analysis we defined the suitable imaging-derived measures and z-score thresholds as follows: only imaging-derived measures where at least 7% of PWE exhibited a z-score of 2.0 or larger were considered within a SuStaIn model; the cut-offs of 1.0 and 2.0 were used for that measure. Further cut-offs of 3.0 and 4.0 were added in circumstances where at least 5% of PWE exceeded that z-score value for that imaging-derived measure. For instances, for left hippocampus volume there may be four severity cut-offs at z=1,2,3,4, while for the FA of the internal capsule tract there were only two severity cut-offs at z=1,2. Finally, to preserve symmetry we added the contralateral feature with the same number of thresholds (in case it was not selected by its own merit).

The SuStaIn algorithm estimates a progression sequence based on maximum likelihood of the data and by using MCMC samples to estimate the uncertainty of the sequence (for further details see Section 3.4.1). Here, the number of subtypes is an input parameter of SuStaIn, and the optimal number of subtypes must be determined empirically from the data. In our case, we used a model comparison approach and computed the CVIC (Gelman, Hwang and Vehtari, 2014) which evaluates the likelihood of the held-out data in a cross-validation setting. A series of CVIC values were computed by varying the number of subtypes from one to five in the SuStaIn model, each time using five-fold cross-

validation. The optimal number of subtypes was determined by minimising the CVIC score. More details of the SuStaIn algorithm and the CVIC metric can be found in Young *et al.*, (2018).

6.2.4 Statistical Analysis

The SuStaIn algorithm assigns each patient a probability of belonging to each of the inferred imaging-derived subtypes based on changes recorded from their MRI scans. To analyse the clinical relevance of these imaging-derived subtypes we only consider confident subtype assignment (with probability > 0.5). Here, we hypothesized that patients assigned to distinct imaging-derived subtypes map to known clinical syndromes, which we investigated using a chi square test. Furthermore, as certain clinical syndromes, for example people with MTLE-HS, tend to be ASM-resistant compared to others, we hypothesized that patients assigned to distinct imaging-derived subtypes were associated with a drug-response status. We used logistic regression to test for associations between imaging-derived subtype assignments and dichotomous outcomes such as ASMs response and IPI. These models were adjusted for age, sex, duration of illness and age of disease onset.

Moreover, based on previous results (Lopez *et al.*, 2022), we hypothesized that patients assigned to advanced stages by SuStaIn were more likely to have a longer duration of illness, to have earlier disease onset, and to be resistant to ASMs. To determine whether individuals' disease stage is related to illness duration or age at onset, we computed Spearman rank correlations between the stage and the duration of illness (in years) at the time of imaging and age at onset, respectively. We also employed a logistic regression model to investigate whether the disease stage served as a predictive factor for the response to ASMs, as well as the IPI status, while adjusting for subtypes, age and sex, duration of illness and age of disease onset.

6.3 Results

Our cohort comprised a range of epilepsy syndromes that were recruited from 15 centres. Table 6.1 and Supplementary Table S5 display the overall demographics from our cohort split by centre and epilepsy syndrome, respectively. For this analysis we used data from 827 healthy controls and 1048 PWE across all included syndromes: 274 left MTLE-HS, 219 right MTLE-HS, 147 left NL-TLE, 109 right NL-TLE, 70 GGE, 120 ETLE and 109 labelled as unspecified. On average, each centre contributed a group of patients, ranging from young adults in their 20s to adults over 60 years (median 36.26 years; IQR 11.65 years) and a similar group of healthy individuals (median 37.1 years; IQR 10.98 years). The sex distribution within the dataset had a slight majority of females (60.40% of PWE and 57.67% of healthy controls). Overall, 1.08% of measures from T1W scans were missing which we imputed as described. Duration of illness and age of disease onset was available for 925 and 983 PWE, respectively. The duration of illness ranged from recently diagnosed to 60 years (median 20.0 years; IQR 13.0 years). Pre-imaging seizure frequency was available for 797 PWE. Of the 50 PWE with the recorded IPI status, 30 PWE had reported an IPI incident, while the remaining 20 PWE did not have any IPI incident.

6.3.1 Imaging-derived features selected for input into SuStaIn:

The features generated by combining FA values from individual tracts were included in our analysis as the corpus callosum, bilateral (left and right) cingulum, internal capsule, fronto-occipital fasciculus and corona radiata (Supplementary Table S6). Of the total 49 imaging-derived features obtained from FA and T1W measures, only those imaging-derived features (n=23) that demonstrated a subject proportion of at least 7% with z-scores above 2 were retained (Supplementary Figure S7). T1W MRI features included here were the bilateral hippocampus and bilateral thalamus volume. Among the analysed features, z-scores of up to 3.0 were observed in the FA of the corpus callosum tracts and z-scores of up to 4.0 in the left and right hippocampal volume.

Table 6.1 Demographics: Demographics of subjects used in analysing subtyping and staging.

Centre	Age controls	Age cases	DURILL cases	AO cases	Total Male controls	Total Female controls	Total controls	Total Male cases	Total Female cases	Total cases	Total n
Bonn	37.9±12.6	41.2±12.5	23.7±14.1	17.5±11.5	12	18	30	28	33	61	91
CUBRIC	26.6±8.1	28.7±7.7	16.2±9.6	12.4±4.0	7	17	24	10	24	34	58
EPICZ	38.4±11.1	38.5±9.5	19.3±12.5	19.2±12.4	55	55	110	40	69	109	219
EPIGEN	34.8±9.5	35.8±9.1	19.4±11.0	16.3±13.3	39	28	67	21	33	54	121
Florence	32.2±8.8	34.4±8.1	19.0±12.1	14.0±9.0	16	14	30	3	2	5	35
HFHS	NA	38.8±13.5	19.1±12.9	19.1±16.9	0	0	0	41	62	103	103
IDIBAPS	33.1±6.0	36.4±9.7	17.3±10.7	18.8±12.0	23	29	52	35	46	81	133
MNI	30.7±7.4	33.1±9.7	16.0±11.2	17.1±9.7	24	22	46	50	64	114	160
MUSC	54.9±8.4	36.7±10.8	18.2±12.0	18.8±13.4	13	44	57	15	28	43	100
NYU	30.3±10.0	32.6±8.9	8.6±9.9	24.0±12.7	11	15	26	17	28	45	71
UCL	37.2±12.4	38.7±11.4	24.7±14.2	13.9±10.7	11	17	28	20	33	53	81
UCSD	38.2±15.9	35.6±11.7	15.9±14.1	19.4±13.4	16	9	25	26	28	54	79
UNAM	33.7±12.1	31.4±11.7	15.5±12.8	15.8±11.1	9	25	34	11	23	34	68
UNICAMP	35.7±10.8	40.3±9.9	27.6±12.3	12.5±9.8	94	166	260	86	149	235	495
MICA	31.9±4.8	36.2±12.1	15.1±12.7	21.2±12.4	20	18	38	12	11	23	61
Total	36.26 ± 11.65	37.1 ± 10.98	19.95 ± 13.34	16.56 ± 11.29	350	477	827	415	633	1048	1875

AO: age of disease onset, DURILL: Duration of illness, Bonn: University Hospital Bonn, CUBRIC: Cardiff University Brain Research Imaging Centre, EPICZ: Epilepsy Centre Cantazaro, EPIGEN: Epilepsy Genetics Dublin, Florence: University of Florence, HFHS: Henry Ford Health System, IDIBAPS: Institut D'Investigacions Biomèdiques August Pi I Sunyer research center, MNI: Montreal Neurological Institute, MUSC: Medical University of South Carolina, NYU: New York University, UCL: University College London, UCSD: University California San Diego, UNAM: Universidad Nacional Autónoma de México, UNICAMP: Universidade Estadual de Campinas, Brazil, MICA: Multimodal Imaging and Connectome Analysis Laboratory from Canada.

6.3.2 Optimal number of subtypes uncovered by SuStaIn

The CVIC plot used to determine the optimal number of imaging-derived subtypes is shown in Supplementary Figure S8. The CVIC score steadily decreased between models with one to four subtypes which indicates improvement of out-of-sample likelihood in the consecutive models. However, the CVIC increased for the model with five subtypes. Thus, four was the optimal number of imaging-derived subtypes was supported by the data.

6.3.3 Imaging-derived subtypes uncovered by SuStaIn:

In our analysis we first tested how the imaging-derived subtypes identified by SuStaIn correspond to the seven different epilepsy syndromes that are included in the ENIGMA cohort. The four imaging-derived subtypes uncovered, based on distinct progression patterns, are shown in Figure 6.1 and Supplementary Figure S9. The first subtype (*Left Limbic)* started with volume decline in the left hippocampus and left thalamus followed by decrease in FA in white matter tracts of the left cingulum, left fornix/stria terminalis and left external capsule, corpus callosum and contralateral regions. Subtype 2 (*Right Limbic) is* very similar to subtype 1 but mirrored, i.e., starting with volume loss in the right hippocampus and right thalamus, left hippocampus followed by decrease in FA in white matter tracts of the right and left cingulum. Subtype 3 (*Late Right Limbic)* started with changes in FA measures of white matter tracts of the bilateral external capsule, corpus callosum, fronto-occipital fasciculus, cingulum followed by changes in right limbic regions from stage 14 onwards. Lastly, subtype 4 (*Bilateral Tracts-Only)* was driven by changes in the white matter tracts of the posterior thalamic radiation, sagittal stratum, corpus callosum and superior longitudinal fasciculus, corona radiata and external capsule bilaterally.

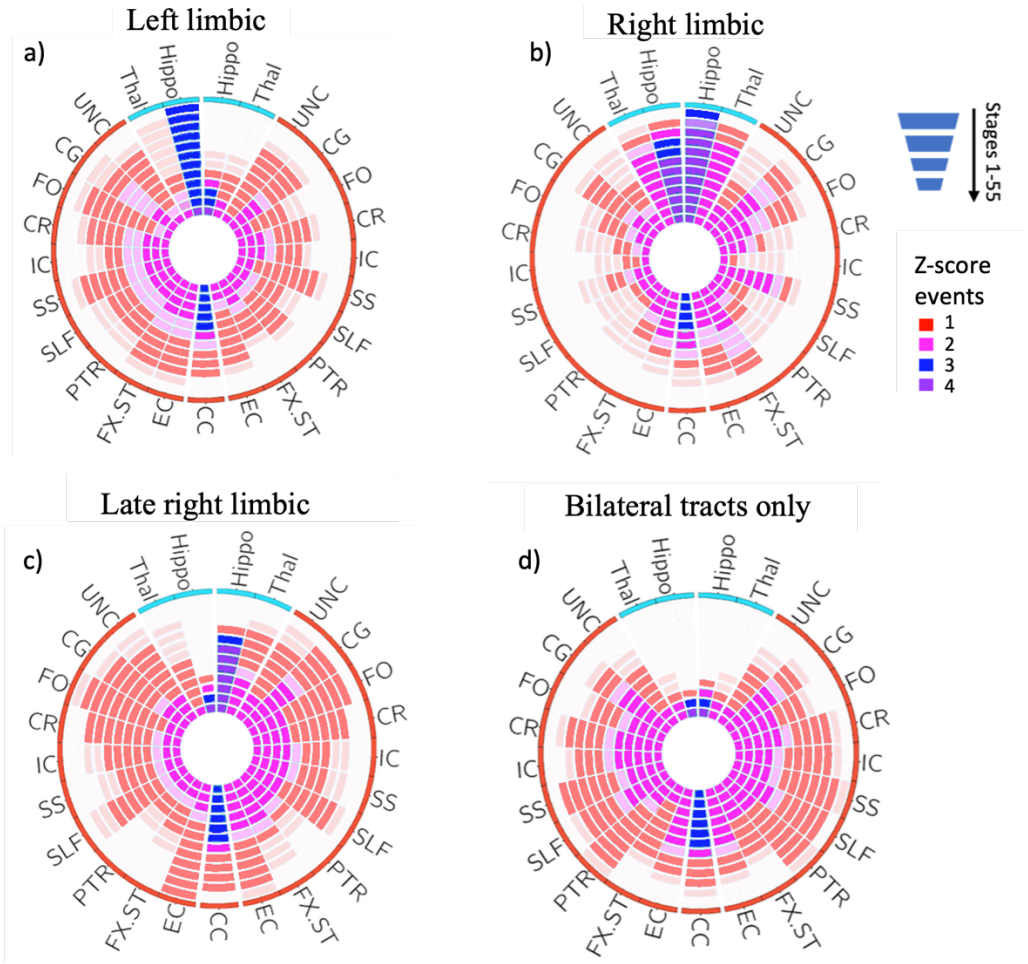

Figure 6.1 Subtypes and their progression patterns uncovered in SuStaIn: Circular plots showing four subtypes with distinct progression patterns identified in SuStaIn. Progression starts from outer-circle and moves inwards. The four colours correspond to the four distinct z-score events, while the transparency represents the uncertainty of assigning the feature at that position, with no transparency indicating the highest certainty. Left Limbic subtype had a high certainty of the first feature as the left hippocampus to become abnormal. Similarly, Right Limbic subtype had a high certainty of changes starting in the right hippocampus. The Late Right Limbic and Bilateral Tracts-Only were mainly driven by changes in white matter tracts. UNC: Uncinate fasciculus, CG: Cingulum, FO: fronto-occipital fasciculus, CR: Corona radiata, IC: Internal capsule, SS: Sagittal stratum, SFL: Superior longitudinal fasciculus, PTR: Posterior thalamic radiations, FX.ST: fornix/stria terminalis, EC: External capsule.

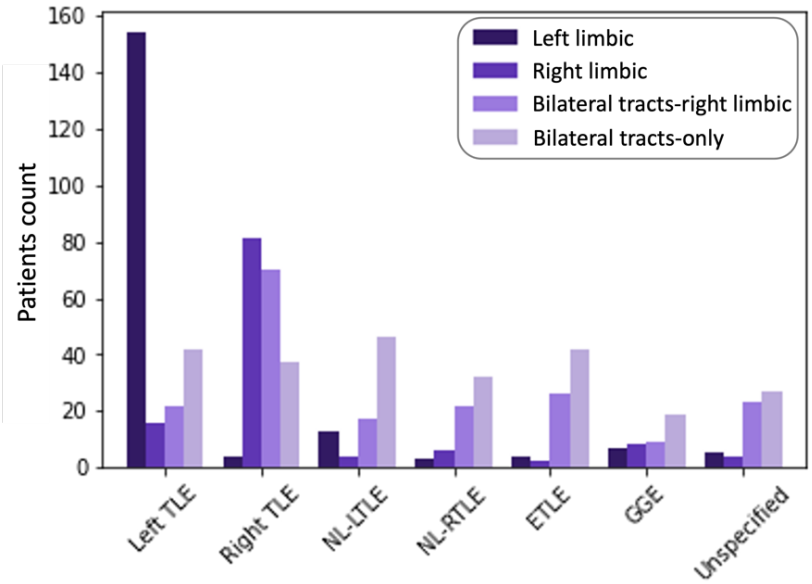

Figure 6.2 Distribution of subjects assigned to subtypes across diagnostic labels in T1W-FA model: Majority of left MTLE-HS were clustered in left limbic subtype, right MTLE-HS patients in right limbic subtype and late right limbic subtype. Bilateral Tracts-Only subtype consisted of a set of the common epilepsies.

6.3.4 Imaging-derived subtypes are associated with epilepsy syndrome, age at imaging and duration of illness

The SuStaIn algorithm estimated on the ENIGMA-Epilepsy cohort can be used to assign PWE into imaging-derived subtypes and place them between stage 0 (i.e., no imaging feature reached a z-score threshold) and stage 48 (i.e., all features exceeded the maximal z-score threshold) as shown in Supplementary Figure S10. To investigate the association of imaging-derived subtypes assigned to PWE and clinical variables, we only considered confident subtype assignments, i.e., assignments with a probability larger than 0.5. Furthermore, since stage 0 represents 'no abnormality' and cannot be attributed to a subtype, we removed 79 PWE placed at stage 0 from further analyses, leaving the following subtyped PWE: 661 with duration of illness, 708 with age of disease onset, 99 that were responsive and 475 that were resistant to ASMs. Patients assigned to the four imaging-derived subtypes had a similar distribution of sex

(χ^2=3.9, p=0.26, dof=3) and age of disease onset (one-way ANOVA t=1.77, p=0.14). Clinical epilepsy syndrome showed a strong association with the imaging-derived subtype (χ^2=495.16, p=1.08x10^{-93}, dof=18; Figure 2).

The Left Limbic subtype was composed of a majority of left MTLE-HS, the Right Limbic subtype of right MTLE-HS, while Late Right Limbic and Bilateral Tracts-Only subtypes were composed of a mixture of all syndromes, including left and right MTLE-HS. In the Late Right Limbic subtype, only patients with right MTLE-HS were placed beyond stage 14, which corresponds to changes in the right hippocampus (Supplementary Figure S11). Thus, the majority of people with right MTLE-HS were distributed between the Right Limbic (36%) and Late Right Limbic subtypes (42%). Right MTLE-HS PWE in the Late Right Limbic subtype displayed lower FA values compared to right MTLE-HS PWE assigned to the Right Limbic subtype (Supplementary Figure S12). Furthermore, there was no difference between people with right MTLE-HS assigned in Right Limbic or Late Right Limbic subtype with respect to age, sex, duration of illness, age of disease onset, centre or the response to ASMs (Supplementary Table S7).

Between the progression subtypes there were also differences in age at imaging (one-way ANOVA t=10.82, p=5.7x10^{-7}), duration of illness (one-way ANOVA t=11.33, p=2.9x10^{-7}) and contributing centre (χ^2=93.19, p=2.4x10^{-6}, dof=39) (Supplementary Figure S11). We report that the subtype assignment was not associated with ASM response in the logistic regression (F=5.9, p=0.11). However, a marginal association was observed while predicting the IPI status from the imaging-derived subtypes in the logistic regression model (F=9.6, p=0.02). Likewise, using logistic regression with IPI status as the response variable, we examined the association between patients in the Left and Right Limbic subtypes, considered as a single group, and those in the white-matter-led subtypes (Late Right Limbic and Bilateral Tracts Only) as another group, resulting in a odds ratio of 0.21, p = 0.04 for the white-matter-led subtypes.

6.3.5 Imaging-derived staging is associated with duration of illness, age of disease onset and initial precipitating injury.

Considering patients across all four imaging-derived subtypes, the inferred disease stage was highly correlated with the duration of illness (Spearman rank correlation, (r=0.23, p=2.24x10^{-09}, N=661) while adjusting for imaging-derived subtype. Overall, PWE assigned to early stages within each subtype showed a relatively shorter illness duration than those in later stages (Table 6.2). However, the significance of the association varied across subtypes, ranging from non-significant in the Left Limbic subtype (ρ=0.03, p=0.68, N=162) to highly significant in the Late Right Limbic subtype (ρ=0.46, p=1.7x10^{-10}, N=169). To corroborate whether the high correlation was led by changes in white matter tracts we recalculated the correlation after excluding PWE with right MTLE-HS in the Late Right Limbic subtype: the association between disease stages and duration of illness remained significant (ρ=0.30, p=0.001, N=107).

Table 6.2 Clinical associations: Associations between imaging-derived disease stages assigned by SuStaIn and clinical variables

Subtype	DURILL vs stages	AO vs stages	ASM RESPONSE vs stages
Left limbic	r=0.03, p=0.68, N=162	r=-0.03, p=0.64, N=181	F=33.7, p=0.38, N1=20, N2=135
Right limbic	r=0.23, p=0.0125, N=112	r=-0.17, p=0.053, N=118	F=26.4, p=0.11, N1=12, N2=88
Late right limbic	r=0.46, p=1.7x10^{-10}, N=169	r=-0.39, p=3x10^{-8}, N=182	F=27.7, p=0.83, N1=27, N2=119
Bilateral tracts-only	r=0.26, p=6x10^{-5}, N=218	r=-0.12, p=0.058, N=227	F=37.22, p=0.41, N1=40, N2=133

r= pearson's correlation; p=p-value; N=sample size; F=F statistic; N1=sample number for ASM responsive patients; N2=sample number for ASM resistant patients.

Like for duration of illness, considering patients across all four imaging-derived subtypes, the inferred disease stage was negatively correlated with the age of disease onset (Spearman rank correlation, (r=-0.13, p=0.0002, N=708) while

adjusting for imaging-derived subtype. Within each imaging-derived subtype, age of onset showed an overall trend of negative correlations with disease stage (Table 6.2). However, magnitude and significance were reduced compared to the associations with duration of illness.

We report that within our cohort the disease stages were not predictive of the response to ASMs (Table 6.2). Here, on an average, patients that were responsive to ASMs (N1=99) were placed in the early stages and those that were resistant (N2=475) were placed in later stages. Interestingly, we observed a marginal association between the disease stages and IPI status from the logistic regression model ($F=40.5$, $p=0.018$).

6.4 Discussion

We applied SuStaIn to a large multi-centre neuroimaging study of epilepsy, identifying distinct patterns of progression of structural changes in the brain, and assigning PWE to four different imaging-derived subtypes. The features used to train our model included z-scores from measures derived from T1W MRI and FA values acquired from DTI scans. These measures represent the pathological impact on grey matter regions and axonal integrity of white matter tracts, respectively. The use of z-scores allowed us to track the severity of structural changes, thus providing a fine-grained measure of progressive changes in regional brain measures.

Among the identified imaging-derived subtypes, the Left Limbic and Right Limbic subtypes predominantly consisted of people with MTLE-HS. Our analysis revealed a localised pattern of limbic system involvement in the Left Limbic subtype, characterised by volume decline in the left hippocampus and thalamus and decreased FA values in key association and commissural fibers that started on the left hemisphere before progressing to the right side. Conversely, the Right Limbic subtype exhibited mirrored structural changes in the right hippocampus and thalamus, along with altered FA values in the right and left cingulum, suggesting potential hemispheric lateralization of limbic

system dysfunction in our study population. This mirroring of structural changes suggests a hemispheric lateralization of limbic system dysfunction in people with MTLE-HS. The distinct structural changes between these two subtypes might reflect the unique functional roles played by each hemisphere, like emotional processing or memory. Overall, this initial sequence involving changes to grey matter in people with MTLE-HS is similar to our previous study (Lopez *et al.*, 2022). Beyond the grey matter, WM changes have been previously reported in ipsilateral and/or contralateral cingulum, fornix/stria terminalis, external capsule and corpus callosum in people with left and right MTLE-HS (Arfanakis *et al.*, 2002; Concha, Beaulieu and Gross, 2005; Gross, Concha and Beaulieu, 2006; Rodrigo *et al.*, 2007; McDonald *et al.*, 2010; Buksakowska *et al.*, 2019). However, our analysis identified the temporal sequence in which these changes occur and we used this sequence to investigate the clinical relevance of progressive structural changes in treatment response.

In addition, we uncovered an alternate progression pattern in people with right MTLE-HS, where changes started in the bilateral white matter tracts before progressing to the right hippocampus and right thalamus. This discovery aligns with recent studies that also document early-stage white matter abnormalities in epilepsy (Chen *et al.*, 2019; Luna-Munguia, Marquez-Bravo and Concha, 2021; Bartoňová *et al.*, 2023). Notably, the findings of Buksakowska *et al.*, (2019), analyzing 32 people with epilepsy, reinforce our observations, highlighting more widespread changes affecting bilateral white matter tracts in right MTLE-HS compared to left MTLE-HS. This result suggests that the progression of structural changes in the brain in left and right MTLE-HS are influenced by distinct pathological mechanisms, impacting grey matter regions and white matter tracts differently.

The progression pattern in the Bilateral Tracts-Only subtype seen in all the epilepsy syndromes, started with changes in white matter tracts that connects the thalamus to the cortex, and progressed to those tracts emerging from the thalamus to the pontine nuclei, and other brainstem structures. A higher proportion of people with GGE and non-lesional epilepsies were assigned to this subtype. This observation may not be immediately apparent when considering

the results of Hatton *et al.*, (2020), where FA measures in white matter tracts displayed distinct alterations between the left and right regions rather than exhibiting a bilateral effect. Here, it's important to note that SuStaIn estimates a imaging-derived subtype based on the best fitting model. The lack of patients assigned to late stages in this subtype suggests that there were no changes in limbic regions considered here.

In contrast, the staging of patients in the Late Right Limbic subtype distinctively indicated the changes in FA values of the left and right external capsule and other association fibers as early disease stages, before progressing to the hippocampus. Here, all syndromes were assigned up to stages representing abnormality in the white matter tracts, while right MTLE-HS patients were assigned to stages representing abnormality predominantly in the right limbic regions. This finding agrees with the earlier univariate analysis in the same cohort, which reported large effect sizes across all of the epilepsy syndromes compared to controls in the bilateral external capsule (Hatton *et al.*, (2020)). The external capsule, which connects the putamen to the cortex, is a route for cholinergic and corticostriatal fibers. Changes to these fibres have been implicated in poor cognitive performance (Nolze-Charron *et al.*, 2020). Hence, microstructural changes in the external capsule, cingulum and corpus callosum as early-stage events suggests an early disruption in fibres connecting the limbic system to the cortex.

The progression sequences of both the Late Right Limbic and the Bilateral Tracts-Only subtypes suggests that an initial disruption in the connecting fibres between neurons may also lead to pathological mechanisms that cause structural changes in the brain. This finding may explain the coexistence of focal and generalized epilepsy in a sub-group of patients with MTLE-HS (Jeha, Morris and Burgess, 2006; Betting *et al.*, 2010; Blume, 2010).

Furthermore, Gleichgerrcht *et al.*, (2021) reported that measures derived from T1W MRI were better in identifying laterality of MTLE-HS, whereas DTI based measures were better at diagnosing MTLE-HS from healthy controls. Similar to

our findings, Gleichgerrcht *et al.*, (2021) could not distinguish patients with NL-TLE from healthy controls. Our cohort with GGEs, NL-TLE, ETLE and unspecified epilepsy indicated grey matter regions analysed were intact. However, previous research has demonstrated that some patients with GGEs have changes in thalamus, superior mesiofrontal lobe and other cortical structures (Ciumas and Savic, 2006; Kim *et al.*, 2007; Boris C. Bernhardt *et al.*, 2009; Lin *et al.*, 2009). Here, the progression sequence estimated for GGEs is constrained by the absence of cortical structures, stemming from our selection criteria. Future analyses may benefit from a more comprehensive and inclusive set of features.

The imaging-derived subtypes we present share similarities with those documented by Xiao *et al.*, (2022), which utilized SuStaIn on a cohort of patients with focal and generalized epilepsies. The first subtype reported in Xiao *et al.*, (2022), was the Hippocampal subtype which was characterized by structural changes in the ipsilateral hippocampus, ipsilateral thalamus and subsequently in other cortical regions. This matches with the two Limbic-led subtypes detected in our cohort. Their second subtype was the Cortical subtype which had widespread changes in the cortical structures, followed by subcortical structures in the late stages, which matches with our Late Right Limbic subtype. Lastly, their Basal Ganglia subtype which had structural changes that started in the globus pallidus before spreading to other basal ganglia region, is similar to our Bilateral Tracts-Only subtype.

Moreover, in Xiao *et al.*, (2022), each of the Cortical and Basal Ganglia subtypes only contained about 10% of people with focal epilepsies, while the rest had generalized epilepsy. On the other hand, our Bilateral Tracts-Only subtype demonstrated a consistent proportion of all seven epilepsy syndromes included in our analysis. Hence, our study unveils a novel observation indicating that a subgroup of PWE may exhibit white matter abnormalities preceding alterations in grey matter regions. Such findings hold potential clinical significance for enhancing treatment outcomes, informing surgical decisions and monitoring disease progression.

We used duration of illness as a proxy for validating the disease stages positions estimated by our model, an approach commonly adopted in cross-sectional studies (Bernhardt et al., 2009; Caciagli et al., 2017; McDonald et al., 2008). With the exception of Left Limbic subtype, our staging distribution of all other subtypes indicated that patients of all syndromes staged early in the progression sequence had a shorter illness duration and a later disease onset. This observation also agrees with our previous finding of weak association of disease stages based on progressive changes and duration of illness (Lopez *et al.*, 2022). Hence, our findings suggest that the association between the duration of illness is more pronounced in relation to changes in white matter tracts as compared to changes in grey matter regions. This observation may be attributed to the greater sensitivity of FA measures in detecting microstructural alterations in white matter tracts, in contrast to the macro-level changes detected by cortical thickness measurements. Although the relationship between FA measures and cortical thickness is typically reported as linear (Kochunov *et al.*, 2011), the ability of FA measures to capture subtle microstructural changes in white matter may contribute to their stronger association with the duration of illness.

Overall, our staging assigned by SuStaIn for all syndromes indicates that response to ASMs was not associated with the extent of structural changes in the brain in epilepsy. In the future, SuStaIn staging information could also be combined with the type of prescribed ASM, seizure semiology, EEG data and type of epilepsy syndrome to predict treatment response. Using such features, previous studies have predicted the ASM efficacy with accuracy of up to 80%. (Wirrell *et al.*, 1996; Nicolson *et al.*, 2004; Mohanraj and Brodie, 2007; Caciagli *et al.*, 2014; Kamitaki *et al.*, 2022).

Our study demonstrates that disease stages were marginally associated with the patients' IPI status. Upon further investigation, we report a higher majority of patients (67%) with an IPI incident compared to those without an IPI incident (60%) were placed before stage 20. This can be attributed to the fact that patients from this centre having an IPI incident at childhood were only considered for presurgical evaluation after the age of 20 years of age.

There were several limitations in our study. First, this ENIGMA-Epilepsy cohort represents data mostly from tertiary epilepsy centres and therefore the findings may not be generalisable to the overall epilepsy population. Also, within the ENIGMA-Epilepsy cohort, we observed sampling bias regarding availability of ASM response data (Supplementary Table S8): PWE with missing response data were younger, diagnosed more recently and had a later age of onset. Second, results would benefit from a validation dataset and predicting other clinical variables such as cognitive score or seizure frequency. Lastly, given a larger cohort of patients with an IPI status, we would be able to further explore the longitudinal effects of an IPI on disease progression and its potential implications for treatment response and long-term outcomes. Additionally, investigating the interaction between an IPI and other relevant clinical factors such as type of ASM administered may provide valuable insights into the underlying mechanisms driving disease trajectories in epilepsy.

In conclusion, we identified four imaging-derived subtypes based on disease progression using features from T1W MRI and DTI scans were used to quantify changes in grey matter and white matter tracts respectively. Disease stages assigned to all syndromes correlated with duration of illness and age of onset. Therefore, once validated in a new cohort, our SuStaIn model trained on the ENIGMA-Epilepsy data could be used to stage patients of these syndromes with relevant clinical data. This could help establish connections between imaging-based disease stages and other clinical features such as seizure frequency, treatment outcomes, ASMs resistance patterns, surgical outcomes and psychiatric comorbidities.

Chapter 7 Conclusion and future work

7.1 Conclusion

We successfully investigated the association of facial asymmetry and structural changes in the brain in PWE, and reported they were independent of each other. Our collaborators also showed that facial asymmetry was higher in patients with focal epilepsy compared to those with IGE or healthy individuals. This indicates that the SAI measured could serve as a valuable tool for gaining insights into the mechanisms underlying focal epilepsy. However, to effectively implement the SAI measure in clinical settings, additional studies are necessary to determine the sensitivity and specificity of SAI measurements across different operators. Furthermore, future work incorporating longitudinal data will help understand the progression of facial asymmetry and severity of structural changes in the brain, and the effect treatments have on them.

We also examined regional brain measures in people with MTLE-HS and controls, unveiling a distinct, progressive sequence of structural changes in grey matter regions. Importantly, the duration of illness correlated with assigned stages, thus validating the identified sequence. Extending our analysis to a wider cohort of common epilepsies, we applied SuStaIn, revealing four imaging-derived subtypes with unique progression patterns in brain structure. These included two limbic-led subtypes, a white matter-led subtype, and a late limbic subtype, suggesting early involvement of both abnormal grey and white matter tracts in disease pathology. Although our study lacked validation on an untrained cohort, we aim to assess the clinical viability of our EBM and SuStaIn model by applying it to an external dataset and evaluating the assigned stages against clinical variables.

7.2 Future work

7.2.1 Investigate association of disease progression and genetics

Several studies have suggested a potential link between alterations in gene expression and structural changes in the brain in neurodegenerative diseases (Julio-César and Rosa-Helena, 2018; Altmann *et al.*, 2020; Guerra-Resendez, Brenner and Hilton, 2022). The findings from Altmann *et al.*, (2020) proposed a more active involvement of specific cell types, such as astrocytes and endothelial cells, in the initiation of neurodegeneration in frontotemporal dementia than previously assumed. Evaluating the correlation between changes in gene expression or genetic mutations and our proposed disease stages has the potential to unveil insights into the molecular mechanisms that affect specific cell populations in the brain. Moreover, such investigations could serve as a foundation for the identification of novel therapeutic targets aimed at preventing brain atrophy and seizures, thereby advancing our ability to develop targeted interventions for PWE.

Bibliography

Adler, S. *et al.* (2018) 'Topographic principles of cortical fluid-attenuated inversion recovery signal in temporal lobe epilepsy', *Epilepsia*, 59(3), pp. 627–635. doi: 10.1111/epi.14017.

Agarwal, N. *et al.* (2017) 'Ketogenic diet: Predictors of seizure control', *SAGE Open Medicine*, 5, p. 205031211771288. doi: 10.1177/2050312117712887.

Ahmadi, M. E. *et al.* (2009) 'Side matters: Diffusion tensor imaging tractography in left and right temporal lobe epilepsy', *American Journal of Neuroradiology*, 30(9), pp. 1740–1747. doi: 10.3174/ajnr.A1650.

Aksman, L. M. *et al.* (2021) 'pySuStaIn: a python implementation of the Subtype and Stage Inference algorithm', *SoftwareX*, 16(December), pp. 1–17. doi: 10.1016/j.softx.2021.100811.

Aksman, L. M. *et al.* (2023) 'A data-driven study of Alzheimer's disease related amyloid and tau pathology progression', *Brain*, awad232. doi: https://doi.org/10.1093/brain/awad232.

Alexander, A. L. *et al.* (2007) 'Diffusion Tensor Imaging of the Brain', *Neurotherapeutics*, 4(3), pp. 316–329. doi: 10.1016/j.nurt.2007.05.011.

Alhusaini, S. *et al.* (2012) 'Asymmetric cortical surface area and morphology changes in mesial temporal lobe epilepsy with hippocampal sclerosis', *Epilepsia*, 53(6), pp. 995–1003. doi: 10.1111/j.1528-1167.2012.03457.x.

Alhusaini, S. *et al.* (2019) 'Normal cerebral cortical thickness in first-degree relatives of temporal lobe epilepsy patients', *Neurology*, 92(4), pp. E351–E358. doi: 10.1212/WNL.0000000000006834.

Allanson, J. E. *et al.* (1993) 'Anthropometric craniofacial pattern profiles in Down syndrome', *American Journal of Medical Genetics*, 47(5), pp. 748–752. doi: 10.1002/ajmg.1320470530.

Altmann, A. *et al.* (2020) 'Analysis of brain atrophy and local gene expression in genetic frontotemporal dementia', *Brain Communications*, 2(2), pp. 1–22. doi: 10.1093/braincomms/fcaa122.

Amar, A. P. *et al.* (1999) 'Long-term multicenter experience with vagus nerve stimulation for intractable partial seizures: Results of the XE5 trial', *Stereotactic and Functional Neurosurgery*, 73(1–4), pp. 104–108. doi: 10.1159/000029764.

An, S. *et al.* (2018) ‘Early Prediction of Drug Resistant Epilepsy using Claims Data’, *Epilepsy and Behavior*, 89, pp. 118–125. doi: 10.1016/j.yebeh.2018.10.013.

Androsova, G. *et al.* (2017) ‘Comparative effectiveness of antiepileptic drugs in patients with mesial temporal lobe epilepsy with hippocampal sclerosis’, *Epilepsia*, 58(10), pp. 1734–1741. doi: 10.1111/epi.13871.

Angus-Leppan, H. (2008) ‘Diagnosing epilepsy in neurology clinics: A prospective study’, *Seizure*, 17(5), pp. 431–436. doi: 10.1016/j.seizure.2007.12.010.

Annegers, J. F. and Rocca, W. A. (1996) ‘Causes of epilepsy: Contributions of the rochester epidemiology project’, *Mayo Clinic Proceedings*. Elsevier Ltd, 71(6), pp. 570–575. doi: 10.4065/71.6.570.

Arfanakis, K. *et al.* (2002) ‘Diffusion tensor MRI in temporal lobe epilepsy’, *Magnetic Resonance Imaging*, 20(7), pp. 511–519. doi: 10.1016/S0730-725X(02)00509-X.

Asadi-Pooya, A. A. *et al.* (2016) ‘Historical Risk Factors Associated with Seizure Outcome after Surgery for Drug-Resistant Mesial Temporal Lobe Epilepsy’, *World Neurosurgery*. Elsevier Inc, 89, pp. 78–83. doi: 10.1016/j.wneu.2016.02.023.

Asadi, S. *et al.* (2019) ‘Dementia with Lewy Bodies Syndrome’, *Journal of Ageing and Restorative Medicine*, 2(1), pp. 64–67.

Asha, K. R. *et al.* (2012) ‘Craniofacial anthropometric analysis in down syndrome’, *New Developments in Down Syndrome Research*, 2, pp. 293–300.

Assenza, G. (2020) ‘Diagnosis and treatment of drug-resistant epilepsy: Present and future perspectives’, *Brain Sciences*, 10(11), pp. 1–3. doi: 10.3390/brainsci10110779.

Balestrini, S. *et al.* (2021) ‘Increased facial asymmetry in focal epilepsies associated with unilateral lesions’, *Brain Communications*, 3(2). doi: 10.1093/braincomms/fcab068.

Bancaud, J. *et al.* (1994) ‘Anatomical origin of déjà vu and vivid “memories” in human temporal lobe epilepsy’, *Brain*, 117(1), pp. 71–90. doi: 10.1093/brain/117.1.71.

Bano, S. *et al.* (2011) ‘Neuroimaging in epilepsy’, *Journal of Pediatric Neurosciences*. Wolters Kluwer -- Medknow Publications, pp. 19–26. doi:

10.4103/1817-1745.84401.
Bartoňová, M. *et al.* (2023) 'White matter alterations in MR-negative temporal and frontal lobe epilepsy using fixel-based analysis', *Scientific Reports*. Nature Publishing Group UK, 13(1), pp. 1–10. doi: 10.1038/s41598-022-27233-4.
Baxendale, S. *et al.* (2019) 'Indications and expectations for neuropsychological assessment in epilepsy surgery in children and adults: Executive summary of the report of the ILAE Neuropsychology Task Force Diagnostic Methods Commission: 2017-2021', *Epilepsia*, 60(9), pp. 1794–1796. doi: 10.1111/epi.16309.
Beghi, E. *et al.* (2019) 'Global, regional, and national burden of epilepsy, 1990–2016: a systematic analysis for the Global Burden of Disease Study 2016', *The Lancet Neurology*, 18(4), pp. 357–375. doi: 10.1016/S1474-4422(18)30454-X.
Beghi, E. (2020) 'The Epidemiology of Epilepsy', *Neuroepidemiology*, 54(2), pp. 185–191. doi: 10.1159/000503831.
Ben-Menachem, E. *et al.* (1995) 'Effects of vagus nerve stimulation on amino acids and other metabolites in the CSF of patients with partial seizures', *Epilepsy Research*, 20(3), pp. 221–227. doi: 10.1016/0920-1211(94)00083-9.
Bender, A. C. *et al.* (2012) 'SCN1A mutations in Dravet syndrome: Impact of interneuron dysfunction on neural networks and cognitive outcome', *Epilepsy and Behavior*, 23(3), pp. 177–186. doi: 10.1016/j.yebeh.2011.11.022.
Bengzon, J. *et al.* (2002) 'Neuronal apoptosis after brief and prolonged seizures', in *Progress in Brain Research*. Elsevier, pp. 111–119. doi: 10.1016/S0079-6123(02)35011-8.
Beniczky, S. *et al.* (2013) 'Standardized Computer-based Organized Reporting of EEG: SCORE', *Epilepsia*, 54(6), pp. 1112–1124. doi: 10.1111/epi.12135.
Berg, A. T. (2004) 'Understanding the Delay before Epilepsy Surgery: Who Develops Intractable Focal Epilepsy and When?', *CNS Spectrums*, 9(2), pp. 136–144. doi: 10.1017/S109285290000849X.
Berg, A. T. *et al.* (2010) 'Revised terminology and concepts for organization of seizures and epilepsies: Report of the ILAE Commission on Classification and Terminology, 2005-2009', *Epilepsia*, 51(4), pp. 676–685. doi: 10.1111/j.1528-1167.2010.02522.x.
Berg, A. T. and Scheffer, I. E. (2011) 'New concepts in classification of the epilepsies: Entering the 21st century', *Epilepsia*, 52(6), pp. 1058–1062. doi:

10.1111/j.1528-1167.2011.03101.x.
Bernasconi, A. *et al.* (2011) 'Advances in MRI for "cryptogenic" epilepsies', *Nature Reviews Neurology*, 7(2), pp. 99–108. doi: 10.1038/nrneurol.2010.199.
Bernasconi, A. *et al.* (2019) 'Recommendations for the use of structural magnetic resonance imaging in the care of patients with epilepsy: A consensus report from the International League Against Epilepsy Neuroimaging Task Force', *Epilepsia*, 60(6), pp. 1054–1068. doi: 10.1111/epi.15612.
Bernasconi, N. *et al.* (2004) 'Whole-brain voxel-based statistical analysis of gray matter and white matter in temporal lobe epilepsy', *NeuroImage*, 23(2), pp. 717–723. doi: 10.1016/j.neuroimage.2004.06.015.
Bernasconi, N., Natsume, J. and Bernasconi, A. (2005) 'Progression in temporal lobe epilepsy: Differential atrophy in mesial temporal structures', *Neurology*, 65(2), pp. 223–228. doi: 10.1212/01.wnl.0000169066.46912.fa.
Bernhardt, B. C. *et al.* (2009) 'Longitudinal and cross-sectional analysis of atrophy in pharmacoresistant temporal lobe epilepsy', *Neurology*, 72(20), pp. 1747–1754. doi: 10.1212/01.wnl.0000345969.57574.f5.
Bernhardt, Boris C. *et al.* (2009) 'Thalamo-cortical network pathology in idiopathic generalized epilepsy: Insights from MRI-based morphometric correlation analysis', *NeuroImage*. Elsevier Inc., 46(2), pp. 373–381. doi: 10.1016/j.neuroimage.2009.01.055.
Bernhardt, B. C. *et al.* (2010) 'Cortical thickness analysis in temporal lobe epilepsy', *Neurology*, 74(22), pp. 1776–84. doi: https://doi.org/10.1212/WNL.0b013e3181e0f80a.
Bernhardt, B. C. *et al.* (2011) 'Graph-theoretical analysis reveals disrupted small-world organization of cortical thickness correlation networks in temporal lobe epilepsy', *Cerebral Cortex*, 21(9), pp. 2147–2157. doi: 10.1093/cercor/bhq291.
Bernhardt, B. C. *et al.* (2012) 'Mapping thalamocortical network pathology in temporal lobe epilepsy', *Neurology*, 78(2), pp. 129–136. doi: 10.1212/WNL.0b013e31823efd0d.
Bernhardt, B. C., Bonilha, L. and Gross, D. W. (2015) 'Network analysis for a network disorder: The emerging role of graph theory in the study of epilepsy', *Epilepsy and Behavior*, 50, pp. 162–170. doi: 10.1016/j.yebeh.2015.06.005.
Bernhardt, B. C., Kim, H. and Bernasconi, N. (2013) 'Patterns of subregional

mesiotemporal disease progression in temporal lobe epilepsy', *Neurology*, 81(21), pp. 1840–1847. doi: 10.1212/01.wnl.0000436069.20513.92.
Bethmann, K. *et al.* (2008) 'Antiepileptic drug resistant rats differ from drug responsive rats in GABAA receptor subunit expression in a model of temporal lobe epilepsy', *Neurobiology of Disease*, 31(2), pp. 169–187. doi: 10.1016/j.nbd.2008.01.005.
Betting, L. E. *et al.* (2010) 'Correlation between quantitative EEG and MRI in idiopathic generalized epilepsy', *Human Brain Mapping*, 31(9), pp. 1327–1338. doi: 10.1002/hbm.20944.
Bihan, L. D. and Breton, E. (1985) 'Imagerie de diffusion in vivo par résonance magnétique nucléaire', *C. R. Académie Sci.*, 301(15), pp. 1109–1112.
Blume, W. T. (2010) 'Focal and Generalized: Both Here and There', *Epilepsy Currents*, 10(5), pp. 115–117. doi: 10.1111/j.1535-7511.2010.01375.x.
Blumenfeld, H. *et al.* (2009) 'Role of hippocampal sodium channel Nav1.6 in kindling epileptogenesis', *Epilepsia*, pp. 44–55. doi: 10.1111/j.1528-1167.2008.01710.x.
Blumenfeld, H. (2014) 'What is a seizure network? Long-range network consequences of focal seizures', *Advances in Experimental Medicine and Biology*, 813, pp. 63–70. doi: 10.1007/978-94-17-8914-1_5.
Bonilha, L. *et al.* (2006) 'Gray matter atrophy associated with duration of temporal lobe epilepsy', *NeuroImage*, 32(3), pp. 1070–1079. doi: 10.1016/j.neuroimage.2006.05.038.
Bonilha, L. *et al.* (2014) 'Neurodevelopmental alterations of large-scale structural networks in children with new-onset epilepsy', *Human Brain Mapping*, 35(8), pp. 3661–3672. doi: 10.1002/hbm.22428.
Bonnett, L. J. *et al.* (2014) 'Treatment outcome after failure of a first antiepileptic drug', *Neurology*, 83(6), pp. 552–560. doi: 10.1212/WNL.0000000000000673.
Boon, P. *et al.* (1999) 'Cost-benefit of vagus nerve stimulation for refractory epilepsy', *Acta Neurologica Belgica*, 99(4), pp. 275–280.
Braak, H. *et al.* (2006) 'Staging of Alzheimer disease-associated neurofibrillary pathology using paraffin sections and immunocytochemistry', *Acta Neuropathologica*. Springer, 112(4), pp. 389–404. doi: 10.1007/s00401-006-0127-z.

Breiman, L. (2001) ‘Random forests’, *Machine Learning*, 45(1), pp. 5–32. doi: 10.1023/A.

Brodtkorb, E. (2013) ‘Common imitators of epilepsy’, *Acta Neurologica Scandinavica*, 127(S196), pp. 5–10. doi: 10.1111/ane.12043.

Buksakowska, I. *et al.* (2019) ‘Distinctive Patterns of Seizure-Related White Matter Alterations in Right and Left Temporal Lobe Epilepsy’, *Frontiers in Neurology*, 10(October), pp. 1–10. doi: 10.3389/fneur.2019.00986.

Van Buren, J. M. *et al.* (1978) ‘Preliminary evaluation of cerebellar stimulation by double-blind stimulation and biological criteria in the treatment of epilepsy’, *Journal of Neurosurgery*, 48(3), pp. 407–416. doi: 10.3171/jns.1978.48.3.0407.

Caciagli, L. *et al.* (2014) ‘Functional network alterations and their structural substrate in drug-resistant epilepsy’, *Frontiers in Neuroscience*, 8(DEC), pp. 1–12. doi: 10.3389/fnins.2014.00411.

Caciagli, L. *et al.* (2017) ‘A meta-Analysis on progressive atrophy in intractable temporal lobe epilepsy: Time is brain?’, *Neurology*, 89(5), pp. 506–516. doi: 10.1212/WNL.0000000000004176.

Camfield, P. R. *et al.* (1997) ‘If a first antiepileptic drug fails to control a child’s epilepsy, what are the chances of success with the next drug?’, *Journal of Pediatrics*, 131(6), pp. 821–824. doi: 10.1016/S0022-3476(97)70027-1.

Cantor-Rivera, D. *et al.* (2015) ‘Detection of temporal lobe epilepsy using support vector machines in multi-parametric quantitative MR imaging’, *Computerized Medical Imaging and Graphics*. Elsevier Ltd, 41, pp. 14–28. doi: 10.1016/j.compmedimag.2014.07.002.

Casazza, M. *et al.* (1997) ‘Lesionectomy in Epileptogenic Temporal Lobe Lesions: Preoperative Seizure Course and Postoperative Outcome’, *Acta Neurochirurgica, Supplement*. Springer Wien, 1997(68), pp. 64–69. doi: 10.1007/978-3-7091-6513-3_12.

Chen, C. H. *et al.* (2013) ‘Genetic topography of brain morphology’, *Proceedings of the National Academy of Sciences of the United States of America*, 110(42), pp. 17089–17094. doi: 10.1073/pnas.1308091110.

Chen, C. Le *et al.* (2019) ‘Premature white matter aging in patients with right mesial temporal lobe epilepsy: A machine learning approach based on diffusion MRI data’, *NeuroImage: Clinical*. Elsevier, 24(October), p. 102033. doi: 10.1016/j.nicl.2019.102033.

Chen, Z. *et al.* (2018) 'Treatment outcomes in patients with newly diagnosed epilepsy treated with established and new antiepileptic drugs a 30-year longitudinal cohort study', *JAMA Neurology*, 75(3), pp. 279–286. doi: 10.1001/jamaneurol.2017.3949.

Chinthapalli, K. *et al.* (2012) 'Atypical face shape and genomic structural variants in epilepsy', *Brain*, 135(10), pp. 3101–3114. doi: 10.1093/brain/aws232.

Chipaux, M. *et al.* (2016) 'Epilepsy diagnostic and treatment needs identified with a collaborative database involving tertiary centers in France', *Epilepsia*, 57(5), pp. 757–769. doi: 10.1111/epi.13368.

Chowdhury, F. A. *et al.* (2021) 'Localisation in focal epilepsy: a practical guide', *Practical neurology*, 21(6), pp. 481–491. doi: 10.1136/practneurol-2019-002341.

Chung, K. L. (1967) *Markov chains with stationary transition probabilities*. 2nd edn, *Springer*. 2nd edn. Berlin; New York.

Ciccarelli, O. *et al.* (2008) 'Diffusion-based tractography in neurological disorders: concepts, applications, and future developments', *The Lancet Neurology*, 7(8), pp. 715–727. doi: 10.1016/S1474-4422(08)70163-7.

Ciumas, C. and Savic, I. (2006) 'Structural changes in patients with primary generalized tonic and clonic seizures', *Neurology*, 67(4), pp. 1–7. doi: https://doi.org/10.1212/01.wnl.0000230171.23913.cf.

Claes, L. *et al.* (2001) 'De novo mutations in the sodium-channel gene SCN1A cause severe myoclonic epilepsy of infancy', *American Journal of Human Genetics*, 68(6), pp. 1327–1332. doi: 10.1086/320609.

Cleton, A., Voskuyl, R. A. and Danhof, M. (1998) 'Adaptive changes in the pharmacodynamics of midazolam in different experimental models of epilepsy: Kindling, cortical stimulation and genetic absence epilepsy', *British Journal of Pharmacology*, 125(4), pp. 615–620. doi: 10.1038/sj.bjp.0702088.

Clusmann, H. *et al.* (2002) 'Prognostic factors and outcome after different types of resection for temporal lobe epilepsy', *Journal of Neurosurgery*, 97(5), pp. 1131–1141. doi: 10.3171/jns.2002.97.5.1131.

Coan, A. C. *et al.* (2009) 'Seizure frequency and lateralization affect progression of atrophy in temporal lobe epilepsy', *Neurology*, 73(11), pp. 834–842. doi: 10.1212/WNL.0b013e3181b783dd.

Coan, A. C. *et al.* (2014) '3T MRI quantification of hippocampal volume and signal in mesial temporal lobe epilepsy improves detection of hippocampal sclerosis', *American Journal of Neuroradiology*, 35(1), pp. 77–83. doi: 10.3174/ajnr.A3640.

Coan, A. C. *et al.* (2015) 'Patterns of seizure control in patients with mesial temporal lobe epilepsy with and without hippocampus sclerosis', *Arquivos de Neuro-Psiquiatria*, 73(2), pp. 79–82. doi: 10.1590/0004-282X20140199.

Coan, A. C. and Cendes, F. (2013) 'Epilepsy as progressive disorders: What is the evidence that can guide our clinical decisions and how can neuroimaging help?', *Epilepsy and Behavior*. Elsevier Inc., 26(3), pp. 313–321. doi: 10.1016/j.yebeh.2012.09.027.

Concha, L. *et al.* (2009) 'White-matter diffusion abnormalities in temporal-lobe epilepsy with and without mesial temporal sclerosis', *Journal of Neurology, Neurosurgery and Psychiatry*, 80(3), pp. 312–319. doi: 10.1136/jnnp.2007.139287.

Concha, L., Beaulieu, C. and Gross, D. W. (2005) 'Bilateral limbic diffusion abnormalities in unilateral temporal lobe epilepsy', *Annals of Neurology*, 57(2), pp. 188–196. doi: 10.1002/ana.20334.

Cover, T. M. and Hart, P. E. (1967) 'Nearest Neighbor Pattern Classification', *IEEE Transactions on Information Theory*, 13(1), pp. 21–27. doi: 10.1109/TIT.1967.1053964.

Croce, P. *et al.* (2021) 'Machine learning for predicting levetiracetam treatment response in temporal lobe epilepsy', *Clinical Neurophysiology*. International Federation of Clinical Neurophysiology, 132(12), pp. 3035–3042. doi: 10.1016/j.clinph.2021.08.024.

Dale, A. M., Fischl, B. and Sereno, M. I. (1999) 'Cortical Surface-Based Analysis: I. Segmentation and Surface Reconstruction Anders', *NeuroImage*, 9(2), pp. 179–194. doi: 10.1006/nimg.1998.0395.

Damadian, R. (1971) 'Tumor detection by nuclear magnetic resonance', *Science*. American Association for the Advancement of Science, 171(3976), pp. 1151–1153. doi: 10.1126/science.171.3976.1151.

Danial, N. N. *et al.* (2013) 'How does the ketogenic diet work? Four potential mechanisms', *Journal of Child Neurology*, 28(8), pp. 1027–1033. doi: 10.1177/0883073813487598.

Dekker, I. *et al.* (2021) 'The sequence of structural, functional and cognitive changes in multiple sclerosis', *NeuroImage: Clinical*. Elsevier Inc., 29(September 2020), p. 102550. doi: 10.1016/j.nicl.2020.102550.

Dempster, A. P., Laird, N. M. and Rubin, D. B. (1977) ' Maximum Likelihood from Incomplete Data Via the EM Algorithm ', *Journal of the Royal Statistical Society: Series B (Methodological)*, 39(1), pp. 1–22. doi: 10.1111/j.2517-6161.1977.tb01600.x.

Depienne, C. *et al.* (2009) 'Spectrum of SCN1A gene mutations associated with Dravet syndrome: Analysis of 333 patients', *Journal of Medical Genetics*, 46(3), pp. 183–191. doi: 10.1136/jmg.2008.062323.

Desikan, R. S. *et al.* (2006) 'An automated labeling system for subdividing the human cerebral cortex on MRI scans into gyral based regions of interest', *NeuroImage*, 31(3), pp. 968–980. doi: 10.1016/j.neuroimage.2006.01.021.

Drenthen, G. S. *et al.* (2021) 'Predictive value of functional MRI and EEG in epilepsy diagnosis after a first seizure', *Epilepsy and Behavior*. The Author(s), 115, p. 107651. doi: 10.1016/j.yebeh.2020.107651.

Du, X. P. *et al.* (2015) 'Semiological and electroencephalographic features of epilepsy with amygdalar lesion', *Epilepsy Research*. Elsevier B.V., 111, pp. 45–53. doi: 10.1016/j.eplepsyres.2015.01.007.

Duncan, J. S. (2010) 'Imaging in the surgical treatment of epilepsy', *Nature Reviews Neurology*, 6(10), pp. 537–550. doi: 10.1038/nrneurol.2010.131.

Duncan, J. S. *et al.* (2016) 'Brain imaging in the assessment for epilepsy surgery', *The Lancet Neurology*, 15(4), pp. 420–433. doi: 10.1016/S1474-4422(15)00383-X.

Elger, C. E. and Schmidt, D. (2008) 'Modern management of epilepsy: A practical approach', *Epilepsy and Behavior*, 12(4), pp. 501–539. doi: 10.1016/j.yebeh.2008.01.003.

Engel, J. (2001) 'A proposed diagnostic scheme for people with epileptic seizures and with epilepsy: Report of the ILAE task force on classification and terminology', *Epilepsia*, 42(6), pp. 796–803. doi: 10.1046/j.1528-1157.2001.10401.x.

Engel, J. J. *et al.* (1993) *Outcome with respect to epileptic seizures*. 2nd edn, *Surgical Treatment of the Epilepsies, Raven Press, New York*. 2nd edn. Edited by J. Engel. New York: Raven Press.

Eshaghi, A. *et al.* (2021) ‘Identifying multiple sclerosis subtypes using unsupervised machine learning and MRI data’, *Nature Communications*. Springer US, 12(1), pp. 1–12. doi: 10.1038/s41467-021-22265-2.
Eyler, L. T. *et al.* (2012) ‘A comparison of heritability maps of cortical surface area and thickness and the influence of adjustment for whole brain measures: A magnetic resonance imaging twin study’, *Twin Research and Human Genetics*, 15(3), pp. 304–314. doi: 10.1017/thg.2012.3.
Falip, M. *et al.* (2012) ‘Prevalence and immunological spectrum of temporal lobe epilepsy with glutamic acid decarboxylase antibodies’, *European Journal of Neurology*, 19(6), pp. 827–833. doi: 10.1111/j.1468-1331.2011.03609.x.
Feldmann, M. and Koepp, M. (2012) ‘P-glycoprotein imaging in temporal lobe epilepsy: in vivo PET experiments with the Pgp substrate [11C]-verapamil.’, *Epilepsia*, 53 Suppl 6, pp. 60–63. doi: 10.1111/j.1528-1167.2012.03704.x.
Ferrari, C. C. *et al.* (2004) ‘Reversible demyelination, blood-brain barrier breakdown, and pronounced neutrophil recruitment induced by chronic IL-1 expression in the brain’, *American Journal of Pathology*, 165(5), pp. 1827–1837. doi: 10.1016/S0002-9440(10)63438-4.
Ferrario, V. F. *et al.* (2005) ‘Soft tissue facial angles in Down’s syndrome subjects: A three-dimensional non-invasive study’, *European Journal of Orthodontics*, 27(4), pp. 355–362. doi: 10.1093/ejo/cji017.
Ferrua, F. *et al.* (2019) ‘Lentiviral haemopoietic stem/progenitor cell gene therapy for treatment of Wiskott-Aldrich syndrome: interim results of a non-randomised, open-label, phase 1/2 clinical study’, *The Lancet Haematology*. The Author(s). Published by Elsevier Ltd. This is an Open Access article under the CC BY 4.0 license, 6(5), pp. e239–e253. doi: 10.1016/S2352-3026(19)30021-3.
Fiest, K. M. *et al.* (2014) ‘Stigma in epilepsy’, *Current Neurology and Neuroscience Reports*, 14(5). doi: 10.1007/s11910-014-0444-x.
Firth, N. C. *et al.* (2020) ‘Sequences of cognitive decline in typical Alzheimer’s disease and posterior cortical atrophy estimated using a novel event-based model of disease progression’, *Alzheimer’s and Dementia*. doi: 10.1002/alz.12083.
Fischl, B. (2012) ‘FreeSurfer’, *NeuroImage*, 62(2), pp. 774–781. doi: 10.1016/j.neuroimage.2012.01.021.
Fisher, R. *et al.* (2010) ‘Electrical stimulation of the anterior nucleus of thalamus for treatment of refractory epilepsy’, *Epilepsia*, 51(5), pp. 899–908. doi:

10.1111/j.1528-1167.2010.02536.x.
Fisher, R. A. (1912) ‘On an absolute criterion for fitting frequency curves’, *Messenger of Mathematics*, 41, pp. 155–160.
Fisher, R. S. *et al.* (2005) ‘Epileptic Seizures and Epilepsy: Definitions proposed by the International League Against Epilepsy (ILAE) and the International Bureau for Epilepsy (IBE)’, *Epilepsia*, 46(10), pp. 1701–1702. doi: 10.1111/j.1528-1167.2005.00273_4.x.
Fisher, R. S. *et al.* (2014) ‘ILAE Official Report: A practical clinical definition of epilepsy’, *Epilepsia*, 55(4), pp. 475–482. doi: 10.1111/epi.12550.
Fisher, R. S. *et al.* (2016) ‘Automatic Vagus Nerve Stimulation Triggered by Ictal Tachycardia: Clinical Outcomes and Device Performance - The U.S. E-37 Trial’, *Neuromodulation*, 19(2), pp. 188–195. doi: 10.1111/ner.12376.
Fisher, R. S. *et al.* (2017) ‘Operational classification of seizure types by the International League Against Epilepsy: Position Paper of the ILAE Commission for Classification and Terminology’, *Epilepsia*, 58(4), pp. 522–530. doi: 10.1111/epi.13670.
Flores-Sobrecueva, A. *et al.* (2020) ‘A relationship between drug-resistant epilepsy and structural abnormalities in neuroimaging’, *Revista Mexicana de Neurociencia*, 21(1), pp. 9–14. doi: 10.24875/rmn.19000090.
Focke, N. K. *et al.* (2008) ‘Voxel-based diffusion tensor imaging in patients with mesial temporal lobe epilepsy and hippocampal sclerosis’, *NeuroImage*. Elsevier Inc., 40(2), pp. 728–737. doi: 10.1016/j.neuroimage.2007.12.031.
Focke, N. K. *et al.* (2009) ‘Automated normalized FLAIR imaging in MRI-negative patients with refractory focal epilepsy’, *Epilepsia*, 50(6), pp. 1484–1490. doi: 10.1111/j.1528-1167.2009.02022.x.
Fonteijn, H. M. *et al.* (2012) ‘An event-based model for disease progression and its application in familial Alzheimer’s disease and Huntington’s disease’, *NeuroImage*. Elsevier Inc., 60(3), pp. 1880–1889. doi: 10.1016/j.neuroimage.2012.01.062.
Fortin, J. P. *et al.* (2018) ‘Harmonization of cortical thickness measurements across scanners and sites’, *NeuroImage*. Elsevier Ltd, 167(June 2017), pp. 104–120. doi: 10.1016/j.neuroimage.2017.11.024.
French, J. A. *et al.* (2003) ‘Dose-response trial of pregabalin adjunctive therapy in patients with partial seizures’, *Neurology*, 60(10), pp. 1631–1637. doi:

10.1212/01.WNL.0000068024.20285.65.
French, J. A. *et al.* (2004) 'Efficacy and tolerability of the new antiepileptic drugs II: Treatment of refractory epilepsy: Report of the Therapeutics and Technology Assessment Subcommittee and Quality Standards Subcommittee of the American Academy of Neurology and the American Epile', *Neurology*, 62(8), pp. 1261–1273. doi: 10.1212/01.WNL.0000123695.22623.32.
Friedman, A., Kaufer, D. and Heinemann, U. (2009) 'Blood-brain barrier breakdown-inducing astrocytic transformation: Novel targets for the prevention of epilepsy', *Epilepsy Research*, 85(2–3), pp. 142–149. doi: 10.1016/j.eplepsyres.2009.03.005.
Fu, L. *et al.* (2020) 'Longitudinal Study of Brain Asymmetries in Autism and Developmental Delays Aged 2–5 Years', *Neuroscience*. IBRO, 432, pp. 137–149. doi: 10.1016/j.neuroscience.2020.02.028.
Gabel, M. C. *et al.* (2020) 'Evolution of white matter damage in amyotrophic lateral sclerosis', *Annals of Clinical and Translational Neurology*, 7(5), pp. 722–732. doi: 10.1002/acn3.51035.
Galizia, E. C. *et al.* (2012) 'Array comparative genomic hybridization: Results from an adult population with drug-resistant epilepsy and co-morbidities', *European Journal of Medical Genetics*, 55(5), pp. 342–348. doi: 10.1016/j.ejmg.2011.12.011.
Galovic, M. *et al.* (2019) 'Progressive Cortical Thinning in Patients with Focal Epilepsy', *JAMA Neurology*, 76(10), pp. 1230–1239. doi: 10.1001/jamaneurol.2019.1708.
Galovic, M. *et al.* (2020) 'Resective surgery prevents progressive cortical thinning in temporal lobe epilepsy', *Brain : a journal of neurology*, 143(11), pp. 3262–3272. doi: 10.1093/brain/awaa284.
Gao, L. *et al.* (2020) 'Dynamic changes of views on the brain changes of Cushing's syndrome using different computer-assisted tool', *Reviews in Endocrine and Metabolic Disorders*. Springer, pp. 185–200. doi: 10.1007/s11154-020-09540-1.
García-Pallero, M. A. *et al.* (2017) 'Effectiveness of vagal nerve stimulation in medication-resistant epilepsy. Comparison between patients with and without medication changes', *Acta Neurochirurgica*, 159(1), pp. 131–136. doi: 10.1007/s00701-016-3027-6.

Gelman, A., Hwang, J. and Vehtari, A. (2014) 'Understanding predictive information criteria for Bayesian models', *Statistics and Computing*, 24(6), pp. 997–1016. doi: 10.1007/s11222-013-9416-2.
Giometto, B. *et al.* (1998) 'Temporal-lobe epilepsy associated with glutamic-acid-decarboxylase autoantibodies', *The Lancet*, 352, pp. 457–458.
Giordano, F. *et al.* (2017) 'Vagus nerve stimulation: Surgical technique of implantation and revision and related morbidity', *Epilepsia*, 58, pp. 85–90. doi: 10.1111/epi.13678.
Gleichgerrcht, E. *et al.* (2021) 'Artificial intelligence for classification of temporal lobe epilepsy with ROI-level MRI data: A worldwide ENIGMA-Epilepsy study', *NeuroImage: Clinical*, 31(July). doi: 10.1016/j.nicl.2021.102765.
Glover, G. H. (2011) 'Overview of functional magnetic resonance imaging', *Neurosurgery Clinics of North America*, 22(2), pp. 133–139. doi: 10.1016/j.nec.2010.11.001.
Govindan, R. M. *et al.* (2008) 'Diffusion tensor analysis of temporal and extra-temporal lobe tracts in temporal lobe epilepsy', *Epilepsy Research*, 80(1), pp. 30–41. doi: 10.1016/j.eplepsyres.2008.03.011.
Gross, D. W., Concha, L. and Beaulieu, C. (2006) 'Extratemporal white matter abnormalities in mesial temporal lobe epilepsy demonstrated with diffusion tensor imaging', *Epilepsia*, 47(8), pp. 1360–1363. doi: 10.1111/j.1528-1167.2006.00603.x.
Guarnieri, F. C. *et al.* (2018) 'Disorders of neurogenesis and cortical development', *Dialogues in Clinical Neuroscience*. Les Laboratoires Seriver, 20(4), pp. 255–266. doi: 10.31887/dcns.2018.20.4/ccardoso.
Guerra-Resendez, R. S., Brenner, D. and Hilton, I. B. (2022) 'Tuning neurodegeneration-linked gene expression, one (edited) base at a time', *Molecular Therapy*, 30(12), pp. 3512–3514. doi: 10.1016/j.ymthe.2022.10.003.
Guerrini, R., Dobyns, W. B. and Barkovich, A. J. (2008) 'Abnormal development of the human cerebral cortex: genetics, functional consequences and treatment options', *Trends in Neurosciences*, 31(3), pp. 154–162. doi: 10.1016/j.tins.2007.12.004.
Guerrini, R., Sicca, F. and Parmeggiani, L. (2003) 'Epilepsy and malformations of the cerebral cortex', *Epileptic Disorders*, 5(SUPPL. 2), p. 14617417.

Hall, P. (1982) ‘Cross-validation in density estimation’, *Biometrika*, 69(2), pp. 383–390. doi: 10.1093/biomet/69.2.383.
Hammond, P. (2007) ‘The use of 3D face shape modelling in dysmorphology’, pp. 1120–1126. doi: 10.1136/adc.2006.103507.
Hammond, P. *et al.* (2008) ‘Face-brain asymmetry in autism spectrum disorders’, *Molecular Psychiatry*, 13(6), pp. 614–623. doi: 10.1038/mp.2008.18.
Handforth, A. *et al.* (1998) ‘Vagus nerve stimulation therapy for partial-onset seizures: A randomized active-control trial’, *Neurology*, 51(1), pp. 48–55. doi: 10.1212/WNL.51.1.48.
Handforth, A., DeSalles, A. A. F. and Krahl, S. E. (2006) ‘Deep brain stimulation of the subthalamic nucleus as adjunct treatment for refractory epilepsy’, *Epilepsia*, 47(7), pp. 1239–1241. doi: 10.1111/j.1528-1167.2006.00563.x.
Hardiman, O. *et al.* (1988) ‘Microdysgenesis in resected temporal neocortex’, *Neurology*, 38(7), pp. 1–6. doi: DOI: https://doi.org/10.1212/WNL.38.7.1041.
Harris, L. and Angus-Leppan, H. (2020) ‘Epilepsy: diagnosis, classification and management’, *Medicine (United Kingdom)*. Elsevier Ltd, 48(8), pp. 522–528. doi: 10.1016/j.mpmed.2020.05.001.
Hatton, S. N. *et al.* (2020) ‘White matter abnormalities across different epilepsy syndromes in adults: An ENIGMA-Epilepsy study’, *Brain*, 143(8), pp. 2454–2473. doi: 10.1093/brain/awaa200.
Hemery, C., Ryvlin, P. and Rheims, S. (2014) ‘Prevention of generalized tonic-clonic seizures in refractory focal epilepsy: A meta-analysis’, *Epilepsia*, 55(11), pp. 1789–1799. doi: 10.1111/epi.12765.
Hitiris, N. *et al.* (2007) ‘Predictors of pharmacoresistant epilepsy’, *Epilepsy Research*, 75(2–3), pp. 192–196. doi: 10.1016/j.eplepsyres.2007.06.003.
Hoerl, A. E. and Kennard, R. W. (1970) ‘Ridge Regression: Biased Estimation for Nonorthogonal Problems’, *Technometrics*, 12(1), pp. 55–67. doi: 10.1080/00401706.1970.10488634.
Hofer, E. *et al.* (2020) ‘Genetic correlations and genome-wide associations of cortical structure in general population samples of 22,824 adults’, *Nature Communications*, 11(1). doi: 10.1038/s41467-020-18367-y.
Hoffmann, K. *et al.* (2006) ‘Expression of the multidrug transporter MRP2 in the blood-brain barrier after pilocarpine-induced seizures in rats’, *Epilepsy*

Research, 69(1), pp. 1–14. doi: 10.1016/j.eplepsyres.2005.12.005.
Hossain, M. A. (2005) 'Molecular mediators of hypoxic-ischemic injury and implications for epilepsy in the developing brain', *Epilepsy and Behavior*, 7(2), pp. 204–213. doi: 10.1016/j.yebeh.2005.05.015.
Huttenlocher, P. R. (1976) 'Ketonemia and Seizures : Metabolic and Anticonvulsant Effects of Two Ketogenic', *Pediatr Res.*, 540, pp. 536–540.
Illman, N. A. *et al.* (2012) 'Déjà Experiences in Temporal Lobe Epilepsy', *Epilepsy Research and Treatment*, 2012, pp. 1–15. doi: 10.1155/2012/539567.
Iorio, R. *et al.* (2015) 'The detection of neural autoantibodies in patients with antiepileptic-drug-resistant epilepsy predicts response to immunotherapy', *European Journal of Neurology*, 22(1), pp. 70–78. doi: 10.1111/ene.12529.
Janahi, M. *et al.* (2022) 'Nomograms of human hippocampal volume shifted by polygenic scores', *eLife*, 11, pp. 1–17. doi: 10.7554/eLife.78232.
Jayakar, P. *et al.* (2016) 'Diagnostic utility of invasive EEG for epilepsy surgery: Indications, modalities, and techniques', *Epilepsia*, 57(11), pp. 1735–1747. doi: 10.1111/epi.13515.
Jeha, L. E., Morris, H. H. and Burgess, R. C. (2006) 'Coexistence of focal and idiopathic generalized epilepsy in the same patient population', *Seizure*, 15(1), pp. 28–34. doi: 10.1016/j.seizure.2005.10.004.
Jehi, L. and Mathern, G. W. (2014) 'Who's responsible to refer for epilepsy surgery? We all are!', *Neurology*, 84(2), pp. 112–113. doi: 10.1212/wnl.0000000000001137.
Jin, B. *et al.* (2018) 'Automated detection of focal cortical dysplasia type II with surface-based magnetic resonance imaging postprocessing and machine learning', *Epilepsia*, 59(5), pp. 982–992. doi: 10.1111/epi.14064.
Jiruska, P. *et al.* (2013) 'Synchronization and desynchronization in epilepsy: Controversies and hypotheses', *Journal of Physiology*, 591(4), pp. 787–797. doi: 10.1113/jphysiol.2012.239590.
Jobst, B. C. and Cascino, G. D. (2015) 'Resective epilepsy surgery for drug-resistant focal epilepsy: A review', *JAMA - Journal of the American Medical Association*, 313(3), pp. 285–293. doi: 10.1001/jama.2014.17426.
Jobst, C. *et al.* (2001) 'Secondarily generalized seizures in mesial temporal epilepsy: Clinical characteristics, lateralizing signs, and association with sleep-wake cycle', *Epilepsia*, 42(10), pp. 1279–1287. doi: 10.1046/j.1528-

1157.2001.09701.x.
Johnson, M. R. *et al.* (2003) 'A twin study of genetic influences on epilepsy outcome', *Twin Res*, 6, pp. 140–146.
Johnson, W. E., Li, C. and Rabinovic, A. (2007) 'Adjusting batch effects in microarray expression data using empirical Bayes methods', *Biostatistics*, 8(1), pp. 118–127. doi: 10.1093/biostatistics/kxj037.
Julio-César, G. and Rosa-Helena, B. (2018) 'The genetic diagnosis of neurodegenerative diseases and therapeutic perspectives', *Brain Sciences*, 8(12), pp. 1–24. doi: 10.3390/brainsci8120222.
Jung, R. and Berger, W. (1979) 'Hans Bergers Entdeckung des Elektrenkephalogramms und seine ersten Befunde 1924-1931', *Archiv für Psychiatrie und Nervenkrankheiten*. Springer-Verlag, 227(4), pp. 279–300. doi: 10.1007/BF00344814.
Kamitaki, B. K. *et al.* (2022) 'Clinical and EEG factors associated with antiseizure medication resistance in idiopathic generalized epilepsy', *Epilepsia*, 63(1), pp. 150–161. doi: 10.1111/epi.17104.
Kang, N. *et al.* (2005) 'White matter fiber tractography via anisotropic diffusion simulation in the human brain', *IEEE Transactions on Medical Imaging*, 24(9), pp. 1127–1137. doi: 10.1109/TMI.2005.852049.
Kasperavičiute, D. *et al.* (2013) 'Epilepsy, hippocampal sclerosis and febrile seizures linked by common genetic variation around SCN1A', *Brain*, 136(10), pp. 3140–3150. doi: 10.1093/brain/awt233.
Keller, S. S. *et al.* (2014) 'Thalamotemporal impairment in temporal lobe epilepsy: A combined MRI analysis of structure, integrity, and connectivity', *Epilepsia*, 55(2), pp. 306–315. doi: 10.1111/epi.12520.
Keller, S. S. and Roberts, N. (2008) 'Voxel-based morphometry of temporal lobe epilepsy: An introduction and review of the literature', *Epilepsia*, 49(5), pp. 741–757. doi: 10.1111/j.1528-1167.2007.01485.x.
Kemmotsu, N. *et al.* (2011) 'MRI analysis in temporal lobe epilepsy: Cortical thinning and white matter disruptions are related to side of seizure onset', *Epilepsia*, 52(12), pp. 2257–2266. doi: 10.1111/j.1528-1167.2011.03278.x.
Kim, J. H. *et al.* (2007) 'Regional grey matter abnormalities in juvenile myoclonic epilepsy: A voxel-based morphometry study', *NeuroImage*, 37(4), pp. 1132–1137. doi: 10.1016/j.neuroimage.2007.06.025.

Kim, J. H. (2017) ‘Grey and White Matter Alterations in Juvenile Myoclonic Epilepsy: A Comprehensive Review’, *Journal of Epilepsy Research*, 7(2), pp. 77–88. doi: 10.14581/jer.17013.

Kim, S. H. *et al.* (2017) ‘Long-term follow-up of anterior thalamic deep brain stimulation in epilepsy: A 11-year, single center experience’, *Seizure*. BEA Trading Ltd, 52, pp. 154–161. doi: 10.1016/j.seizure.2017.10.009.

Ko, T. S. and Holmes, G. L. (1999) ‘EEG and clinical predictors of medically intractable childhood epilepsy’, *Clinical Neurophysiology*, 110(7), pp. 1245–1251. doi: 10.1016/S1388-2457(99)00068-1.

Kobayashi, E. *et al.* (2002) ‘Magnetic resonance imaging evidence of hippocampal sclerosis in asymptomatic, first-degree relatives of patients with familial mesial temporal lobe epilepsy’, *Archives of Neurology*, 59(12), pp. 1891–1894. doi: 10.1001/archneur.59.12.1891.

Kochunov, P. *et al.* (2011) ‘Fractional anisotropy of cerebral white matter and thickness of cortical gray matter across the lifespan’, *NeuroImage*, 58(1), pp. 41–49. doi: 10.1016/j.neuroimage.2011.05.050.

Kochunov, P. *et al.* (2014) ‘Multi-site study of additive genetic effects on fractional anisotropy of cerebral white matter: Comparing meta and megaanalytical approaches for data pooling’, *NeuroImage*, 95, pp. 136–150. doi: 10.1016/j.neuroimage.2014.03.033.

Koepp, M. J. and Woermann, F. G. (2005) ‘Imaging structure and function in refractory focal epilepsy’, *Lancet Neurology*, pp. 42–53. doi: 10.1016/S1474-4422(04)00965-2.

Kong, X. Z. *et al.* (2018) ‘Mapping cortical brain asymmetry in 17,141 healthy individuals worldwide via the ENIGMA consortium’, *Proceedings of the National Academy of Sciences of the United States of America*, 115(22), pp. E5154–E5163. doi: 10.1073/pnas.1718418115.

Kousar, S. *et al.* (2015) ‘Clinical relevance of genetic polymorphism in the CYP2C9 gene to pharmacodynamics and pharmacokinetics of phenytoin in epileptic patients: Validatory pharmacogenomic approach to pharmacovigilance’, *International Journal of Clinical Pharmacology and Therapeutics*, 53(7), pp. 504–516. doi: 10.5414/CP202112.

Koutcher, J. A., Goldsmith, M. and Damadian, R. (1978) ‘NMR in cancer.X. A malignancy index to discriminate normal and cancerous tissue’, *Cancer*. John

Wiley & Sons, Ltd, 41(1), pp. 174–182. doi: 10.1002/1097-0142(197801)41:1<174::AID-CNCR2820410126>3.0.CO;2-2.

Kuzmanovski, I. *et al.* (2016) 'Seizure outcome following medical treatment of mesial temporal lobe epilepsy: Clinical phenotypes and prognostic factors', *Clinical Neurology and Neurosurgery*. Elsevier B.V., 144, pp. 91–95. doi: 10.1016/j.clineuro.2016.03.018.

Kuzniecky, R. I. (2005) 'Neuroimaging of epilepsy: Therapeutic implications', *NeuroRx*. American Society for Experimental Neurotherapeutics, 2(2), pp. 384–393. doi: 10.1602/neurorx.2.2.384.

Kwan, P., Li, H. M., *et al.* (2010) 'Association between temporal lobe P-glycoprotein expression and seizure recurrence after surgery for pharmacoresistant temporal lobe epilepsy', *Neurobiology of Disease*. Elsevier Inc., 39(2), pp. 192–197. doi: 10.1016/j.nbd.2010.04.006.

Kwan, P., Arzimanoglou, A., *et al.* (2010) 'Definition of drug resistant epilepsy: Consensus proposal by the ad hoc Task Force of the ILAE Commission on Therapeutic Strategies', *Epilepsia*, 51(6), pp. 1069–1077. doi: 10.1111/j.1528-1167.2009.02397.x.

Kwan, P. and Brodie, M. J. (2000) 'Early identification of refractory epilepsy', *The New England Journal of Medicine*, 342(5), pp. 314–319.

Kwan, P. and Brodie, M. J. (2001) 'Effectiveness of first antiepileptic drug', *Epilepsia*, 42(10), pp. 1255–1260. doi: 10.1046/j.1528-1157.2001.04501.x.

Kwon, C. S. *et al.* (2016) 'Resective focal epilepsy surgery - Has selection of candidates changed? A systematic review', *Epilepsy Research*. Elsevier B.V., 122, pp. 37–43. doi: 10.1016/j.eplepsyres.2016.02.007.

Kwon, O. Y. and Park, S. P. (2014) 'Depression and anxiety in people with epilepsy', *Journal of Clinical Neurology (Korea)*, 10(3), pp. 175–188. doi: 10.3988/jcn.2014.10.3.175.

Labate, A. *et al.* (2011) 'Neocortical thinning in "benign" mesial temporal lobe epilepsy', *Epilepsia*, 52(4), pp. 712–717. doi: 10.1111/j.1528-1167.2011.03038.x.

Lakhan, R. *et al.* (2009) 'Differential role of sodium channels SCN1A and SCN2A gene polymorphisms with epilepsy and multiple drug resistance in the north Indian population', *British Journal of Clinical Pharmacology*. Wiley-Blackwell, 68(2), pp. 214–220. doi: 10.1111/j.1365-2125.2009.03437.x.

Larivière, S. *et al.* (2021) 'The ENIGMA Toolbox: multiscale neural contextualization of multisite neuroimaging datasets', *Nature Methods*. Springer US, 18(7), pp. 698–700. doi: 10.1038/s41592-021-01186-4.
Larsen, J. *et al.* (2015) 'The role of SLC2A1 mutations in myoclonic astatic epilepsy and absence epilepsy, and the estimated frequency of GLUT1 deficiency syndrome', *Epilepsia*, 56(12), pp. e203–e208. doi: 10.1111/epi.13222.
Lee, C. Y. *et al.* (2014) 'Diffusional kurtosis imaging reveals a distinctive pattern of microstructural alternations in idiopathic generalized epilepsy', *Acta Neurologica Scandinavica*, 130(3), pp. 148–155. doi: 10.1111/ane.12257.
Lee, J. W. *et al.* (1995) 'Morphometry in temporal lobe epilepsy', *Magnetic Resonance Imaging*, 13(8), pp. 1073–1080. doi: 10.1016/0730-725X(95)02015-L.
Lee, K. J., Jang, K. S. and Shon, Y. M. (2006) 'Chronic deep brain stimulation of subthalamic and anterior thalamic nuclei for controlling refractory partial epilepsy', *Acta Neurochirurgica, Supplementum*, (99), pp. 87–91. doi: 10.1007/978-3-211-35205-2_17.
Lee, K. J., Shon, Y. M. and Cho, C. B. (2012) 'Long-term outcome of anterior thalamic nucleus stimulation for intractable epilepsy', *Stereotactic and Functional Neurosurgery*, 90(6), pp. 379–385. doi: 10.1159/000339991.
Li, M. *et al.* (2014) 'Abnormal cortical thickness in heroin-dependent individuals', *NeuroImage*. Elsevier Inc., 88, pp. 295–307. doi: 10.1016/j.neuroimage.2013.10.021.
Lin, K. *et al.* (2009) 'Voxel-based morphometry evaluation of patients with photosensitive juvenile myoclonic epilepsy', *Epilepsy Research*, 86(2–3), pp. 138–145. doi: 10.1016/j.eplepsyres.2009.05.016.
Liu, H. *et al.* (2018) 'Ketogenic diet for treatment of intractable epilepsy in adults: A meta-analysis of observational studies', *Epilepsia Open*, 3(1), pp. 9–17. doi: 10.1002/epi4.12098.
Long, L. *et al.* (2020) 'Shared hippocampal abnormalities in sporadic temporal lobe epilepsy patients and their siblings', *Epilepsia*, 61(4), pp. 735–746. doi: 10.1111/epi.16477.
Lopez, S. M. *et al.* (2022) 'Event-based modelling in temporal lobe epilepsy demonstrates progressive atrophy from cross- sectional data', pp. 6–7. doi:

10.1111/epi.17316.
Löscher, W. *et al.* (2009) 'The clinical impact of pharmacogenetics on the treatment of epilepsy', *Epilepsia*, 50(1), pp. 1–23. doi: 10.1111/j.1528-1167.2008.01716.x.
Löscher, W. *et al.* (2020) 'Drug resistance in epilepsy: Clinical impact, potential mechanisms, and new innovative treatment options', *Pharmacological Reviews*, 72(3), pp. 606–638. doi: 10.1124/pr.120.019539.
Löscher, W. and Potschka, H. (2005) 'Drug resistance in brain diseases and the role of drug efflux transporters', *Nature Reviews Neuroscience*, 6(8), pp. 591–602. doi: 10.1038/nrn1728.
Löscher, W. and Schmidt, D. (2004) 'New horizons in the development of antiepileptic drugs: The search for new targets', *Epilepsy Research*, 60(2-3 SPEC. ISS.), pp. 77–159. doi: 10.1016/j.eplepsyres.2004.06.004.
Lossin, C. *et al.* (2003) 'Epilepsy-Associated Dysfunction in the Voltage-Gated Neuronal Sodium Channel SCN1A', *Journal of Neuroscience*, 23(36), pp. 11289–11295. doi: 10.1523/jneurosci.23-36-11289.2003.
Lowenstein, D. H. and Alldredge, B. (1998) 'Clinical features of generalized status epilepticus', *N Engl J Med*, 338(14), pp. 970–976.
Luciano, A. L. and Shorvon, S. D. (2007) 'Results of treatment changes in patients with apparently drug-resistant chronic epilepsy', *Annals of Neurology*, 62(4), pp. 375–381. doi: 10.1002/ana.21064.
Luna-Munguia, H., Marquez-Bravo, L. and Concha, L. (2021) 'Longitudinal changes in gray and white matter microstructure during epileptogenesis in pilocarpine-induced epileptic rats', *Seizure*, 90(August), pp. 130–140. doi: 10.1016/j.seizure.2021.02.011.
Maller, J. J. *et al.* (2019) 'Revealing the Hippocampal Connectome through Super-Resolution 1150-Direction Diffusion MRI', *Scientific Reports*. Springer US, 9(1), pp. 1–13. doi: 10.1038/s41598-018-37905-9.
Malter, M. P. *et al.* (2015) 'Treatment of immune-mediated temporal lobe epilepsy with GAD antibodies', *Seizure*. BEA Trading Ltd, 30, pp. 57–63. doi: 10.1016/j.seizure.2015.05.017.
Marcián, V. *et al.* (2016) 'Cerebellar dysfunction and ataxia in patients with epilepsy: Coincidence, consequence, or cause?', *Tremor and Other Hyperkinetic Movements*, 2016, pp. 9–11. doi: 10.7916/D8KH0NBT.

Marinescu, R. V. *et al.* (2019) 'BrainPainter: A Software for the Visualisation of Brain Structures, Biomarkers and Associated Pathological Processes', *Lecture Notes in Computer Science (including subseries Lecture Notes in Artificial Intelligence and Lecture Notes in Bioinformatics)*, 11846 LNCS, pp. 112–120. doi: 10.1007/978-3-030-33226-6_13.

Marini, C. *et al.* (2009) 'SCN1A duplications and deletions detected in Dravet syndrome: Implications for molecular diagnosis', *Epilepsia*, 50(7), pp. 1670–1678. doi: 10.1111/j.1528-1167.2009.02013.x.

Marquand, A. F. *et al.* (2016) 'Understanding Heterogeneity in Clinical Cohorts Using Normative Models: Beyond Case-Control Studies', *Biological Psychiatry*. Elsevier, 80(7), pp. 552–561. doi: 10.1016/j.biopsych.2015.12.023.

Martin, D. R. and Semelka, R. C. (2006) 'Health effects of ionising radiation from diagnostic CT', *Lancet*, 367(9524), pp. 1712–1714. doi: 10.1016/S0140-6736(06)68748-5.

Martire, D. J. *et al.* (2020) 'Temporal-plus epilepsy in children: A connectomic analysis in magnetoencephalography', *Epilepsia*, 61(8), pp. 1691–1700. doi: 10.1111/epi.16591.

Martlé, V. *et al.* (2015) 'Brain Stimulation The Effect of Vagus Nerve Stimulation on CSF Monoamines and the PTZ Seizure Threshold in Dogs', 8(September 2013), pp. 1–6. doi: 10.1016/j.brs.2014.07.032.

Mathern, G. W., Pretorius, J. K. and Babb, T. L. (1995) 'Influence of the type of initial precipitating injury and at what age it occurs on course and outcome in patients with temporal lobe seizures', *Journal of Neurosurgery*, 82(2), pp. 220–227. doi: 10.3171/jns.1995.82.2.0220.

Mathon, B. *et al.* (2017) 'Predictive factors of long-term outcomes of surgery for mesial temporal lobe epilepsy associated with hippocampal sclerosis', *Epilepsia*, 58(8), pp. 1473–1485. doi: 10.1111/epi.13831.

McDaniel, S. S. *et al.* (2011) 'The ketogenic diet inhibits the mammalian target of rapamycin (mTOR) pathway', *Epilepsia*, 52(3), pp. e7–e11. doi: 10.1111/j.1528-1167.2011.02981.x.

McDonald, C. R. *et al.* (2008) 'Regional neocortical thinning in mesial temporal lobe epilepsy', *Epilepsia*, 49(5), pp. 794–803. doi: 10.1111/j.1528-1167.2008.01539.x.

McDonald, C. R. *et al.* (2010) 'Changes in fiber tract integrity and visual fields

after anterior temporal lobectomy', *Neurology*, 75(18), pp. 1631–1638. doi: 10.1212/WNL.0b013e3181fb44db.
McGonigal, A. and Chauvel, P. (2004) 'Frontal lobe epilepsy: Seizure semiology and presurgical evaluation', *Practical Neurology*, 4(5), pp. 260–273. doi: 10.1111/j.1474-7766.2004.00244.x.
McKnight, K. *et al.* (2005) 'Serum antibodies in epilepsy and seizure-associated disorders', *Neurology*, 65(11), pp. 1730–1736. doi: 10.1212/01.wnl.0000187129.66353.13.
Metropolis, N. *et al.* (1953) 'Equation of state calculations by fast computing machines', *The Journal of Chemical Physics*, 21(6), pp. 1087–1092. doi: 10.1063/1.1699114.
Milder, J. B. and Patel, M. (2012) 'Modulation of oxidative stress and mitochondrial function by the ketogenic diet', *Epilepsy Res.*, 100(3), pp. 295–303. doi: 10.1016/j.eplepsyres.2011.09.021.
Mishra, V., Gautier, N. M. and Glasscock, E. (2018) 'Simultaneous video-EEG-ECG monitoring to identify neurocardiac dysfunction in mouse models of epilepsy', *Journal of Visualized Experiments*, 2018(131), pp. 1–20. doi: 10.3791/57300.
Mohanraj, R. and Brodie, M. J. (2007) 'Outcomes of newly diagnosed idiopathic generalized epilepsy syndromes in a non-pediatric setting', *Acta Neurologica Scandinavica*, 115(3), pp. 204–208. doi: 10.1111/j.1600-0404.2006.00791.x.
Morin-Brureau, M. *et al.* (2011) 'Epileptiform activity induces vascular remodeling and zonula occludens 1 downregulation in organotypic hippocampal cultures: Role of VEGF signaling pathways', *Journal of Neuroscience*, 31(29), pp. 10677–10688. doi: 10.1523/JNEUROSCI.5692-10.2011.
Mountcastle, V. B. (1997) 'The columnar organization of the neocortex', *Brain*, 120(4), pp. 701–722. doi: 10.1093/brain/120.4.701.
Moyano, L. M. *et al.* (2014) 'Neurocysticercosis as a Cause of Epilepsy and Seizures in Two Community-Based Studies in a Cysticercosis-Endemic Region in Peru', *PLoS Neglected Tropical Diseases*, 8(2). doi: 10.1371/journal.pntd.0002692.
Myint, P. K., Staufenberg, E. F. A. and Sabanathan, K. (2006) 'Post-stroke seizure and post-stroke epilepsy', *Postgraduate Medical Journal*, 82(971), pp. 568–572. doi: 10.1136/pgmj.2005.041426.

Naldini, L. (2011) ‘Ex vivo gene transfer and correction for cell-based therapies’, *Nature Reviews Genetics*. Nature Publishing Group, 12(5), pp. 301–315. doi: 10.1038/nrg2985.

Nass, R. D. *et al.* (2017) ‘The role of postictal laboratory blood analyses in the diagnosis and prognosis of seizures’, *Seizure*. BEA Trading Ltd, 47, pp. 51–65. doi: 10.1016/j.seizure.2017.02.013.

Neligan, A. *et al.* (2011) ‘How refractory is refractory epilepsy? Patterns of relapse and remission in people with refractory epilepsy’, *Epilepsy Research*. Elsevier B.V., 96(3), pp. 225–230. doi: 10.1016/j.eplepsyres.2011.06.004.

Nicolson, A. *et al.* (2004) ‘The relationship between treatment with valproate, lamotrigine, and topiramate and the prognosis of the idiopathic generalised epilepsies’, *Journal of Neurology, Neurosurgery and Psychiatry*, 75(1), pp. 75–79.

Nobili, L. *et al.* (2020) ‘Standard procedures for the diagnostic pathway of sleep-related epilepsies and comorbid sleep disorders: A European Academy of Neurology, European Sleep Research Society and International League against Epilepsy-Europe consensus review’, *Journal of Sleep Research*, 29(6), pp. 1–18. doi: 10.1111/jsr.13184.

Nolze-Charron, G. *et al.* (2020) ‘Tractography of the external capsule and cognition: A diffusion MRI study of cholinergic fibers’, *Experimental Gerontology*. Elsevier, 130(November 2019), p. 110792. doi: 10.1016/j.exger.2019.110792.

Odani, A. *et al.* (1997) ‘Genetic polymorphism of the CYP2C subfamily and its effect on the pharmacokinetics of phenytoin in Japanese patients with epilepsy’, *Clinical Pharmacology and Therapeutics*, 62(3), pp. 287–292. doi: 10.1016/S0009-9236(97)90031-X.

Oh, Y. S. *et al.* (2012) ‘Cognitive improvement after long-term electrical stimulation of bilateral anterior thalamic nucleus in refractory epilepsy patients’, *Seizure*, 21(3), pp. 183–187. doi: 10.1016/j.seizure.2011.12.003.

Orlandi, A. *et al.* (2018) ‘Clinical reappraisal of the influence of drug-transporter polymorphisms in epilepsy’, *Expert Opinion on Drug Metabolism and Toxicology*, 14(5), pp. 505–512. doi: 10.1080/17425255.2018.1473377.

Ottman, R. *et al.* (1995) ‘Localization of a gene for partial epilepsy to chromosome 10q’, *Nature Genetics*, 10(may), pp. 56–60.

Oxtoby, N. P. *et al.* (2021) ‘Sequence of clinical and neurodegeneration events in Parkinson’s disease progression’, *Brain*, pp. 1–14. doi: 10.1093/brain/awaa461.
Pal, D. K., Carpio, A. and Sander, J. W. A. S. (2000) ‘Neurocysticercosis and epilepsy in developing countries’, *Journal of Neurology Neurosurgery and Psychiatry*, 68, pp. 137–143. doi: 10.1136/jnnp.70.5.707.
Panizzon, M. S. *et al.* (2009) ‘Distinct genetic influences on cortical surface area and cortical thickness’, *Cerebral Cortex*, 19(11), pp. 2728–2735. doi: 10.1093/cercor/bhp026.
Parrini, E. *et al.* (2016) ‘Genetic basis of brain malformations’, *Molecular Syndromology*, 7(4), pp. 220–233. doi: 10.1159/000448639.
Pedregosa, F. *et al.* (2011) ‘Scikit-learn: Machine learning in Python’, *Journal of Machine Learning Research*, 12, pp. 2825–2830.
Peltola, J. *et al.* (2000) ‘Autoantibodies to glutamic acid decarboxylase in patients with therapy-resistant epilepsy’, *Neurology*, 55(1), pp. 46–50. doi: 10.1212/wnl.55.1.46.
Pereira, F. R. S. *et al.* (2010) ‘Asymmetrical hippocampal connectivity in mesial temporal lobe epilepsy: Evidence from resting state fMRI’, *BMC Neuroscience*, 11, pp. 1–48. doi: 10.1186/1471-2202-11-66.
Petroff, O. A. C. *et al.* (1996) ‘The effect of gabapentin on brain gamma-aminobutyric acid in patients with epilepsy’, *Annals of Neurology*, 39(1), pp. 95–99. doi: 10.1002/ana.410390114.
Petrovski, S. *et al.* (2010) ‘Neuropsychiatric symptomatology predicts seizure recurrence in newly treated patients’, *Neurology*, 75(11), pp. 1015–1021. doi: 10.1212/WNL.0b013e3181f25b16.
Piacentino, M. *et al.* (2015) ‘Anterior thalamic nucleus deep brain Stimulation (DBS) for drug-resistant complex partial seizures (CPS) with or without generalization: long-term evaluation and predictive outcome’, *Acta Neurochirurgica*, 157(9), pp. 1525–1532. doi: 10.1007/s00701-015-2498-1.
Pilz, D. T. *et al.* (1998) ‘LIS1 and XLIS (DCX) mutations cause most classical lissencephaly, but different patterns of malformation’, *Human Molecular Genetics*, 7(13), pp. 2029–2037. doi: 10.1093/hmg/7.13.2029.
Pohlen, M. S. *et al.* (2017) ‘Pharmacoresistance with newer anti-epileptic drugs in mesial temporal lobe epilepsy with hippocampal sclerosis’, *Epilepsy*

Research. Elsevier B.V., 137, pp. 56–60. doi: 10.1016/j.eplepsyres.2017.09.012.
Postema, M. C. *et al.* (2019) 'Altered structural brain asymmetry in autism spectrum disorder in a study of 54 datasets', *Nature Communications*, 10(1), pp. 1–12. doi: 10.1038/s41467-019-13005-8.
Potschka, H., Fedrowitz, M. and Löscher, W. (2003) 'Multidrug resistance protein MRP2 contributes to blood-brain barrier function and restricts antiepileptic drug activity', *Journal of Pharmacology and Experimental Therapeutics*, 306(1), pp. 124–131. doi: 10.1124/jpet.103.049858.
Pulsipher, D. T. *et al.* (2007) 'MRI volume loss of subcortical structures in unilateral temporal lobe epilepsy', *Epilepsy Behav*, 11(3), pp. 442–449. doi: 10.1016/j.yebeh.2007.08.007.
Rafael Covenas, F. M. W. (2015) 'Neuropeptides and Neurotransmitters Involved in Generalized Epilepsy: How Can the Antiepileptic Effect be Improved?', *Journal of Neurology & Neurophysiology*, 06(04), pp. 4–7. doi: 10.4172/2155-9562.1000303.
Rakic, P. (1995) 'A small step for the cell, a giant leap for mankind: a hypothesis of neocortical expansion during evolution', *Trends in Neurosciences*, 18(9), pp. 383–388. doi: 10.1016/0166-2236(95)93934-P.
Ramaraju, S. *et al.* (2020) 'Removal of Interictal MEG-Derived Network Hubs Is Associated With Postoperative Seizure Freedom', *Frontiers in Neurology*, 11(September), pp. 1–9. doi: 10.3389/fneur.2020.563847.
Rathore, C. *et al.* (2013) 'Calcified neurocysticercosis lesions and antiepileptic drug-resistant epilepsy: A surgically remediable syndrome?', *Epilepsia*, 54(10), pp. 1815–1822. doi: 10.1111/epi.12349.
Ravizza, T. and Vezzani, A. (2006) 'Status epilepticus induces time-dependent neuronal and astrocytic expression of interleukin-1 receptor type I in the rat limbic system', *Neuroscience*, 137(1), pp. 301–308. doi: 10.1016/j.neuroscience.2005.07.063.
Remy, S., Gabriel, S., *et al.* (2003) 'A novel mechanism underlying drug resistance in chronic epilepsy', *Annals of Neurology*, 53(4), pp. 469–479. doi: 10.1002/ana.10473.
Remy, S., Urban, B. W., *et al.* (2003) 'Anticonvulsant pharmacology of voltage-gated Na+ channels in hippocampal neurons of control and chronically epileptic rats', *European Journal of Neuroscience*, 17(12), pp. 2648–2658. doi:

10.1046/j.1460-9568.2003.02710.x.
Révész, D., Rydenhag, B. and Ben-Menachem, E. (2016) ‘Complications and safety of vagus nerve stimulation: 25 years of experience at a single center’, *Journal of Neurosurgery: Pediatrics*, 18(1), pp. 97–104. doi: 10.3171/2016.1.PEDS15534.
Riban, V., Fitzsimons, H. L. and During, M. J. (2009) ‘Gene therapy in epilepsy’, *Epilepsia*, 50(1), pp. 24–32. doi: 10.1111/j.1528-1167.2008.01743.x.
Riney, K. *et al.* (2021) ‘ILAE Classification and Definition of Epilepsy Syndromes with Onset at a Variable Age: Position Statement by the ILAE Task Force on Nosology and Definitions’, *Ilae*, p. 75. Available at: https://www.ilae.org/files/dmfile/Riney_VariableAges_7Apr21.pdf.
Rodrigo, S. *et al.* (2007) ‘Uncinate fasciculus fiber tracking in mesial temporal lobe epilepsy. Initial findings’, *European Radiology*, 17(7), pp. 1663–1668. doi: 10.1007/s00330-006-0558-x.
Rogawski, M. A. (2013) ‘The intrinsic severity hypothesis of pharmacoresistance to antiepileptic drugs.’, *Epilepsia*, 54 Suppl 2, pp. 33–40. doi: 10.1111/epi.12182.
Rogawski, M. A. and Johnson, M. R. (2008) ‘Intrinsic Severity as a Determinant of Antiepileptic Drug Refractoriness’, *Epilepsy Currents*, 8(5), pp. 127–130. doi: 10.1111/j.1535-7511.2008.00272.x.
Roger, J. *et al.* (1989) ‘Proposal for Revised Classification of Epilepsies and Epileptic Syndromes.’, *Epilepsia*, 30(4), pp. 389–399. doi: 10.1111/j.1528-1157.1989.tb05316.x.
Rosenow, F. *et al.* (2016) ‘Revised version of quality guidelines for presurgical epilepsy evaluation and surgical epilepsy therapy issued by the Austrian, German, and Swiss working group on presurgical epilepsy diagnosis and operative epilepsy treatment’, *Epilepsia*, 57(8), pp. 1215–1220. doi: 10.1111/epi.13449.
Ryvlin, P. and Rheims, S. (2008) ‘Epilepsy surgery: Eligibility criteria and presurgical evaluation’, *Dialogues in Clinical Neuroscience*, 10(1), pp. 91–103. doi: 10.31887/dcns.2008.10.1/pryvlin.
Salanova, V. *et al.* (2021) ‘The SANTÉ study at 10 years of follow-up: Effectiveness, safety, and sudden unexpected death in epilepsy’, *Epilepsia*, 62(6), pp. 1306–1317. doi: 10.1111/epi.16895.

Salar, S. *et al.* (2014) 'Blood-brain barrier dysfunction can contribute to pharmacoresistance of seizures', *Epilepsia*, pp. 1255–1263. doi: 10.1111/epi.12713.

Salmenpera, T. M. and Duncan, J. S. (2005) 'Imaging in epilepsy', *Neurology in Practice*. BMJ Publishing Group Ltd, pp. 2–10. doi: 10.1136/jnnp.2005.075135.

Sander, J. W. (2014) 'Epilepsy; Epidemiology', *Encyclopedia of the Neurological Sciences*, 2, pp. 108–111. doi: 10.1016/B978-0-12-385157-4.00284-0.

Sandu, C. *et al.* (2019) 'Ketogenic Diet in Patients with GLUT1 Deficiency Syndrome', *MAEDICA-a Journal of Clinical Medicine*, 14(2), pp. 93–97. Available at: https://doi.org/10.26574/maedica.2019.14.2.93.

Scanlon, C. *et al.* (2013) 'Grey and white matter abnormalities in temporal lobe epilepsy with and without mesial temporal sclerosis', *Journal of Neurology*, 260(9), pp. 2320–2329. doi: 10.1007/s00415-013-6974-3.

Scharfman, H. E. (2007) 'The neurobiology of epilepsy', *Current Neurology and Neuroscience Reports*, 7(4), pp. 348–354. doi: 10.1007/s11910-007-0053-z.

Scheffer, I. E. *et al.* (2017) 'ILAE classification of the epilepsies: position paper of the ILAE Commission for Classification and Terminology', *Epilepsia*, 58(4), pp. 512–521. doi: doi:10.1111/epi.13709.

Schiller, Y. and Najjar, Y. (2008) 'Quantifying the response to antiepileptic drugs: effect of past treatment history', *Neurology*, 70, pp. 54–65.

Schmidt, D., Baumgartner, C. and Löscher, W. (2004) 'Seizure Recurrence after Planned Discontinuation of Antiepileptic Drugs in Seizure-free Patients after Epilepsy Surgery: A Review of Current Clinical Experience', *Epilepsia*, 45(2), pp. 179–186. doi: 10.1111/j.0013-9580.2004.37803.x.

Schmidt, D. and Löscher, W. (2005) 'Drug resistance in epilepsy: Putative neurobiologic and clinical mechanisms', *Epilepsia*, 46(6), pp. 858–877. doi: 10.1111/j.1528-1167.2005.54904.x.

Schmidt, D. and Löscher, W. (2009) 'New Developments in Antiepileptic Drug Resistance: An Integrative View', *Epilepsy Currents*, 9(2), pp. 47–52. doi: 10.1111/j.1535-7511.2008.01289.x.

Schmitt, J. E. *et al.* (2020) 'The genetics of cortical myelination in young adults and its relationships to cerebral surface area, cortical thickness, and intelligence: A magnetic resonance imaging study of twins and families: Genetics of Cortical

Myelination, Area, Thickness, and Int', *NeuroImage*. Elsevier Ltd, 206(October 2019), p. 116319. doi: 10.1016/j.neuroimage.2019.116319.
Seidenberg, M. *et al.* (2008) 'Thalamic atrophy and cognition in unilateral temporal lobe epilepsy', *Journal of the International Neuropsychological Society*, 14(3), pp. 384–393. doi: 10.1017/S1355617708080399.
Seifert, C. L. *et al.* (2015) 'Reduced volume of the nucleus accumbens in heroin addiction', *European Archives of Psychiatry and Clinical Neuroscience*. Springer Berlin Heidelberg, 265(8), pp. 637–645. doi: 10.1007/s00406-014-0564-y.
Shin, J. W. *et al.* (2016) 'Clinical applications of simultaneous PET/MR imaging using R-[11C]-verapamil with cyclosporin a: Preliminary RESULTS on a surrogate marker of drug-resistant epilepsy', *American Journal of Neuroradiology*, 37(4), pp. 600–606. doi: 10.3174/ajnr.A4566.
Shorvon, S. D. (2011) 'The etiologic classification of epilepsy', *Epilepsia*, 52(6), pp. 1052–1057. doi: 10.1111/j.1528-1167.2011.03041.x.
Shorvon, S. D., Guerrini, R. and Andermann, F. (2011) 'Introduction to the concept of provoked epilepsy', in *The Causes of Epilepsy: Common and Uncommon Causes in Adults and Children*. Cambridge University Press, pp. 625–630. doi: 10.1017/CBO9780511921001.090.
Sillanpaa, M. and Schmidt, D. (2008) 'Early seizure frequency and aetiology predict long-term medical outcome in childhood-onset epilepsy', *Brain*, 132(4), pp. 989–998. doi: 10.1093/brain/awn357.
Sillanpää, M. and Schmidt, D. (2006) 'Natural history of treated childhood-onset epilepsy: Prospective, long-term population-based study', *Brain*, 129(3), pp. 617–624. doi: 10.1093/brain/awh726.
Silverman, B. W. (1982) 'Algorithm AS 176: kernel density estimation using the fast Fourier transform', *Journal of the Royal Statistical Society: Series C (Applied Statistics)*, 31(1), pp. 93–99.
Simasathien, T. *et al.* (2013) 'Improved outcomes with earlier surgery for intractable frontal lobe epilepsy', *Annals of Neurology*, 73(5), pp. 646–654. doi: 10.1002/ana.23862.
Singh, N. A. *et al.* (1998) 'A novel potassium channel gene, KCNQ2, is mutated in an inherited epilepsy of newborns', *Nature*, 18, pp. 25–29.
Singhi, P. (2011) 'Infectious causes of seizures and epilepsy in the developing

world', *Developmental Medicine and Child Neurology*, 53(7), pp. 600–609. doi: 10.1111/j.1469-8749.2011.03928.x.
Sinha, N. *et al.* (2021) 'Focal to bilateral tonic–clonic seizures are associated with widespread network abnormality in temporal lobe epilepsy', *Epilepsia*, 62(3), pp. 729–741. doi: 10.1111/epi.16819.
Sisodiya, S. M. (2003) 'Mechanisms of antiepileptic drug resistance', *Current Opinion in Neurology*, 16(2), pp. 197–201. doi: 10.1097/01.wco.0000063771.81810.6c.
Sisodiya, S. M. (2004) 'Malformations of cortical development: Burdens and insights from important causes of human epilepsy', *Lancet Neurology*. Lancet Publishing Group, pp. 29–38. doi: 10.1016/S1474-4422(03)00620-3.
Sisodiya, S. M. *et al.* (2020) 'The ENIGMA-Epilepsy working group: Mapping disease from large data sets', *Human Brain Mapping*, (May), pp. 1–16. doi: 10.1002/hbm.25037.
Sisodiya, S. M., Heffernan, J. and Squier, M. V. (1999) 'Over-expression of P-glycoprotein in malformations of cortical development', *NeuroReport*, 10(16), pp. 3437–3441. doi: 10.1097/00001756-199911080-00032.
Sokol, D. K. *et al.* (2004) 'Antiphospholipid and glutamic acid decarboxylase antibodies in patients with focal epilepsy', *Neurology*, 62(3), pp. 517–518. doi: 10.1212/01.WNL.0000106821.83436.59.
Son, B. C. *et al.* (2016) 'Clinical Outcome of Patients with Deep Brain Stimulation of the Centromedian Thalamic Nucleus for Refractory Epilepsy and Location of the Active Contacts', *Stereotactic and Functional Neurosurgery*, 94(3), pp. 187–197. doi: 10.1159/000446611.
Srivastava, A. K. *et al.* (2013) 'Rapid loss of efficacy to the antiseizure drugs lamotrigine and carbamazepine: A novel experimental model of pharmacoresistant epilepsy', *Epilepsia*, 54(7), pp. 1186–1194. doi: 10.1111/epi.12234.
Stieger, K. *et al.* (2007) 'Oral administration of doxycycline allows tight control of transgene expression: A key step towards gene therapy of retinal diseases', *Gene Therapy*, 14(23), pp. 1668–1673. doi: 10.1038/sj.gt.3303034.
Stigler, S. M. (1981) 'Gauss and the invention of least squares', *Annals of Statistics*, 9(3), pp. 465–474. doi: https://doi.org/10.1214/aos/1176345451.
Stoyke, C., Bilgin, Ö. and Noachtar, S. (2011) 'Video atlas of lateralising and

localising seizure phenomena', *Epileptic Disorders*, 13(2), pp. 113–124. doi: 10.1684/epd.2011.0433.
Szaflarski, J. P. *et al.* (2013) 'The relationship between the localization of the generalized spike and wave discharge generators and the response to valproate', *Epilepsia*, 54(3), pp. 471–480. doi: 10.1111/epi.12062.
Szaflarski, J. P. *et al.* (2016) 'White matter abnormalities in patients with treatment-resistant genetic generalized epilepsies', *Medical Science Monitor*, 22, pp. 1966–1975. doi: 10.12659/MSM.897002.
T. Hastie, R. Tibshirani, J. F. (2008) *The Elements of Statistical Learning*. 2nd edn, *Springer Series in Statistics*. 2nd edn. Springer.
Takahashi, H. *et al.* (2020) 'Convolutional neural network with autoencoder-assisted multiclass labelling for seizure detection based on scalp electroencephalography', *Computers in Biology and Medicine*. Elsevier Ltd, 125, p. 104016. doi: 10.1016/j.compbiomed.2020.104016.
Tang, F., Hartz, A. M. S. and Bauer, B. (2017) 'Drug-resistant epilepsy: Multiple hypotheses, few answers', *Frontiers in Neurology*, 8(JUL), pp. 1–19. doi: 10.3389/fneur.2017.00301.
Tatum, W. O. *et al.* (2018) 'Clinical utility of EEG in diagnosing and monitoring epilepsy in adults', *Clinical Neurophysiology*, 129(5), pp. 1056–1082. doi: 10.1016/j.clinph.2018.01.019.
Tellez-Zenteno, J. F. *et al.* (2006) 'Hippocampal electrical stimulation in mesial temporal lobe epilepsy', *Neurology*, 66(10), pp. 1490–1494. doi: 10.1212/01.wnl.0000209300.49308.8f.
Thom, M. *et al.* (2011) 'Neurofibrillary tangle pathology and Braak staging in chronic epilepsy in relation to traumatic brain injury and hippocampal sclerosis: A post-mortem study', *Brain*, 134(10), pp. 2969–2981. doi: 10.1093/brain/awr209.
Thom, M. *et al.* (2012) 'Variability of sclerosis along the longitudinal hippocampal axis in epilepsy: A post mortem study', *Epilepsy Research*. Elsevier B.V., 102(1–2), pp. 45–59. doi: 10.1016/j.eplepsyres.2012.04.015.
Thurman, D. J. *et al.* (2017) 'The burden of premature mortality of epilepsy in high-income countries: A systematic review from the Mortality Task Force of the International League Against Epilepsy', *Epilepsia*, 58(1), pp. 17–26. doi: 10.1111/epi.13604.

Tibshirani, R. (1996) ‘Regression Shrinkage and Selection Via the Lasso’, *Journal of the Royal Statistical Society: Series B (Methodological)*, 58(1), pp. 267–288. doi: 10.1111/j.2517-6161.1996.tb02080.x.

De Tisi, J. *et al.* (2011) ‘The long-term outcome of adult epilepsy surgery, patterns of seizure remission, and relapse: A cohort study’, *The Lancet*. Elsevier Ltd, 378(9800), pp. 1388–1395. doi: 10.1016/S0140-6736(11)60890-8.

Toma, A. M. *et al.* (2009) ‘Reproducibility of facial soft tissue landmarks on 3D laser-scanned facial images’, *Orthodontics and Craniofacial Research*, 12(1), pp. 33–42. doi: 10.1111/j.1601-6343.2008.01435.x.

Tondelli, M. *et al.* (2020) ‘Valproate Use Is Associated With Posterior Cortical Thinning and Ventricular Enlargement in Epilepsy Patients’, *Frontiers in Neurology*, 11(July). doi: 10.3389/fneur.2020.00622.

Touma, L. *et al.* (2022) ‘Neurostimulation in people with drug-resistant epilepsy: Systematic review and meta-analysis from the ILAE Surgical Therapies Commission’, *Epilepsia*, 63(6), pp. 1314–1329. doi: 10.1111/epi.17243.

Trinka, E. *et al.* (2015) ‘A definition and classification of status epilepticus - Report of the ILAE Task Force on Classification of Status Epilepticus’, *Epilepsia*, 56(10), pp. 1515–1523. doi: 10.1111/epi.13121.

Troyanskaya, O. *et al.* (2001) ‘Missing value estimation methods for DNA microarrays’, *Bioinformatics*, 17(6), pp. 520–525. doi: 10.1093/bioinformatics/17.6.520.

Tsai, M.-H. *et al.* (2013) ‘Etiology of hippocampal sclerosis: Evidence for a predisposing familial morphologic anomaly’, *Neurology*, 81(2), pp. 144–149. doi: 10.1212/wnl.0b013e31829a33ac.

Tufenkjian, K. and Lüders, H. O. (2012) ‘Seizure semiology: Its value and limitations in localizing the epileptogenic zone’, *Journal of Clinical Neurology (Korea)*, 8(4), pp. 243–250. doi: 10.3988/jcn.2012.8.4.243.

Tugcu, B. *et al.* (2016) ‘Outcome of surgical treatment of hippocampal sclerosis from relatively new epilepsy surgery center’, *Journal of Neurosurgical Sciences*, 60(2), pp. 159–168.

Vaughan, D. N. *et al.* (2016) ‘MRI-negative temporal lobe epilepsy: A network disorder of neocortical connectivity.’, *Neurology*, 87(18), pp. 1934–1942. doi: 10.1212/WNL.0000000000003289.

Vaughan, D. N. *et al.* (2017) 'Tract-specific atrophy in focal epilepsy: Disease, genetics, or seizures?', *Annals of Neurology*, 81(2), pp. 240–250. doi: 10.1002/ana.24848.

Vaughan, K. A. *et al.* (2019) 'An estimation of global volume of surgically treatable epilepsy based on a systematic review and meta-analysis of epilepsy', *Journal of Neurosurgery*, 130(4), pp. 1127–1141. doi: 10.3171/2018.3.JNS171722.

Vehmeijer, F. O. L. *et al.* (2015) 'Can we predict efficacy of the ketogenic diet in children with refractory epilepsy?', *European Journal of Paediatric Neurology*. Elsevier Ltd, 19(6), pp. 701–705. doi: 10.1016/j.ejpn.2015.06.004.

Velasco, A. L. *et al.* (2006) 'Neuromodulation of the centromedian thalamic nuclei in the treatment of generalized seizures and the improvement of the quality of life in patients with Lennox-Gastaut syndrome', *Epilepsia*, 47(7), pp. 1203–1212. doi: 10.1111/j.1528-1167.2006.00593.x.

Velasco, F. *et al.* (2000) 'Predictors in the treatment of difficult-to-control seizures by electrical stimulation of the centromedian thalamic nucleus', *Neurosurgery*, 47(2), pp. 295–305. doi: 10.1097/00006123-200008000-00007.

Velasco, F. *et al.* (2005) 'Double-blind, randomized controlled pilot study of bilateral cerebellar stimulation for treatment of intractable motor seizures', *Epilepsia*, 46(7), pp. 1071–1081. doi: 10.1111/j.1528-1167.2005.70504.x.

Velasco, M. *et al.* (2000) 'Subacute electrical stimulation of the hippocampus blocks intractable temporal lobe seizures and paroxysmal EEG activities', *Epilepsia*, 41(2), pp. 158–169. doi: 10.1111/j.1528-1157.2000.tb00135.x.

Vezzani, A. *et al.* (2016) *Infections, inflammation and epilepsy*, *Acta Neuropathol*. doi: 10.1007/s00401-015-1481-5.Infections.

Vogt, V. L. *et al.* (2017) 'Current standards of neuropsychological assessment in epilepsy surgery centers across Europe', *Epilepsia*, 58(3), pp. 343–355. doi: 10.1111/epi.13646.

Volk, H. A. *et al.* (2006) 'Antiepileptic drug-resistant rats differ from drug-responsive rats in hippocampal neurodegeneration and GABAA receptor ligand binding in a model of temporal lobe epilepsy', *Neurobiology of Disease*, 21(3), pp. 633–646. doi: 10.1016/j.nbd.2005.09.006.

Vorravanpreecha, N. *et al.* (2018) 'Studying Down syndrome recognition probabilities in Thai children with de-identified computer-aided facial analysis',

American Journal of Medical Genetics, Part A, 176(9), pp. 1935–1940. doi: 10.1002/ajmg.a.40483.

Vreugdenhil, M. and Wadman, W. J. (1999) 'Modulation of sodium currents in rat CA1 neurons by carbamazepine and valproate after kindling epileptogenesis', *Epilepsia*, 40(11), pp. 1512–1522. doi: 10.1111/j.1528-1157.1999.tb02034.x.

Whelan, C. D. *et al.* (2018) 'Structural brain abnormalities in the common epilepsies assessed in a worldwide ENIGMA study', *Brain*, 141(2), pp. 391–408. doi: 10.1093/brain/awx341.

Wiebe, S. and Jette, N. (2012) 'Pharmacoresistance and the role of surgery in difficult to treat epilepsy', *Nature Reviews Neurology*. Nature Publishing Group, 8(12), pp. 669–677. doi: 10.1038/nrneurol.2012.181.

Wieser, G. H. (1988) 'Selective Amygdalo-Hippocampectomy for Temporal Lobe Epilepsy', 29(2), pp. S100–S113. doi: 10.1111/j.1528-1157.1988.tb05793.x.

Wieser, H. G. *et al.* (2001) 'Proposal for a new classification of outcome with respect to epileptic seizures following epilepsy surgery', *Epilepsia*, 42(2), pp. 282–286. doi: 10.1046/j.1528-1157.2001.35100.x.

Winston, G. P. *et al.* (2014) 'Progressive white matter changes following anterior temporal lobe resection for epilepsy', *NeuroImage: Clinical*, 4, pp. 190–200. doi: 10.1016/j.nicl.2013.12.004.

Wirrell, E. *et al.* (2012) 'Predictors and course of medically intractable epilepsy in young children presenting before 36 months of age: A retrospective, population-based study', *Epilepsia*, 53(9), pp. 1563–1569. doi: 10.1111/j.1528-1167.2012.03562.x.

Wirrell, E. C. *et al.* (1996) 'Long-term prognosis of typical childhood absence epilepsy: Remission or progression to juvenile myoclonic epilepsy', *Neurology*, 47(4), pp. 912–918. doi: 10.1212/WNL.47.4.912.

Woermann, F. G. *et al.* (2000) 'Reduction of frontal neocortical grey matter associated with affective aggression in patients with temporal lobe epilepsy-an objective voxel-by-voxel analysis of automatically segmented MRI', *NeuroImage*, 9(6 PART II), pp. 162–169.

Xiao, F. *et al.* (2022) 'Artificial intelligence and MRI: the source of a new epilepsy taxonomy', *MedRxiv*, (82001369), pp. 1–6. doi: https://doi.org/10.1101/2022.11.10.22282047.

Xue-Ping, W. *et al.* (2019) 'Risk factors for drug-resistant epilepsy', *Medicine*. Lippincott Williams and Wilkins, 98(30), p. e16402. doi: 10.1097/MD.0000000000016402.

Yamazaki, T., Igarashi, J. and Yamaura, H. (2021) 'Human-scale Brain Simulation via Supercomputer: A Case Study on the Cerebellum', *Neuroscience*. Elsevier Ltd. doi: 10.1016/j.neuroscience.2021.01.014.

Yang, Y. *et al.* (2018) 'Electroclinical characteristics of seizures arising from the precuneus based on stereoelectroencephalography (SEEG)', *BMC Neurology*. BMC Neurology, 18(1), pp. 1–11. doi: 10.1186/s12883-018-1119-z.

Yasuda, C. L. *et al.* (2010) 'Dynamic changes in white and gray matter volume are associated with outcome of surgical treatment in temporal lobe epilepsy', *NeuroImage*, 49(1), pp. 71–79. doi: 10.1016/j.neuroimage.2009.08.014.

Yoo, J. Y. *et al.* (2014) 'Ictal spread of medial temporal lobe seizures with and without secondary generalization: An intracranial electroencephalography analysis', *Epilepsia*, 55(2), pp. 289–295. doi: 10.1111/epi.12505.

Young, A. L. *et al.* (2014) 'A data-driven model of biomarker changes in sporadic Alzheimer's disease', *Brain*, 137(9), pp. 2564–2577. doi: 10.1093/brain/awu176.

Young, A. L. *et al.* (2018) 'Uncovering the heterogeneity and temporal complexity of neurodegenerative diseases with Subtype and Stage Inference', *Nature Communications*, 9(1), pp. 1–16. doi: 10.1038/s41467-018-05892-0.

Young, A.L., Oxtoby, N.P., Garbarino, S. *et al.* Data-driven modelling of neurodegenerative disease progression: thinking outside the black box. *Nat. Rev. Neurosci.* **25**, 111–130 (2024). https://doi.org/10.1038/s41583-023-00779-6.

Yuan, Y. *et al.* (2009) 'Gray matter density negatively correlates with duration of heroin use in young lifetime heroin-dependent individuals', *Brain and Cognition*. Elsevier Inc., 71(3), pp. 223–228. doi: 10.1016/j.bandc.2009.08.014.

Yudkoff, M. *et al.* (2008) 'Ketosis and brain handling of glutamate, glutamine, and GABA', *Epilepsia*, 49(SUPPL. 8), pp. 73–75. doi: 10.1111/j.1528-1167.2008.01841.x.

Zeng, L. H., Rensing, N. R. and Wong, M. (2009) 'The mammalian target of rapamycin signaling pathway mediates epileptogenesis in a model of temporal lobe epilepsy', *Journal of Neuroscience*, 29(21), pp. 6964–6972. doi: 10.1523/JNEUROSCI.0066-09.2009.

Zhang, H. *et al.* (2012) 'NODDI: Practical in vivo neurite orientation dispersion and density imaging of the human brain', *NeuroImage*, 61(4), pp. 1000–1016. doi: 10.1016/j.neuroimage.2012.03.072.
Zhang, Z. *et al.* (2017) 'Hippocampus-associated causal network of structural covariance measuring structural damage progression in temporal lobe epilepsy', *Human Brain Mapping*, 38(2), pp. 753–766. doi: 10.1002/hbm.23415.
Zhao, X. *et al.* (2017) 'Role of conventional magnetic resonance imaging in the screening of epilepsy with structural abnormalities: a pictorial essay.', *American journal of nuclear medicine and molecular imaging*, 7(3), pp. 126–137.
Zhu, W., Zeng, N. F. and Wang, N. (2010) '1 Sensitivity , Specificity , Accuracy , Associated Confidence Interval and ROC Analysis with Practical SAS'.

Supplementary Table

Supplementary Table S1 Features selection frequency: Table lists the 57 BASI features computed from 57 left and 57 right individual brain regions, including side of lesion on MRI scan and epilepsy type the patient was categorised in. The selection frequency represents the number of times the features were included for prediction by the LASSO model. The table below corresponds to the model trained on subjects from all categories, BASI features, epilepsy category and lesion laterality on MRI scan. (CT: cortical thickness, SA: surface area, V: volume, SF: hippocampus subfield)

BASI features	Selection frequency
BASI_entorhinal_CT	258
BASI_fimbria_SF	256
BASI_pallidium_V	252
BASI_frontalpole_CT	168
BASI_caudalanteriorcingulate_CT	165
MRI_leasion_side	150
BASI_inferiortemporal_CT	146
BASI_lateraloccipital_CT	142
BASI_caudalmiddlefrontal_CT	130
BASI_Lateral_Ventricle_V	123
BASI_superiorparietal_CT	120
BASI_isthmuscingulate_CT	115
BASI_hata_SF	90
BASI_parsopercularis_CT	85
BASI_precentral_CT	80
BASI_transversetemporal_CT	70
BASI_parsorbitalis_CT	65
BASI_gc_ML_DG_SF	60
BASI_CA1_SF	55
BASI_paracentral_CT	50
BASI_hemisphere_SA	50
BASI_postcentral_CT	42
BASI_cuneus_CT	40

BASI_fusiform_CT	35
BASI_middletemporal_CT	32
BASI_pericalcarine_CT	28
BASI_CA4_SF	20
BASI_inferiorparietal_CT	17
BASI_presubiculum_SF	14
BASI_temporalpole_CT	12
BASI_superiortemporal_CT	11
BASI_accumbens_V	11
BASI_whole_hippocampus_SF	10
BASI_bankssts_CT	10
BASI_medialorbitofrontal_CT	10
BASI_CA3_SF	10
BASI_lingual_CT	9
BASI_parahippocampal_CT	9
BASI_precuneus_CT	9
BASI_parasuniculum_SF	9
BASI_posteriorcingulate_CT	8
BASI_rostralmiddlefrontal_CT	8
BASI_supramarginal_CT	7
Epilepsy_category	6
BASI_insula_CT	6
BASI_lateralorbitofrontal_CT	6
BASI_parstriangularis_CT	5
BASI_putamen_V	5
BASI_rostralanteriorcingulate_CT	4
BASI_superiorfrontal_CT	4
BASI_hippocampal_tail_SF	3
BASI_amygdala_V	3
BASI_caudate_V	3
BASI_hippocampus_V	2
BASI_thalamus_V	2

BASI_hippocampal_fissure_SF	1
BASI_molecular_layer_hp_SF	1
BASI_subiculum_SF	1
BASI_Hemisphere_CT	0

Supplementary Table S2 Summary of centres demographics: Table shows summary of sample size of controls, left MTLE-HS and right MTLE-HS from each centre along with the location and period of recruitment used in EBM.

Centre	Female controls	Female cases	Total controls	Total cases	L MTLE-HS cases	R MTLE-HS cases	Total *n*
Bern	41	9	78	18	10	8	96
Bonn	41	62	80	112	74	38	192
CUBRIC	34	0	48	0	0	0	48
EKUT	9	0	18	0	0	0	18
EPICZ	59	26	116	46	19	27	162
EPIGEN_3T	30	6	70	13	8	5	83
Florence	14	0	30	0	0	0	30
Genova	8	1	20	1	0	1	21
Greifswald	59	0	99	0	0	0	99
HFHS	0	15	0	20	9	11	20
IDIBAPS	29	29	52	53	17	36	105
KCL_CNS	54	11	101	15	6	9	116
KCL_CRF	16	1	26	5	3	2	31
KUOPIO	33	5	67	9	0	9	76
MICA	18	7	38	14	12	2	52
MNI	22	48	46	83	45	38	129
MUSC	45	17	58	27	21	6	85
NYU	62	12	118	19	8	11	137
RMH	11	13	27	35	22	13	62
UCL	17	21	29	37	24	13	66
UCSD	16	15	37	26	16	10	63
UMG	12	12	21	20	10	10	41
UNAM	25	12	35	20	10	10	55
UNICAMP	249	113	398	191	107	84	589
XMU	4	15	13	40	25	15	53
Total	**908**	**450**	**1625**	**804**	**446**	**358**	**2429**

Supplementary Table S3 List of classic and robust Cohen's d and corresponding brain regions: BASI=Brain Asymmetry Index; IPS=ipsilateral; Contra= contralateral, CT=cortical thickness, SA=surface area, V=volume.

Feature	Robust Cohen's d
BASI Hippocampus V	-2.6829179
I Hippocampus V	-1.7582463
I Thalamus V	-0.6664918
I precuneus CT	-0.5467175
I superiorparietal CT	-0.5380512
C superiorparietal CT	-0.5209357
I superiortemporal CT	-0.4723382
I lingual CT	-0.4631141
I Pallidum V	-0.458555
I Putamen V	-0.4504646
C precentral CT	-0.4451158
C precuneus CT	-0.4443393
C Thalamus V	-0.4344409
C postcentral CT	-0.4331437
I precentral CT	-0.4222914
I paracentral CT	-0.4218226
C caudalmiddlefrontal CT	-0.4162054
I superiorfrontal CT	-0.3899213
I postcentral CT	-0.3874891
BASI Amygdala V	-0.3866285
I lateraloccipital CT	-0.3854351
C supramarginal CT	-0.3842853
C paracentral CT	-0.3835202
C superiorfrontal CT	-0.3805965
I supramarginal CT	-0.3803446
C lateraloccipital CT	-0.3801412
I caudalmiddlefrontal CT	-0.378605
C Putamen V	-0.3742566
I middletemporal SA	-0.3738439
C Pallidum V	-0.3705729
I inferiorparietal CT	-0.3645912
I cuneus CT	-0.3626711
C inferiorparietal CT	-0.3520396
I parstriangularis CT	-0.3443501
C cuneus CT	-0.3397424
I fusiform CT	-0.3375276
I inferiortemporal SA	-0.3368785
I pericalcarine CT	-0.3275078
C parsopercularis CT	-0.3188425
C transversetemporal CT	-0.3119499
C pericalcarine CT	-0.3117247
BASI middletemporal SA	-0.3027246
I middletemporal CT	-0.3017855

I parahippocampal CT	-0.2930618
BASI inferiorparietal SA	-0.2891688
I parsopercularis CT	-0.2889303
I Caudate V	-0.2880701
I temporalpole CT	-0.27784
I transversetemporal CT	-0.2759336
I inferiorparietal SA	-0.2683861
I temporalpole SA	-0.2677421
I bankssts CT	-0.2596088
C lingual CT	-0.2581602
C rostralmiddlefrontal CT	-0.2566672
C parstriangularis CT	-0.2522852
I entorhinal CT	-0.2500147
BASI inferiortemporal SA	-0.2483479
BASI temporalpole CT	-0.2452617
I precentral SA	-0.2407922
BASI Thickness	-0.2351717
I Amygdala V	-0.228986
BASI superiortemporal SA	-0.2254611
BASI parahippocampal CT	-0.2192267
BASI Thalamus V	-0.2173022
C parsorbitalis CT	-0.2121693
I parstriangularis SA	-0.2120204
I parahippocampal SA	-0.2068277
BASI parsorbitalis SA	-0.206631
BASI lingual CT	-0.2051527
BASI rostralmiddlefrontal SA	-0.2017726
I cuneus SA	-0.2004569
BASI entorhinal CT	-0.1995361
BASI frontalpole SA	-0.1971317
BASI superiorparietal SA	-0.1962724
I parsorbitalis SA	-0.1933529
BASI superiortemporal CT	-0.1901711
BASI fusiform CT	-0.189665
I rostralmiddlefrontal SA	-0.1878315
I SurfArea	-0.1862529
C Caudate V	-0.1860718
C posteriorcingulate CT	-0.1853445
C bankssts CT	-0.1838757
I rostralmiddlefrontal CT	-0.1803568
C superiortemporal CT	-0.1774301
I superiortemporal SA	-0.1753831
I postcentral SA	-0.1727137
I insula SA	-0.1698279
I bankssts SA	-0.1677565
BASI cuneus SA	-0.1673264
BASI Putamen V	-0.1672498
I inferiortemporal CT	-0.1627242

C precentral SA	-0.1606092
BASI inferiortemporal CT	-0.1584654
C lateralorbitofrontal CT	-0.1566637
C parsopercularis SA	-0.1562873
BASI SurfArea	-0.1559051
BASI parstriangularis SA	-0.1551918
C parahippocampal SA	-0.1540064
BASI bankssts SA	-0.1514161
I lateralorbitofrontal SA	-0.1503787
I superiorfrontal SA	-0.1458241
C caudalanteriorcingulate CT	-0.1451751
C Hippocampus V	-0.14319
C middletemporal CT	-0.1426917
BASI temporalpole SA	-0.1327397
I Accumbens V	-0.1327248
I parsorbitalis CT	-0.1292584
BASI middletemporal CT	-0.1290904
BASI superiorparietal CT	-0.1250625
C caudalmiddlefrontal SA	-0.1235376
I superiorparietal SA	-0.1226229
C frontalpole CT	-0.1204295
I posteriorcingulate CT	-0.1192416
I lateralorbitofrontal CT	-0.1176395
BASI posteriorcingulate SA	-0.116049
BASI paracentral SA	-0.1130479
I entorhinal SA	-0.1126223
BASI pericalcarine SA	-0.1126034
C medialorbitofrontal CT	-0.1072757
C rostralanteriorcingulate SA	-0.1068092
I caudalanteriorcingulate SA	-0.1067414
C fusiform CT	-0.1062734
BASI parahippocampal SA	-0.1049692
BASI lateraloccipital CT	-0.1026907
I lateraloccipital SA	-0.0948732
C transversetemporal SA	-0.0938629
C lateraloccipital SA	-0.093557
C Accumbens V	-0.0913876
C insula CT	-0.0903123
C temporalpole CT	-0.0894061
I posteriorcingulate SA	-0.0883885
BASI fusiform SA	-0.0881418
I fusiform SA	-0.0879827
I caudalmiddlefrontal SA	-0.0860714
I parsopercularis SA	-0.0859082
C insula SA	-0.0857329
BASI precentral SA	-0.0849061
C fusiform SA	-0.0848152
C paracentral SA	-0.0844464

C isthmuscingulate SA	-0.0815205
C postcentral SA	-0.080863
I frontalpole CT	-0.0797915
BASI Caudate V	-0.0771777
BASI precuneus SA	-0.0754572
C entorhinal CT	-0.0751199
I medialorbitofrontal SA	-0.0742784
I medialorbitofrontal CT	-0.0736646
BASI entorhinal SA	-0.0723618
C rostralmiddlefrontal SA	-0.0722609
I isthmuscingulate CT	-0.0714677
BASI medialorbitofrontal SA	-0.070861
BASI superiorfrontal SA	-0.0703944
C parahippocampal CT	-0.068767
BASI insula SA	-0.0646701
C posteriorcingulate SA	-0.0630943
I pericalcarine SA	-0.060347
C superiorfrontal SA	-0.0600856
BASI precuneus CT	-0.0591003
BASI pericalcarine CT	-0.0566343
BASI lateralorbitofrontal SA	-0.0537998
C caudalanteriorcingulate SA	-0.0529875
C inferiortemporal SA	-0.0424029
I paracentral SA	-0.0412793
C superiortemporal SA	-0.0412381
BASI postcentral SA	-0.0396793
C lateralorbitofrontal SA	-0.0396383
BASI lateraloccipital SA	-0.039085
BASI paracentral CT	-0.0382261
BASI bankssts CT	-0.035709
I precuneus SA	-0.0351027
C cuneus SA	-0.0336586
C temporalpole SA	-0.0302501
BASI caudalanteriorcingulate SA	-0.0275075
BASI Pallidum V	-0.0233492
BASI supramarginal SA	-0.0200667
BASI caudalmiddlefrontal SA	-0.017667
BASI superiorfrontal CT	-0.0157578
I frontalpole SA	-0.015389
C middletemporal SA	-0.0131659
C entorhinal SA	-0.0116351
C isthmuscingulate CT	-0.0115805
BASI frontalpole CT	-0.0088867
BASI Accumbens V	-0.0065703
BASI parstriangularis CT	-0.0056471
C inferiortemporal CT	-0.0009267
I lingual SA	0.00300391
BASI parsopercularis CT	0.0077404

I insula CT	0.0096573
BASI postcentral CT	0.00979354
BASI transversetemporal CT	0.00997855
BASI posteriorcingulate CT	0.01070268
BASI inferiorparietal CT	0.01107456
BASI precentral CT	0.01665731
BASI rostralanteriorcingulate CT	0.01928661
C superiorparietal SA	0.02132597
C lingual SA	0.02277294
BASI isthmuscingulate CT	0.02439135
C SurfArea	0.02487679
I transversetemporal SA	0.02490681
C parsorbitalis SA	0.02745711
C bankssts SA	0.02800504
BASI medialorbitofrontal CT	0.02888847
BASI lateralorbitofrontal CT	0.03268548
C precuneus SA	0.03765065
C medialorbitofrontal SA	0.03786681
BASI supramarginal CT	0.03942664
BASI lingual SA	0.0405
BASI cuneus CT	0.04124328
C pericalcarine SA	0.04423045
BASI parsorbitalis CT	0.04947811
I caudalanteriorcingulate CT	0.05240513
C supramarginal SA	0.07132833
I supramarginal SA	0.07164339
I isthmuscingulate SA	0.07213289
C rostralanteriorcingulate CT	0.07223438
I rostralanteriorcingulate SA	0.08276231
I rostralanteriorcingulate CT	0.08474284
C parstriangularis SA	0.08665371
BASI caudalmiddlefrontal CT	0.08741198
C inferiorparietal SA	0.09426966
BASI isthmuscingulate SA	0.09982338
BASI rostralmiddlefrontal CT	0.10202985
BASI insula CT	0.11399903
BASI parsopercularis SA	0.13987967
BASI caudalanteriorcingulate CT	0.15544052
C frontalpole SA	0.17046372
BASI rostralanteriorcingulate SA	0.17375967
BASI Lateral Ventricle V	0.18917073
BASI transversetemporal SA	0.20267358
C Amygdala V	0.2042172
I Thickness	0.20783915
C Thickness	0.21171169
C Lateral Ventricle V	0.44088061
I Lateral Ventricle V	0.5389778

Supplementary Table S4 Association between availability of ASM data and demographic and clinical variables in the ENIGMA-Epilepsy cohort: Columns correspond to the examined demographic and clinical variables. Diagnosis refers to left or right MTLE-HS. Rows: 'Test' indicates the applied test (Chi squared test or t-test); 'Statistic' provides the test statistic (and degrees of freedom (df); 'Mean difference' provides the difference of the variable between PWE with missing ASM response data and PWE with available response data; 'p-value' provides the resulting p-value.

	Sex	**Diagnosis**	**Age**	**Duration of illness**	**Age of onset**	**Site**
Test	Chi-sq	Chi-sq	t-test	t-test	t-test	Chi-sq
Statistic	1.02; df=1	0.67; df=1	-2.54	-4.96	3.49	426; df=19
Mean difference			-2.08	-5.26	3.02	
p-value	0.31	0.41	0.011	$8.88x10^{-07}$	0.0005	$1.11x10^{-78}$

Supplementary Table S5: Demographics of patients across the assigned syndromes: The demographic variables available for analysis included age, duration of illness, and age of disease onset.

Syndrome	**Age**	**DURILL**	**Age of disease onset**	**Total n**
GGE	32.0±9.5	18.9±10.2	13.0±7.0	70
L MTLE-HS	39.0±10.6	24.3±13.7	14.4±11.7	274
R MTLE-HS	40.2±10.7	24.7±14.0	15.5±11.4	219
L NL-MTLE	36.3±10.4	17.4±11.6	18.7±11.4	147
R NL-MTLE	36.1±11.3	15.7±11.2	20.6±13.4	109
ETLE	32.6±10.7	14.8±11.7	17.6±12.2	120
Unspecified	36.4±11.3	16.9±11.1	19.6±14.3	109

Supplementary Table S6 Combination of DTI measures from white matter tracts: Regional FA and MD measures combined based on origin of white matter tracts. Adapted from Kochunov *et al.*, (2014).

Left or right regional FA and MD measures added	Overall FA and MD measures across left or right white matter tracts region based on origin in the brain
Anterior limb of internal capsule (ALIC) Posterior limb of internal capsule (PLIC) Retrolenticular part of internal capsule (RLIC)	Internal capsule (IC)
Inferior fronto-occipital fasciculus (IFO) Superior fronto-occipital fasciculus (SFO)	Fronto-occipital fasciculus (FO)
Anterior corona radiata (ACR) Superior corona radiata (SCR) Posterior corona radiata (PCR)	Corona radiata (CR)
Cingulum/cingulate gyrus (CGC) Cingulum/hippocampus (CGH)	Cingulum (CG)
(connecting left to right regions) Genu of corpus callosum (GCC) Body of corpus callosum (BCC) Splenium of corpus callosum (SCC)	(connecting left to right regions) Corpus callosum (CC)

Supplementary Table S7: Association between demographic and clinical variables in right MTLE-HS patients assigned to subtype 2 and subtype 3: Columns correspond to the examined demographic and clinical variables. Rows: 'Test' indicates the applied test (Chi squared test or t-test); 'Statistic' provides the test statistic (and degrees of freedom (df); 'Mean difference' provides the difference of the variable between patients with right MTLE-HS in subtype 2 and subtype 3; 'p-value' provides the resulting p-value; NA (Not applicable)

	Sex	**ASM response**	**Age**	**Duration of illness**	**Age of disease onset**	**Site**
Test	Chi-sq	Chi-sq	t-test	t-test	t-test	Chi-sq
Statistic	0.01; df=1	1.0; df=1	1.09	1.67	-1.12	9.39; df=9
Mean difference	NA	NA	1.95	3.98	-2.09	NA
p-value	0.908	1.000	0.27	0.095	0.261	0.401

Supplementary Table S8: Association between availability of ASM data and demographic and clinical variables in the ENIGMA-Epilepsy cohort: Columns correspond to the examined demographic and clinical variables. Diagnosis refers to left or right MTLE-HS, ETLE, unspecified/bilateral, GGEs, left and right NL-TLEs. Rows: 'Test' indicates the applied test (Chi squared test or t-test); 'Statistic' provides the test statistic (and degrees of freedom (df); 'Mean difference' provides the difference of the variable between PWE with missing AMS response data and PWE with available response data; 'p-value' provides the resulting p-value.

	Sex	**Diagnosis**	**Age**	**Duration of illness**	**Age of onset**	**Site**
Test	Chi-sq	Chi-sq	t-test	t-test	t-test	Chi-sq
Statistic	0.24; df=1	59.23; df=6	2.35	3.92	-2.59	452.27; df=14
Mean difference	NA	NA	2.25	4.96	-2.84	NA
p-value	0.619	6.44×10^{-11}	0.018	9.4×10^{-5}	0.009	1.17×10^{-87}

Supplementary Figure

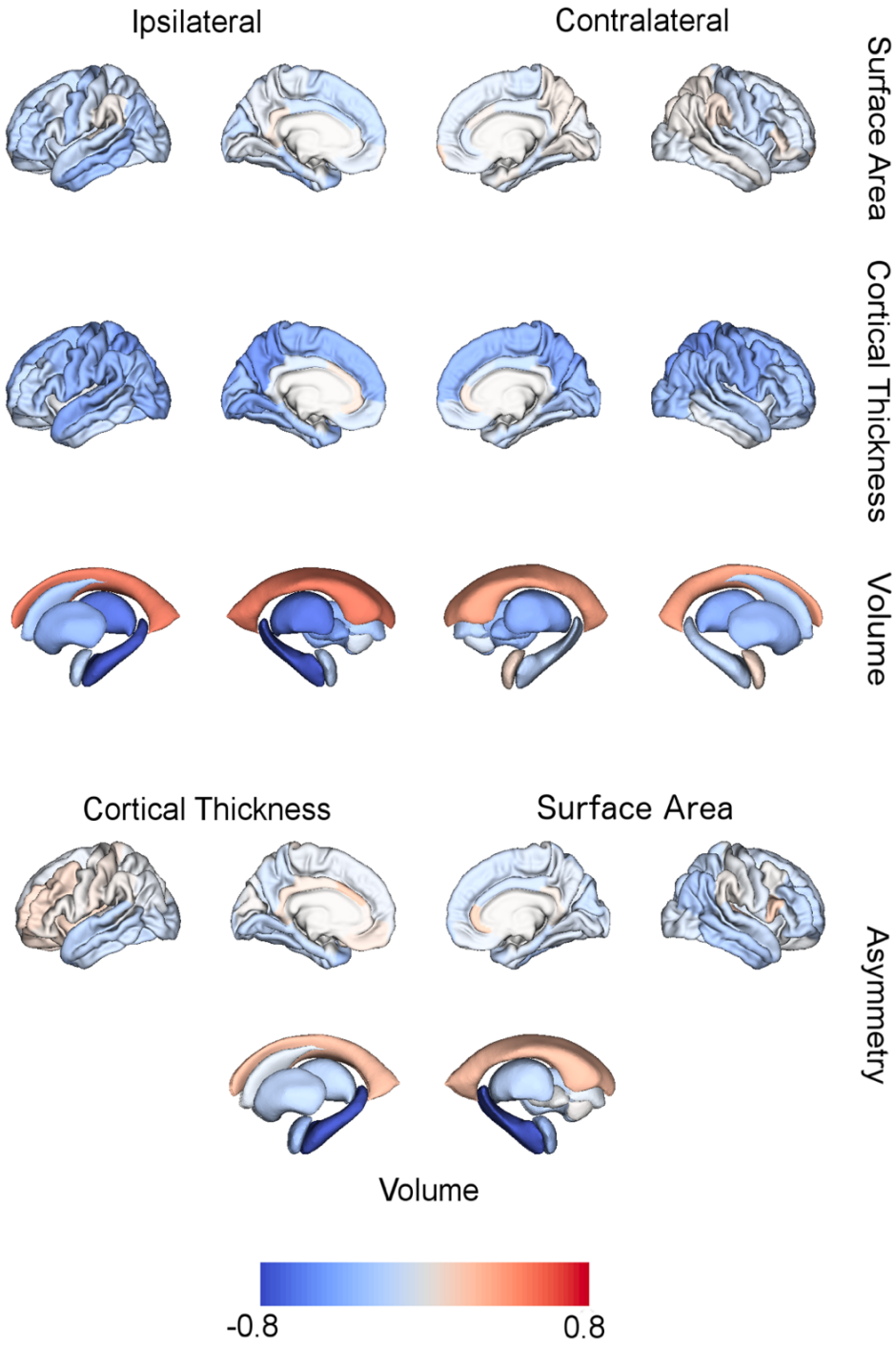

Supplementary Figure S1: Regional differences in MTLE-HS compared to Controls. Effect size between MTLE-HS cases and controls measured as *robust* Cohens' *d* for Surface Area, Cortical Thickness and Volumes depicted ipsilateral or contralateral to the seizure focus (top three rows). The bottom two rows depict effect sizes for asymmetry features.

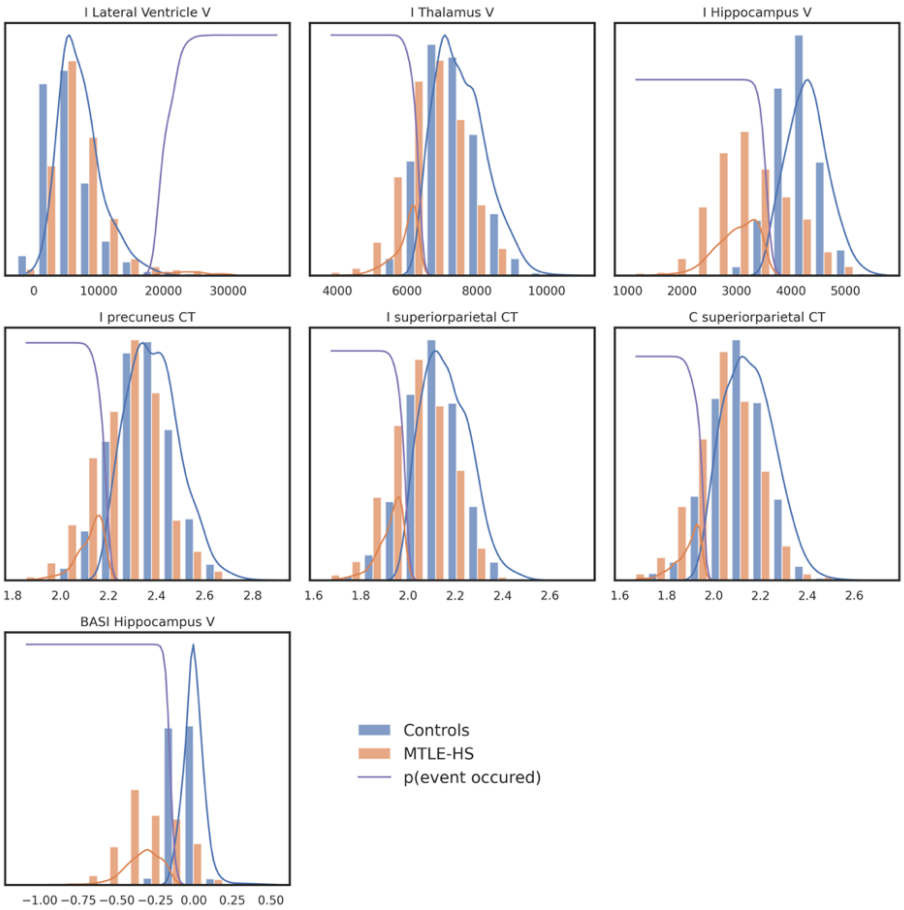

Supplementary Figure S2 Mixture models for the imaging features: Histograms of the feature distribution for cases (orange) and controls (blue). The estimated density using KDE is indicated in solid lines of the same color. The resulting probability that the event has occurred (i.e., the feature value is considered abnormal) is indicated by a purple solid line.

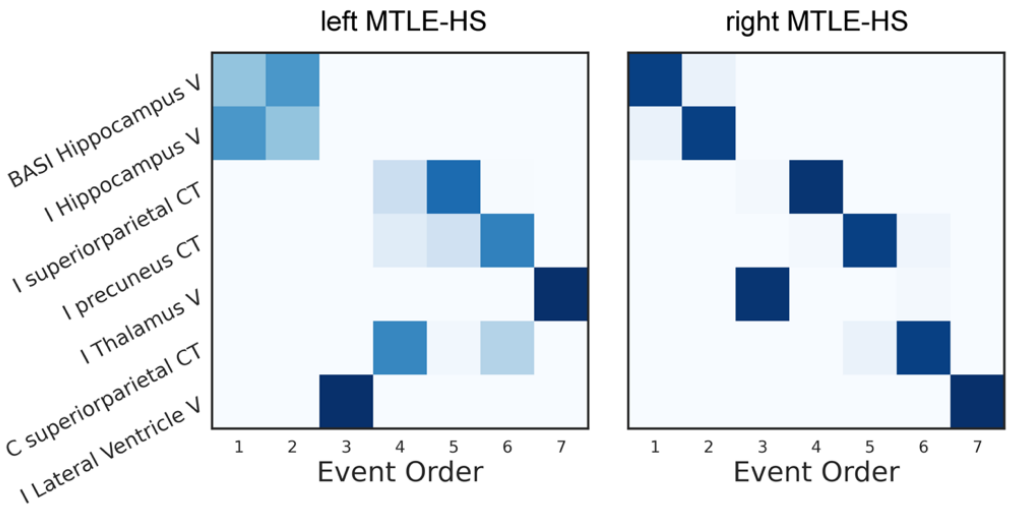

Supplementary Figure S3 Positional variance diagram of left and right MTLE-HS cases: The EBM was estimated using only left MTLE-HS cases (left panel) or only right MTLE-HS cases (right panel). To assist comparisons of the order in which structural changes occur, the y-axis ordering was based on the full EBM (Figure 3). The right MTLE-HS PVD indicates a preferred start with hippocampal volume asymmetry and in addition places reduced ipsilateral thalamic volume on position three instead of five. The left MTLE-HS follows roughly the same ordering, however, increase in ipsilateral lateral ventricle volume was placed at position three followed by decreased cortical thickness in the contralateral superior parietal gyrus. CT=cortical thickness, V=Volume, BASI=Brain Asymmetry Index, I=ipsilateral, C=contralateral.

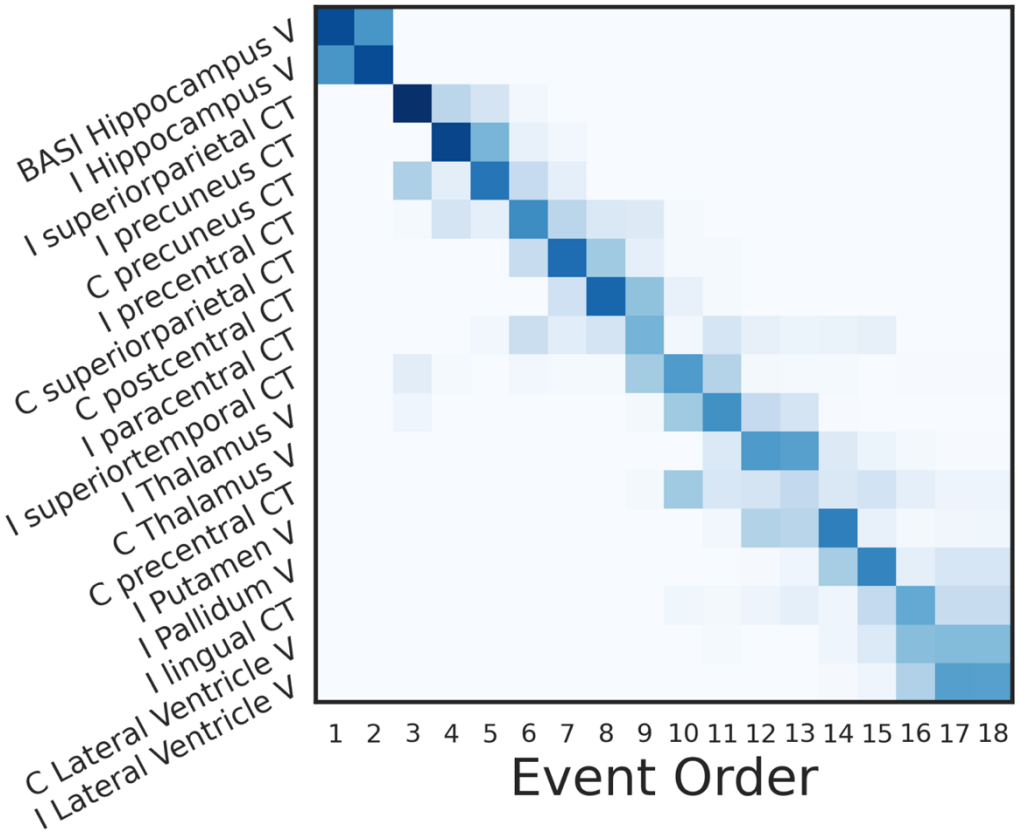

Supplementary Figure S4 Positional variance diagram for features above Cohen's d of 0.4: Positional variance diagram for the full dataset with 19 features passing the more lenient Cohens' d cut-off ($|d| \geq 0.4$). Fitting of the KDE mixture model for the feature 'C caudalmiddlefrontal CT' failed and the feature was therefore excluded from EBM modelling, leaving 18 features in the model. The ordering agrees with the original EBM: hippocampal features are followed by reduced cortical thickness, mainly in the parietal and frontal lobes. Next, there is a reduction in bilateral thalamic volumes and other subcortical structures. At the end of the sequence there is an increase in bilateral lateral ventricle volume. CT=cortical thickness, V=Volume, BASI=Brain Asymmetry Index, I=ipsilateral, C=contralateral.

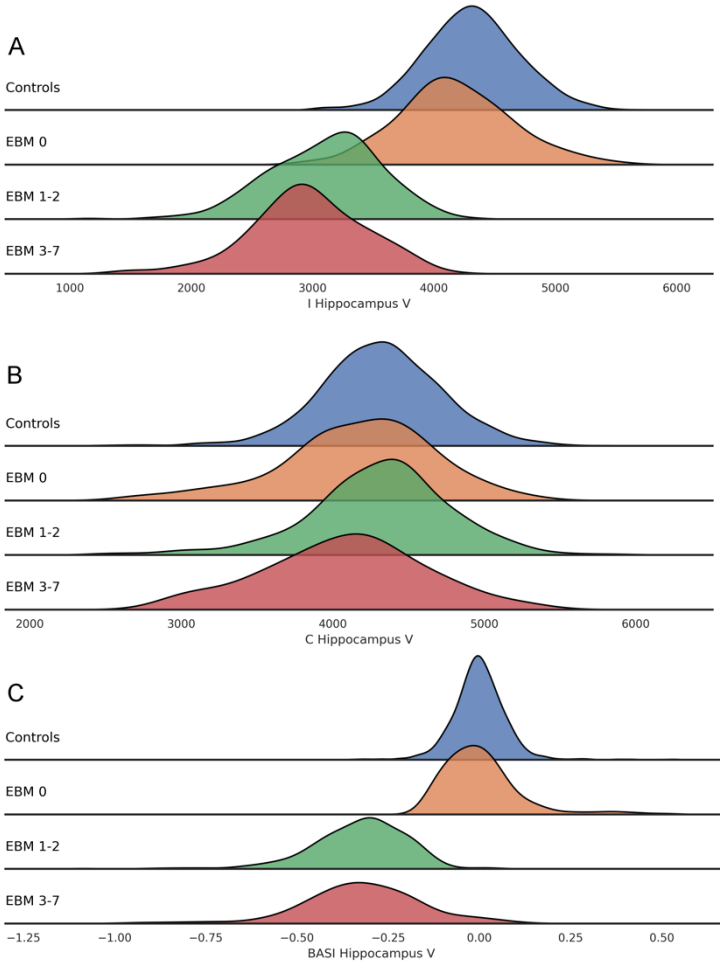

Supplementary Figure S5 Ridgeplots of hippocampal features in controls and MTLE-HS cases at different EBM stages: Each panel shows a series of density plots for hippocampal features, i.e., ipsilateral hippocampal volume (**A**), contralateral hippocampal volume (**B**) and BAIS of hippocampal volume (**C**). In each panel subjects are grouped into Controls and (top ridge) and EBM stages for MTLE-HS cases. For MTLE cases at stage 0 (EBM 0), hippocampal asymmetry is the same as in controls and ipsilateral hippocampal volume is only slightly decreased compared to controls. MTLE cases at stages 1 and 2 (EBM 1-2) show increased hippocampal volume asymmetry, reduction in ipsilateral volume but no decrease in contralateral hippocampal volume.

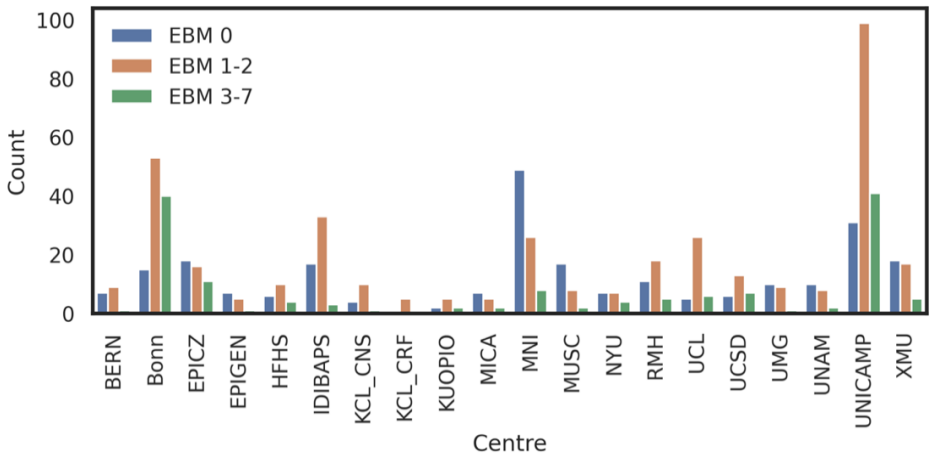

Supplementary Figure S6 Distribution of stages in MTLE-HS cases by contributing centre: Distribution of MTLE-HS cases placed in stage 0, stages 1-2 and stages 3-7 from individual centres. Some centres have a high fraction of MTLE-HS cases with EBM stage 0 (blue bars) potentially indicating different protocols and sensitivities in establishing sclerosis of the hippocampus or the mesial temporal lobe.

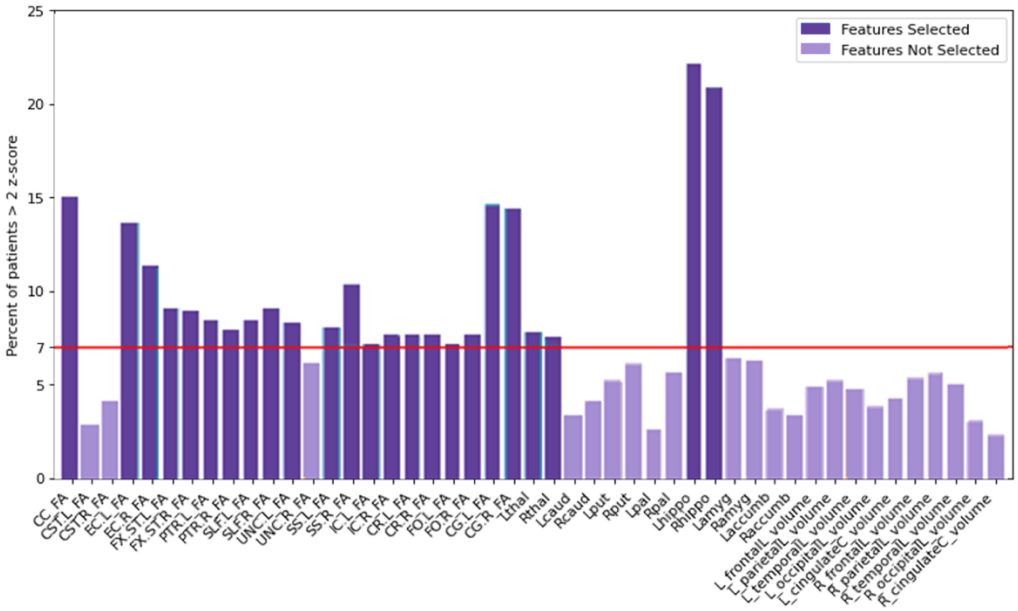

Supplementary Figure S7 Features selected: 23 features were selected based on a cut-off of atleast 7% of PWE with z-score greater than 2. CC: Corpus callosum UNC: Uncinate fasciculus, CG: Cingulum, FO: fronto-occipital fasciculus, CR: Corona radiata, IC: Internal capsule, SS: Sagittal stratum, SFL: Superior longitudinal fasciculus, PTR: Posterior thalamic radiations, FX.ST: fornix/stria terminalis, EC: External capsule, CST: Corticospinal tract.

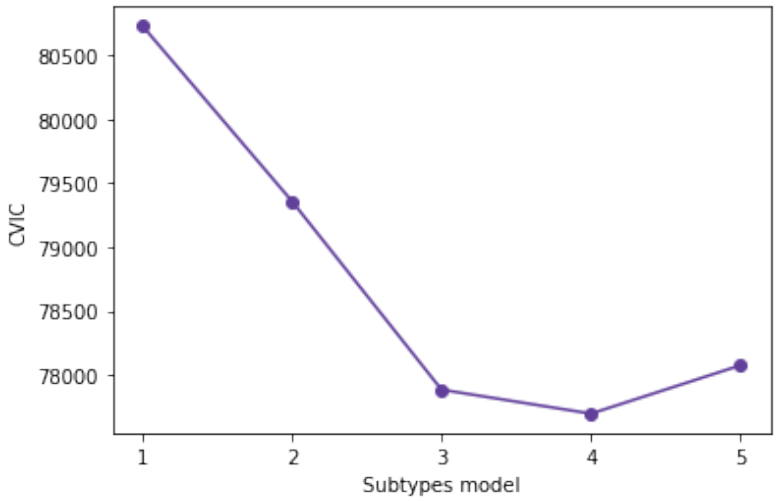

Supplementary Figure S8 CVIC of SuStaIn models: CVIC progressively decreased after considering 2, 3 and 4 subtypes and increased after considering 5 subtypes in SuStaIn.

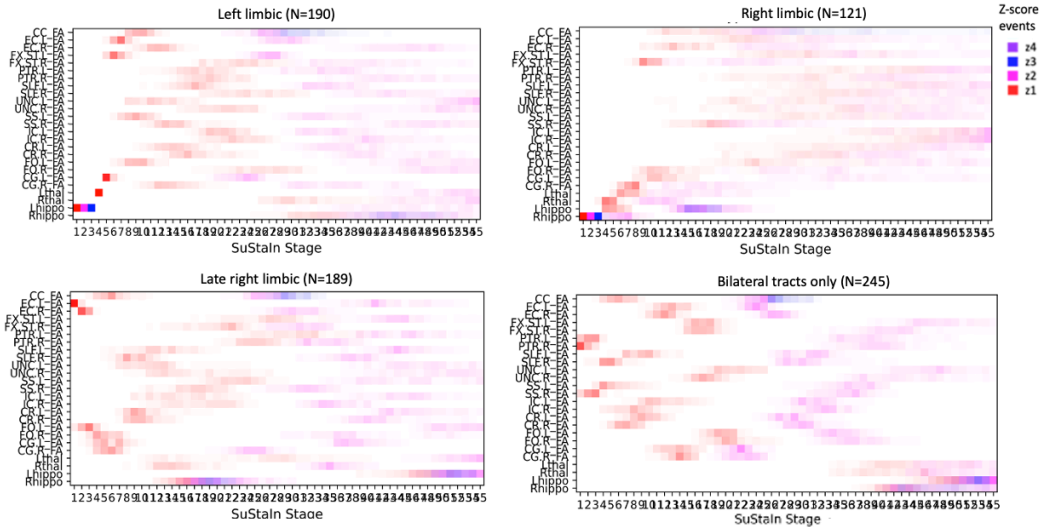

Supplementary Figure S9 Detailed progression patterns of subtypes uncovered: The Variance Diagrams (PVDs) shows the progression of disease severity, where z1, z2,..,z4 correspond to z-scores 1, 2,..,4 for each of the features arranged as rows. The colour intensity of each box marks the probability or certainty that the feature has surpassed an event score at that stage. For instance, in the left limbic subtype, the changes in left hippocampal volume is very severe with a z-score of 3 at an early (stage 3) with a high certainty.

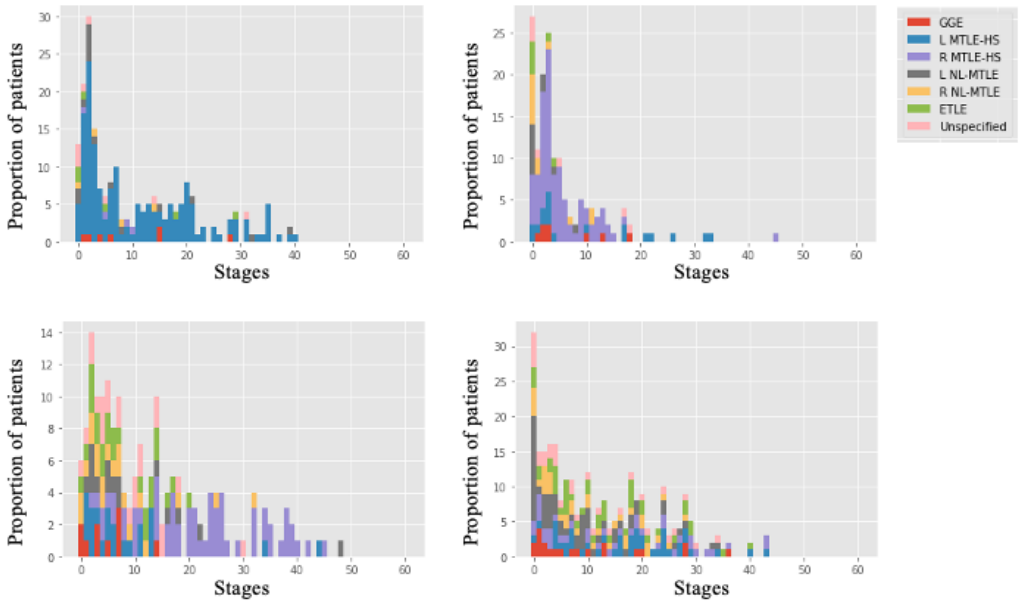

Supplementary Figure S10 SuStaIn stage distribution: Histogram showing stages (x-axis) assigned to PWE and the corresponding count (y-axis) across the four subtypes. These staging indicate around 30-40 features are affected in each of the subtypes.

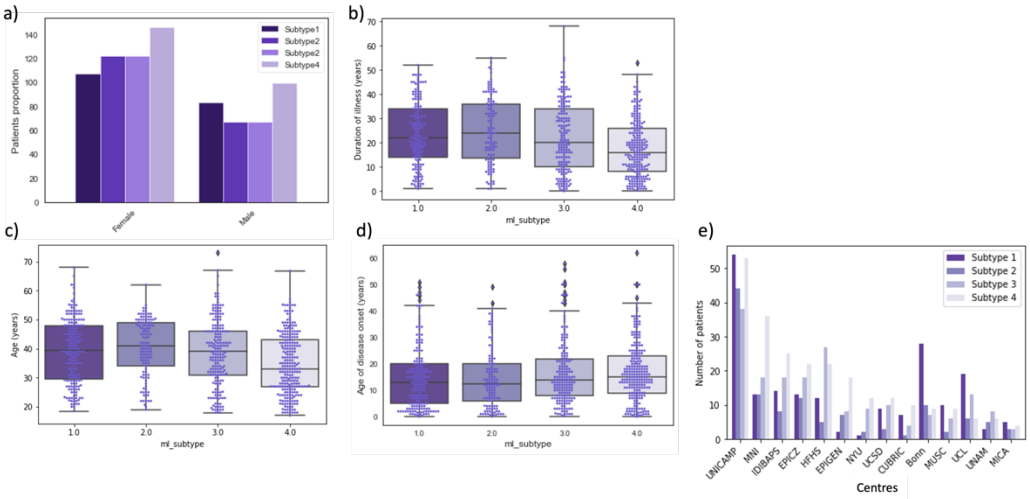

Supplementary Figure S11 Demographics of SuStaIn subtypes: The four subtypes uncovered by SuStaIn did not differ in sex (a) or age of disease onset (d), but did with respect to duration of illness (b) age (c), and centres (e). Majority of patients from MNI were assigned in subtype 1 while majority of patients from Bonn and UCL were assigned in subtype 2.

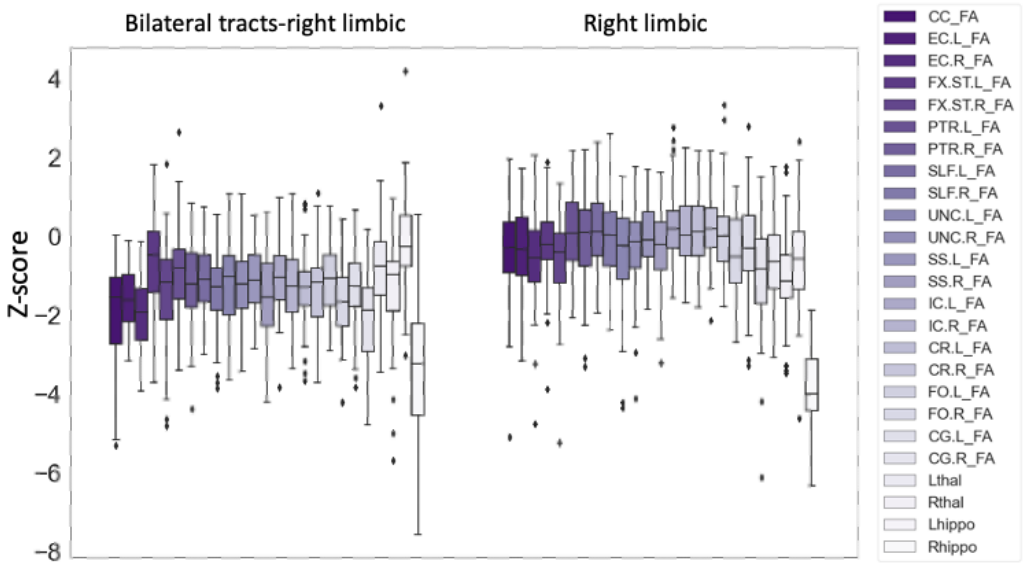

Supplementary Figure S12 Comparison of z-scores between subtypes: Box-plots showing right MTLE-HS patients assigned in Late Right Limbic subtype had lower FA values in white matter tracts than those assigned to the Right Limbic subtype.